ULTIMATE BEARING CAPACITY OF SHALLOW FOOTINGS IN LAYERED COHESIONLESS SOIL

THESIS SUBMITTED IN PARTIAL FULFILLMENT FOR THE AWARD OF THE DEGREE
of
MASTER OF CIVIL ENGINEERING
in
SOIL MECHANICS AND FOUNDATION ENGINEERING

By

RITABRATA ADHIKARI
UNIVERSITY REGD. NO. – **140640 of 2017-18**
CLASS ROLL NO. - **001710402013**
EXAM ROLL NO. – **M4CIV19017**

Under The Guidance of

Dr. Sibapriya Mukherjee
Professor

Dr. Gupinath Bhandari
Associate Professor

CIVIL ENGINEERING DEPARTMENT
JADAVPUR UNIVERSITY

MAY 2019

JADAVPUR UNIVERSITY
FACULTY OF ENGINEERING AND TECHNOLOGY
DEPARTMENT OF CIVIL ENGINEERING

DECLARATION OF ORIGINALITY AND COMPLIANCE OF ACADEMIC ETHICS

I hereby declare that this thesis contains literature survey and original research works by the undersigned candidate, as part of the Master of Civil Engineering in Soil Mechanics & Foundation Engineering studies.

All the information in this document have been obtained and presented in accordance with academic rules and ethical conduct.

I also declare that, as required by these rules and conduct, I have fully cited and referenced all material and results that are not original to this work.

Name – Ritabrata Adhikari
University Regd. No. – 140640 of 2017-18
Class Roll No. - 001710402013
Exam Roll No. - M4CIV19017
Thesis Title – **"Ultimate Bearing Capacity of shallow footings in Layered Cohesionless Soil"**

Signature with Date

JADAVPUR UNIVERSITY
FACULTY OF ENGINEERING AND TECHNOLOGY
DEPARTMENT OF CIVIL ENGINEERING

CERTIFICATE OF RECOMMENDATION

I hereby recommend that the thesis prepared under my supervision by Ritabrata Adhikari (Exam Roll No. M4CIV19017) entitled "**Ultimate Bearing Capacity of Shallow Footings in Layered Cohesionless Soil**" be accepted in partial fulfillment of the requirements for the Degree of Master of Civil Engineering with specialization in Soil Mechanics and Foundation Engineering from Jadavpur University during the year 2018-2019.

In-Charge of thesis :

Dr. Sibapriya Mukherjee
Professor

Dr. Gupinath Bhandari
Associate Professor

Department of Civil Engineering
Faculty of Engineering and Technology
Jadavpur University

Countersigned by :

Head of the Department
Department of Civil Engineering
Faculty of Engineering and Technology
Jadavpur University

Dean
Faculty of Engineering and Technology
Jadavpur University

JADAVPUR UNIVERSITY
FACULTY OF ENGINEERING AND TECHNOLOGY
DEPARTMENT OF CIVIL ENGINEERING

CERTIFICATE OF APPROVAL

The foregoing thesis entitled "**Ultimate Bearing Capacity of Shallow Footings in Layered Cohesionless Soil**", is hereby approved as a creditable study of an Engineering subject carried out and presented in a manner, satisfactory to warrant its acceptance as a pre-requisite to the degree for which it has been submitted. It is understood that by this approval the undersigned do not necessarily endorse or approve any statement made, opinion expressed or conclusion drawn therein, but approve this thesis only for the purpose for which it is submitted.

Board of Thesis Examiners:

1……

2……

3……

JADAVPUR UNIVERSITY
FACULTY OF ENGINEERING AND TECHNOLOGY
DEPARTMENT OF CIVIL ENGINEERING

ACKNOWLEDGEMENT

I would like to express my special thanks and gratitude to the professors of Civil Engineering Department, Jadavpur University who gave me the golden opportunity to do this wonderful study on the topic "**Ultimate Bearing Capacity of Shallow Footings in Layered Cohesionless Soil**". I am extremely grateful to Prof. S. P. Mukherjee, and Prof. G. Bhandari, for their persistent and valuable guidance, vigilant supervision, critical evaluation, constant support and encouragement throughout my work. Again, I am indebted to Prof. R. B. Sahu, Prof. P. Aitch, Prof. S. K. Biswas and Prof. N. Roy for their precious advice and guidance.

I express my thanks to all the staff members of Civil Engineering Department, Jadavpur University for providing me timely assistance in the course of this study.

I am also thankful to my friends for their help, moral support, constant encouragement and quality discussion on geotechnical concepts.

Place : **Kolkata**

Date : **29th May, 2019**

RITABRATA ADHIKARI
CLASS ROLL NO - 001710402013
EXAM ROLL NO – M4CIV19017
FACULTY OF ENGINEERING AND TECHNOLOGY
JADAVPUR UNIVERSITY
KOLKATA – 700032

List of Contents

CHAPTER	DESCRIPTION	PAGE NO

LIST OF FIGURES

LIST OF TABLES

LIST OF SYMBOLS

B = Least lateral dimension or width of footing (m)

L = Length of footing (m)

C = Cohesion of soil (kN/m^2)

φ = Angle of internal friction of soil (Degree)

ψ = Dilatancy angle of soil (Degree)

γ = Bulk density of soil (kN/m^3)

E = Young's modulus of elasticity of soil (kN/m^2)

ν = Poisson's ratio of soil

D_f = Depth of foundation (m)

L_1 = Depth of top layer in two-layer subsoil system (m)

L_2 = Depth of bottom layer in two layer subsoil system (m)

K_0 = Earth pressure coefficient at rest

K_a = Active earth pressure coefficient

K_p = Passive earth pressure coefficient

σ_v = Total vertical pressure (kN/m^2)

σ_h = Total horizontal pressure (kN/m^2)

β = Inclination angle of backfill to the horizontal

q = Bearing capacity of soil (kN/m^2)

N_c , N_q , N_γ = Bearing capacity coefficients

S_c , S_q , S_γ = shape factors

dc, dq, dγ = Depth Factors

ic, iq, iγ = Inclination Factor

gc, gq, gγ = Ground Factor

bc, bq, bγ = Base Factor

ABSTRACT

Traditional bearing capacity theories for determining the ultimate load carrying capacity of shallow foundations assume that the thickness of the bearing stratum is homogenous and infinite. However, this is not true in all cases. Multilayer soils are commonly encountered in practice as naturally occurring soils are often deposited in layers. It is possible to encounter a rigid layer at shallow depth or the soil may be layered and have different shear strength parameters (Bowles, 1988). A layer of deposits below shallow foundation which influences the bearing capacity is called subsoil. In the present study the bearing capacity is analyzed in one type of subsoil combination: Medium dense sand layer is overliad loose sand layer.

From the review of literature, it may be noted that the bearing capacity equations proposed for the homogenous soils by Terzaghi (1943), Meyerhof (1951) and are not applicable to layered soils. Hence it is necessary to develop an approach for predicting the bearing capacity of layered soils. The best estimation of bearing capacity and settlement in layered soil are possible only, if the pressure-settlement characteristics of the foundation-soil are known for the size of the footing.

In this present study numerical modeling and analysis of shallow footings have been carried out for layered cohesionless soils using finite element software PLAXIS 2D and the corresponding load settlement curves have been studied to evaluate the ultimate bearing capacity. This fecitilates to carry out a parametric study to understand the influence of different parameters like footing width, thickness of different layers etc. on ultimate bearing capacity of shallowfootings. In case of two-layered cohesive soil system, the influence depth varies with varying the thickness of the top layer which is well addressed in the present study. Such assessment is possible by investigating the failure mechanism and addressing the failure surface in the subsoil. Attempt has also been made to develop curves for design of shallow footing on layered cohesionless soil with non-dimensional forms of parameters considered in the study. Multiple linear regressions have been carried out to obtain an empirical relationship for ultimate bearing capacity of footings in terms of depth of footing and ratio of top layer thickness to bottom layer thickness.

CHAPTER 1: INTRODUCTION

1.0 GENERAL

For most structures including buildings, bridges, earth fills, earth and concrete dams, it is the earth that provides the ultimate support. The behaviour of the supporting ground must, therefore, affect the stability of the structure. The supporting ground is invariably a soil (sound rocky stratum being rare) which is weaker than any construction material like wood, concrete, steel or masonry. Hence, compared to structural members made out of these materials , a larger area or mass of soil is necessarily involved in carrying the same load. Structural foundations are the substructure elements which transmit the structural load to the earth in such a way that the supporting soil is not overstressed and not undergo deformations that would cause excessive settlement of the structure.

Traditional bearing capacity theories for determining the ultimate load carrying capacity of shallow foundations assume that the thickness of the bearing stratum is homogenous and infinite. However, this is not true in all cases. Multilayered soils are commonly encountered in practice. It is also possible to encounter a rigid layer at shallow depth or the soil may be layered and have different shear strength parameters (Bowles, 1988). The best estimation of bearing capacity and settlement on layered soil are possible only if the pressure-settlement characteristics of the foundation-soil are known for the given size of the footing.

Naturally occurring soils are often deposited in layers. Within each layer the soil may, typically, be assumed to be homogeneous, although the strength properties of adjacent layers are generally quite different. If a foundation is placed on the surface of a layered soil for which the thickness of the top layer is large when compared to the width of the foundation, then realistic estimates of the bearing capacity may be obtained using conventional bearing capacity theory. However, this approach may not be appropriate, if the thickness of the top layer is not large when compared to width of thefooting. Such studies of bearing capacity can be judged by conducting laboratory model tests of footings. But model tests being influenced by boundary conditions may deviate from actual field scenario where as the arrangement of actual field test being hefty it is not often possible to be adopted in practice. On such

occasions numerical analysis could be an useful tool for such analysis. There are various software packages available such as PLAXIS, ABAQUS, GEOSTUDIO, FLAC etc.,which, are being used worldwide for numerical modeling and analysis of any geotechnical problem and are popular for their robust and accurate simulation techniques.

In the present investigation attempt has been made to study the ultimate bearing capacity of shallow footings (e.g. circular and strip footings) in layered cohesionless soils using numerical modeling and analysis in finite element software package **PLAXIS 2D v 8.4 2002**. It is a two-dimensional finite element program especially developed for the analysis for foundation structures. It combines simple graphical input procedures, which allow the user to automatically generate complex finite element models, with robust calculation procedures and advanced outputfacilities. An attempt has also been made to carry out a parametric study to understand the influence of different parameters like footing width, thickness of different layers etc. on ultimate bearing capacity of shallow footings. This facilitates preparing of curves for design of shallow footing on layered cohesionless soil with non-dimensional forms of parameters considered in thestudy.

1.1 MOTIVATION OF WORK

From the literature study carried out in Chapter 2, it has been found that there are many well established theoretical equations (Terzaghi 1943, Meyerhoff 1963) to assess the bearing capacity of shallow foundations in homogenous soil deposits. It has also been found that there are many experimental (Brown and Meyerhof 1969, 1979) and analytical (Georgiadis and Michalopoulos 1985, Ming Zhu 2004) works on layered cohesive soil. But it is observed that only a few studies have been carried out on the bearing capacity of layered cohesionless soil and also to assess the variation of influence depth with varying the thickness of the top layer of layered soil stratum. In the present study attempts have been made to take care of these potential points.

1.2 OBJECTIVES OF PRESENT STUDY

Following objectives have been investigated in this present study :-

a) To carry out analysis of bearing capacity of shallow foundation in a layered cohesionless soil deposit using PLAXIS 2D software.

b) To carry out a parametric study to understand the influence of different parameters like footing width, thickness of different layers etc. on ultimate bearing capacity of shallow footings.

1.3 SCOPE OF PRESENT STUDY

The scope of the work is outlined as follows:

a) Numerical modeling and analysis of shallow footings have been carried out for layered cohesionless soils using finite element software PLAXIS 2D and the corresponding load settlement curves have been studied to evaluate the ultimate bearing capacity.

b) Thickness of the top layer (L_1) is one of the key factors in evaluation of bearing capacity in layered soil. Thickness of the top layer has been expressed in terms of the ratio L_1/L_2 (where $L_1 + L_2 = 2B$) where B is the width of footing. The following parameters has been used in the present analysis:

   i. Type of Footings – Strip and Circular
   ii. Width (B) of the footing is varied as 2.0 m and 3.0 m
   iii. D_f/B is varied as 0.5, 1, 1.5
   iv. L_1/L_2 is varied as 1/3, 1, 3
   v. Top soil layer : Loose Sand Layer ($\varphi = 28°$)
      Bottom soil layer: Medium Desnse Sand Layer ($\varphi = 31°$)

c) Multiple linear regressions have been carried out to obtain an empirical relationship for ultimate bearing capacity of footings in terms of depth of footing and ratio of top layer thickness to bottom layer thickness.

1.4 ORGANIZATION OF THE THESIS

The thesis has been organized with **seven** different chapters as follows:

An **Introduction** to the current research work has been presented in the **Chapter 1.** This chapter also deals with objective and scope of the study.

Chapter 2 presents a detailed **Literature Review** related to both experimental and theoretical studies separately on the relevant field of research.

Chapter 3 deals with **Materials and Methodology,** which deals with properties of the materials used for the study, properties of the different Subsoil and footing properties adopted for Plaxis 2d numerical analysis is stated in this chapter. Program of finite element numerical model analysis is also discussed here.

Chapter 4 describes **Numerical study by finite element method in plaxis 2D**. In this chapter, algorithms and theorems required to solve a problem by finite element in plaxis 2d is discussed.

Chapter 5 presents methodology of **Numerical Analysis** and **Presentation of finite element numerical modelling results.** Result of each model is presented here in this chapter.

Chapter 6 incorporates a detailed **Discussion on Results of Numerical Studies** on model in plaxis.

Chapter 7 brings out the **Summary, Conclusions and Suggestions for Further Research**.
An **Abstract** of the dissertation has been presented at the beginning of this dissertation.

CHAPTER 2. LITERATURE REVIEW

2.0 GENERAL :

This chapter presents the review of literature relevant to the present topic of research in chronological order.

2.1 REVIEW BASED ON CLASICAL BEARING CAPACITY THEORIES :

William John Macquorn Rankine's theory (1857) is a stress field solution that predicts active and passive earth pressure. It assumes that the soil is cohesionless, the wall is frictionless, the soil-wall interface is vertical, the failure surface on which the soil moves is planar, and the resultant force is angled parallel to the backfill surface. The equations for active and passive lateral earth pressure coefficients are given below. φ is the angle of shearing resistance of the soil and the backfill is inclined at angle β to the horizontal.

$$K_a = \frac{\cos\beta - (\cos^2\beta - \cos^2\varphi)^{1/2}}{\cos\beta + (\cos^2\beta - \cos^2\varphi)^{1/2}} \qquad \text{……...(2.1)}$$

$$K_p = \frac{\cos\beta + (\cos^2\beta - \cos^2\varphi)^{1/2}}{\cos\beta - (\cos^2\beta - \cos^2\varphi)^{1/2}} \qquad \text{……..(2.2)}$$

Rankine's Theory assumes that failure will occur when the maximum principal stress at any point reaches a value equal to the tensile stress in a simple tension specimen at failure. This theory does not take into account the effect of the other two principal stresses. Rankine's theory is satisfactory for brittle materials, and not applicable to ductile materials. This theory is also called the Maximum Stress Theory. Ultimate bearing capacity of soil is given as

$$q_{ult} = \frac{1}{2}\gamma b N_\gamma + \gamma D_f N_q^2 \qquad \text{……....(2.3)}$$

Where,

$$N_\gamma = \frac{1}{2}\sqrt{N_\varphi}(N_\varphi^2 - 1) \qquad \text{……....(2.4)}$$

$$N_q = N_\varphi^2 \qquad \text{……..(2.5)}$$

Pauker, a Russian military engineer (1889) is credited to have derived one of the oldest formulae for the bearing capacity of a foundation in cohesionless soil and the minimum depth of foundation. He was supposed to have used his formula in 1850s during the construction of fortifications and sea batteries for Czarist naval base of Kronstadt. His theory was once very popular and was extensively used in Czarist Russia, before the revolution. Pauker's equation is written as:

$$q_{ult} = H_e \tan^4(45^0 + \frac{\varphi}{2}) \quad \text{……..(2.6)}$$

This may be written in the following form also

$$H_e = \frac{q_{ult}}{\gamma} \quad \text{……..(2.7)}$$

$$q_{ult} = \gamma D_f \tan^4(45^0 + \frac{\varphi}{2}) \quad \text{…….(2.8)}$$

Bell (1915) modified Pauker-Rankine's formula to be applicable for cohesive soils; both friction and cohesion were considered in his equation. He derived the effect of cohesion on the passive pressure and his solution for a soil with horizontal surface is given by:

$$p_p = \gamma h \tan^4\left(45^0 + \frac{\varphi}{2}\right) + 2c\tan^4\left(45^0 + \frac{\varphi}{2}\right) = K_p \gamma h + 2c\sqrt{K_p} \quad \text{…....(2.9)}$$

Incurring up his solution to Rankine's equation, he proposed a bearing capacity equation for cohesive soil:

$$q_{ult} = \gamma D_f \tan^4\left(45^0 + \frac{\varphi}{2}\right) + 2c\tan^4\left(45^0 + \frac{\varphi}{2}\right) \quad \text{……...(2.10)}$$

Terzaghi (1943) considered the case of rough foundation bases resting on a soil mass that possesses weight. He developed a general bearing capacity equation for a uniformly loaded strip footing.

Terzaghi's theory is based on the following **assumptions**:

1. Soil is homogeneous and isotropic.

2. The shear strength of soil is represented by Mohr Coulombs Criteria.

3. The footing is of strip footing type with rough base. It is essentially a two dimensional plane strain problem.

4. Failure mode is General shear failure.

5. Failure zone is not extended above, beyond the base of the footing. Shear resistance of soil above the base of footing is neglected. The soil above the base of the footing is substituted by an equivalent surcharge ($q = \gamma * D_f$), where γ = unit weight of soil above the base of thefooting.
6. Method of superposition is valid.
7. Passive pressure force has three components (P_{pc} produced by cohesion, P_{pq} produced by surcharge and $P_{p\gamma}$ produced by weight of shearzone).
8. Effect of water table is neglected.
9. Footing carries concentric and vertical loads.
10. Footing and ground are horizontal.
11. Limit equilibrium is reached simultaneously at all points. Complete shear failure is mobilized at all points at the same time.
12. The properties of foundation soil do not change during the shear failure.

A strip footing of width B gradually compresses the foundation soil underneath due to the vertical load from superstructure. Let q_f be the final load at which the foundation soil experiences failure due to the mobilization of plastic equilibrium. According to Terzaghi, the soil mass above the failure surface consists of three zones:

Zone I: Because of friction and adhesion between the soil and the base of the footing, this zone cannot spread laterally. It moves downward as an elastic wedge and the soil in this zone behaves as if it is a part of the footing. The two sides of the wedge ac and bc make angle ϕ with the horizontal.

Zone II: The zones aef and bed are under this zone, which are called zones of radial shear. The soil in this zone is pushed into zone III.

Zone III: These are the two passive Rankine zones, boundaries of which make angles $(45° - \phi/2)$ with the horizontal.

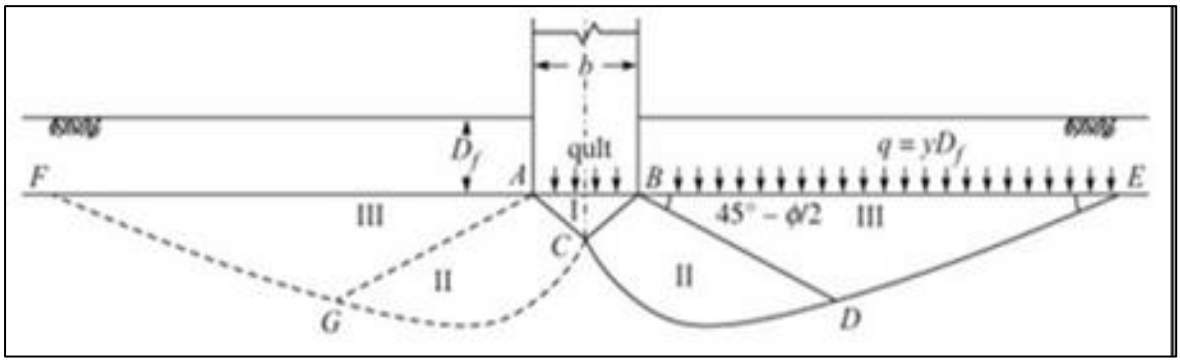

Fig 2.1 :- Terzaghi's System for ideal soil, rough base and Surcharge

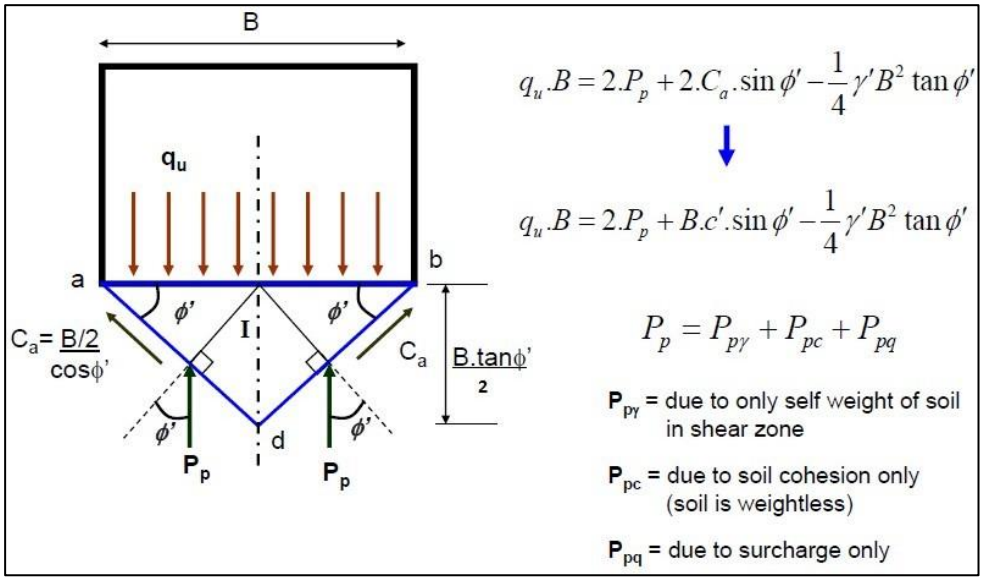

Fig 2.2 :- Terzaghi's Failure Mechanism & Govering Formula

Terzaghi has determined the bearing capacity factors N_C, N_q and N_γ as functions of the angle of internal friction ϕ as given in the table below.

Table 2.1:- Terzaghi's Bearing Capacity Factors

φ°	N_c	N_q	N_γ	φ°	N_c	N_q	N_γ
0	5.7	1	0	26	27.09	14.21	9.84
1	6	1.1	0.01	27	29.24	15.9	11.6
2	6.3	1.22	0.04	28	31.61	17.81	13.7
3	6.62	1.35	0.06	29	34.24	19.98	16.18
4	6.97	1.49	0.1	30	37.16	22.46	19.13
5	7.34	1.64	0.14	31	40.41	25.28	22.65
6	7.73	1.81	0.2	32	44.04	28.52	26.87
7	8.15	2	0.27	33	48.09	32.23	31.94
8	8.6	2.21	0.35	34	52.64	36.5	38.04
9	9.09	2.44	0.44	35	57.75	41.44	45.41
10	9.61	2.69	0.56	36	63.53	47.16	54.36
11	10.16	2.98	0.69	37	70.01	53.8	65.27
12	10.76	3.29	0.85	38	77.5	61.55	78.61
13	11.41	3.63	1.04	39	85.97	70.61	95.03
14	12.11	4.02	1.26	40	95.66	81.27	115.31
15	12.86	4.45	1.52	41	106.81	93.85	140.51
16	13.68	4.92	1.82	42	119.67	108.75	171.99
17	14.6	5.45	2.18	43	134.58	126.5	211.56
18	15.12	6.04	2.59	44	151.95	147.74	261.6
19	16.56	6.7	3.07	45	172.28	173.28	325.34
20	17.69	7.44	3.64	46	196.22	204.19	407.11
21	18.92	8.26	4.31	47	224.55	241.8	512.84
22	20.27	9.19	5.09	48	258.28	287.85	650.67
23	21.75	10.23	6	49	298.71	344.63	831.99
24	23.36	11.4	7.08	50	347.5	415.14	1072.8
25	25.13	12.72	8.34				

When, $\phi = 0$, in case of pure cohesive soils, $N_C = 3\ \pi/2+1 = 5.71$ (Calculated by applying L'Hospital's Rule to the N_C function, because with $\phi = 0$ the $N_C = 0$), $N_q = 1$ and $N_\gamma = 0$.

Terzaghi's method of analysis of the bearing capacity of a cohesive soil is independent of the width of the footing. The settlement, however, of a cohesive soil is inversely proportional to the width 'b' of the footing.

The shape of footing influences the bearing capacity. Terzaghi and other contributors have suggested the correction to the bearing capacity equation for shapes other than strip footing based on their experimental findings. The following are the corrections for circular, square and rectangular footings.

For Circular Footing

$$\mathbf{q_f = 1.3cN_C + qN_q + 0.3\gamma BN_\gamma} \qquad \text{……..(2.11)}$$

For Square Footing

$$\mathbf{q_f = 1.3cN_C + qN_q + 0.4\gamma BN_\gamma} \qquad \text{……....(2.12)}$$

For Rectangular footing

$$q_f=(1+0.3B/L)cN_c+qN_q+(1-0.2B/L)0.5\gamma BN_\gamma \quad \text{.....(2.13)}$$

The equation for bearing capacity explained above is applicable for soil experiencing general shear failure. If a soil is relatively loose and soft, it fails in local shear failure. Such a failure is accounted in bearing capacity equation by reducing the magnitudes of strength parameters c and ϕ as follows:

$$C' = \frac{2}{3} C \quad \text{.....(2.14)}$$

$$\varphi' = \tan^{-1}\left(\frac{2}{3} tan\varphi\right) \quad \text{.....(2.15)}$$

The following table summarizes the bearing capacity factors to be used under different situations. If ϕ is less than 36^0 and more than 28^0, it is not sure whether the failure is of general or local shear type. In such situations, linear interpolation can be made and the region is called mixed zone.

Local Shear Failure	Mixed Zone	General Shear Failure
$\Phi < 28^0$	$28^0 < \phi < 36^0$	$\Phi > 36^0$

Terzaghi's theory has the following **limitations**:

1. The theory is applicable to shallow foundations.
2. As the soil compresses, ϕ increases which is not considered. Hence fully plastic zone may not develop at the assumed ϕ.
3. All points need not experience limit equilibrium condition at different loads.
4. Method of superstition is not acceptable in plastic conditions as the ground is near failure zone.

Meyerhof (1963) extended Terzaghi's analysis of the plastic equilibrium of the surface footing to shallow and deep foundations, considering the shear strength of overburden. Figure

2.3 shows the failure mechanism for shallow and deep foundations according to both Terzaghi and Meyerhof's analysis

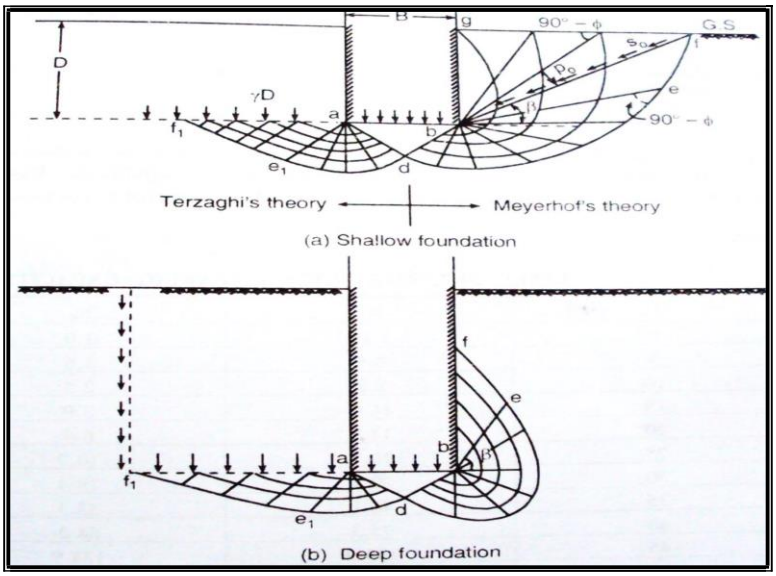

Fig 2.3 :- Meyerhof's Analysis (1963)

In the Meyerhof's analysis, abd is the elastic zone, bde is the radial shear zone and befg is the zone of mixed shear in which shear varies between radial and plane shear, which depend upon the depth and roughness of the foundation. The plastic equilibrium in all these zones is established from the boundary conditions starting from the foundation shaft. To make analysis simpler, Meyerhof introduced a parameter β, the angle to define the line bf, joining point b to f where the boundary failure slip line intersects the soil surface. The resultant effects of the wedge bfg are represented by normal stress and tangential stress, p_0 and s_0 on bf.The plane bf is termed as the equivalent free surface, and p0 and s0 are termed as the equivalent free surface stresses. The value of β increases with depth, and becomes 90° for deep foundations. The equation for ultimate bearing capacity (taking into account the shape, depth and inclination factors) can be expressed as,

$$\boldsymbol{q_u = c.N_c.s_c.d_c.i_c + q.N_q.s_q.d_q.i_q + 0.5\gamma.B.N_\gamma.s_\gamma.d_q.i_\gamma} \qquad \text{……..(2.16)}$$

Where shape factors ($\boldsymbol{s_c, s_q, s_\gamma}$), depth factors ($d_c, d_q, d_q$) and inclinations factors (i_c, i_q, i_γ) have been introduced.

Where

$$N_{\emptyset} = \tan^2\left(45 + \frac{\emptyset'}{2}\right).e^{\pi\tan\emptyset'} \quad \text{.....(2.17)}$$

$$N_c = (N_q - 1)\cot\emptyset' \quad \text{.....(2.18)}$$

$$N_\gamma = (N_q - 1)\tan(1.4\emptyset') \quad \text{.....(2.19)}$$

Above expression is of the same form as that of Terzaghi, but N_C, N_q and N_γ hold different values as follows:

Table 2.2:- Meyerhof's Bearing Capacity Factors

BEARING CAPACITY FACTORS

ϕ (Degrees)	N_c	N_q	$N\gamma$
0	5.14	1.00	0.00
5	6.49	1.57	0.45
10	8.35	2.47	1.22
15	10.98	3.94	2.65
20	14.83	6.40	5.39
25	20.72	10.66	10.88
30	30.14	18.40	22.40
35	46.12	33.30	48.03
40	75.31	64.20	109.41
45	138.88	134.88	271.76
50	266.89	319.07	762.89

NOTE — For obtaining values of N'_c, N'_q and $N'\gamma$, calculate $\phi' = \tan^{-1}(0.67 \tan \phi)$. Read N_c, N_q, and N_γ, from the Table corresponding to the value of ϕ' instead of ϕ which are values of N'_c, N'_q, $N'\gamma$ respectively.

IS code (IS: 6403-1981) recommended a bearing capacity equation which is similar in nature to those given by Vesic, Meyerhof and Brinch Hansen. IS code recommended following bearing capacity equation:

Net ultimate bearing Capacity,

$$q_{nu} = c.N_c.s_c.d_c.i_c + q.(N_q - 1).s_q.d_q.i_q + 0.5\gamma BN_\gamma.s_\gamma.d_\gamma.i_\gamma \quad \text{.....(2.20)}$$

For Cohesive soil, $q_{nu} = c.N_c.s_c.d_c.i_c$, where N_c = 5.14

N_C, N_q and N_γ are as per Vesic (1973) recommendations. Vesic's recommendation for the bearing capacity factors N_C and N_q are same as those recommended by Meyerhof but N_γ holds a different equation as follows:

By Vesic (1973),

$$N_\gamma = 2(N_q + 1)\tan(\emptyset') \quad \text{.....(2.21)}$$

Shape Factors for rectangle,

$$S_c = 1 + 0.2\frac{B}{L} \quad \text{……(2.22)}$$

$$S_q = 1 + 0.2\frac{B}{L} \quad \text{……..(2.23)}$$

$$S_\gamma = 1 - 0.4\frac{B}{L} \quad \text{……..(2.24)}$$

For Square, S_c =1.3, S_q = 1.2, S γ= 0.8;

For Circular, S_c =1.3, S_q = 1.2, S γ= 0.6

And the inclination factors are,

$$i_c = i_q = \left(1 - \frac{\beta^0}{90}\right)^2 \quad \text{…….(2.25)}$$

$$i_\gamma = \left(1 - \frac{\beta}{\emptyset'}\right) \quad \text{…….(2.26)}$$

Effect of water table as per IS Code is as follows:

a) If the water table is likely to permanently remain at or below a depth of (D + B) beneath the ground level surrounding the footing then W=1.
b) If the water table is located at a depth D or likely to rise to the base of the footing or above then the value of W' shall be taken as 0.5.
c) If the water table is likely to permanently got located at depth D < Dw < (D + B), then the value of W' be obtained by linear interpolation.

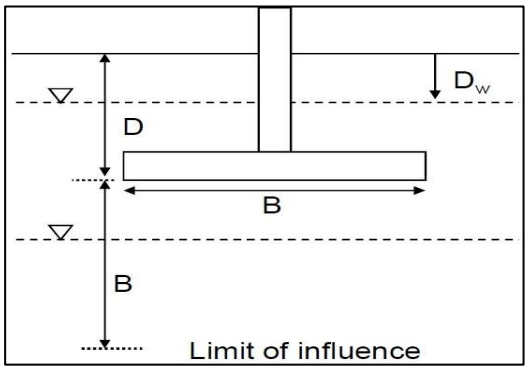

Fig 2.4 :- Effect of water table, IS Code

2.2 REVIEW BASED ON BEARING CAPACITY IN LAYERED SOIL :

Button (1953) analyzed the bearing capacity of a strip footing resting on two layers of clay. He assumed that the cohesive soils in both layers are consolidated approximately to the same degree. In order to determine the ultimate bearing capacity of the foundation, he assumed that the failure surface at the ultimate load is cylindrical, where the curve lies at the edge of the footing. The bearing capacity factor used depends on the upper soil layer and on the ratio of the cohesions of the lower/ upper claylayers.

Brown and Meyerhof (1969) investigated foundations resting on a stiff clay layer overlying a soft clay layer deposit, and the case of a soft layer overlying a stiff layer. They assumed that the footing fails by punching through the top layer for the first case, and with full development of the bearing capacity of the lower layer in the second case. Equations and charts giving the appropriate modified bearing capacity factors were given, derived from the empirical relationships obtained based on the experimental results. The results of the investigation are summarized in charts, which may be used in evaluating the bearing capacity of layered clay foundations, but these results are essentially experimental, and therefore are strongly affected by the characteristics of the claytested.

The purpose of this paper was to present the results of a series of model footing tests carried out on two- layered clay soils, and the models have many limitations. First, they were limited to one type of clay, although the strength of the clay was varied, the deformation properties remained constant. Second, studies were limited to surface loading only, using rigid strip and circular footings with rough bases. Third, all studies were made in terms of the undrained shear strength of the clay, using the $\Phi = 0$ analyses.

They also conducted a series of tests on footings in homogeneous clay. They observed that the pattern of failure beneath a footing is a function of the physical mode of rupture of the clay, which is strongly dependent on the structure of the clay. The failure mechanism of the structure of the clay is not adequately defined by conventional Mohr-Coulomb concepts of cohesion and friction.

Meyerhof (1974) investigated the case of sand layer overlying clay: dense sand on soft clay and loose sand on stiff clay. The analyses of different modes of failure were compared with the results of model test results on circular and strip footings and field data.

In the case of dense sand overlying a soft clay deposit, the failure mechanism was assumed as an approximately truncated pyramidal shape, pushed into the clay so that, in the case of general shear failure, the friction angle Φ of the sand and the undrained cohesion C of the clay are mobilized in the combined failure zones. Based on this theory, semi-empirical formulae were developed to calculate the bearing capacity of strip and circular footings resting on dense sand overlying soft clay. He conducted model tests on strip and circular footings on the surface and at shallow depths in the dense sand layer overlying clay. The results of these tests, and the filed observations were found to agree with the theory developed.

In the case of loose sand on stiff clay, the sand mass beneath the footing failed laterally by squeezing at an ultimate load. Formulae for the ultimate bearing capacity of strip and circular footings were developed. Model tests were carried out on strip and circular footings, and the results also agreed with the theory developed.

Theory and test results showed that the influence of the sand layer thickness beneath the footing depends mainly on the bearing capacity ratio of the clay to the sand, the friction angle Φ of the sand, the shape and depth of the foundation.

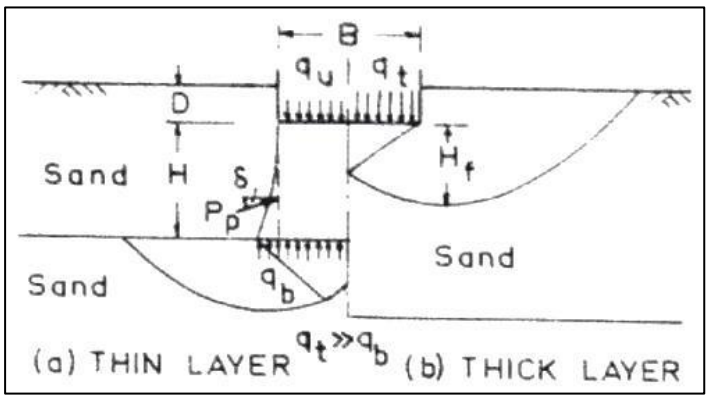

Fig 2.5 :- Reference Diagram (Meyerhof,1974)

Hanna and Meyerhof (1979) extended their previous theory of the ultimate bearing capacity of two-layer soils to the case of three-layer soils. The analysis compared well with the results of model tests of strip and circular footings in a three-layer soil. Only one case was considered in this paper, that for footings subjected to vertical loads and resting on a subsoil consisting of two strong layers overlying a weak deposit.

The same theoretical failure mechanism was assumed by considering a soil mass of the upper

two layers is pushed into the lower layer and the same forces acting on the failure surface was assumed as well. Formulae and charts were developed and can be used in designing foundations having the same conditions. Model tests on rough strip and circular footings under central vertical loads were made on the surface of three-layer sand consisting of two dense upper layers and a loose lower one. By comparing the results of the model tests with the results of the punching theory, good agreement was found. Briefly, this paper is an extension of the previous theory in order to include the case of the three-layer soil. But, it is restricted to only one case of three-layer soil, and it needs more development to include all possible cases of three-layer soils.

Pfeifle and Das (1979) presented laboratory model tests results for the case of rough rectangular footings in sand with a rigid rough base located at a limited depth. The results were compared to the predicted results of Mandel and Salencon (1972) and Meyerhof (1974). The authors concluded that the critical depth of location of the rough rigid base beyond which it has no effect on the value of the ultimate bearing capacity is about 50% - 75% higher than that predicted by the theory. And the previous theories do not predict correctly the bearing capacity for the case when the rigid base is located at shallow depth. This experimental investigation is very limited to one case of layered soils, and the friction angle Φ of the sand used varies in a small range (42° - 45°), and the conclusion may be valid only for this range ofΦ.

Hanna and Meyerhof (1981) investigated experimentally the ultimate bearing capacity of footings subjected to axially inclined loads by conducting tests on model strip and circular footings on homogeneous sand and clay. The results were analyzed to determine the inclination factors, depth factors and the shape factors incorporated in the general bearing capacity equation for shallow foundations. These values were compared with the recommended values given in the Canada Foundation Engineering Manual. The values of these factors given in the manual agree reasonably well with the experimental ones, except for the depth and shape factors, for which the theoretical values are on the conservative side when applied to inclined loads.

Hanna (1981) extended his previous theory to cover the case of footings resting on subsoil

consisting of a strong sand layer overlying a weak sand deposit. Applying the same theory that at ultimate load, a soil mass of the upper layer is pushed to the lower sand layer, and by calculating the forces on the assumed vertical punching failure surface, the ultimate bearing capacity can be calculated theoretically. Charts are presented in this paper and can be used in the design of footings. In order to verify the theory presented, model tests on strip and circular footings resting on a dense sand layer overlying loose sand layer were done and the results of the tests agreed well with the theory presented.

Hanna (1981) conducted an experimental investigation on the ultimate bearing capacity of strip and circular model footings on a two-layered soil in order to verify the validity of the empirical method proposed by Satyanarayana and Garg (1980) to predict numerically the ultimate bearing capacity of footings on layered soils. Summary of the results was presented in the form of comparative charts in order to compare the experimental and theoretical results. The author concluded that by extensive comparisons between the observed ultimate bearing capacity values and those calculated by the method reveal discrepancies ranging between 70% to 85%. Thus, the method needs more refinement and further investigation before it can be recommended for practical applications.

Hanna (1982) investigated the case of footings resting on subsoil consisting of a weak sand layer overlying a dense sand deposit. Based on model tests of strip and circular footings, the author extended the classical equation of bearing capacity to cover cases of these footings in layered sand; consisting of weak sand layer overlying a dense sand deposit. In order to calculate the ultimate bearing capacity of these footings, the author proposed to use the classical equation of homogeneous sand in conjunction with the modified bearing capacity factors. These factors depend on the relative strength of the upper and lower layers and the thickness of the upper weak sand layer, and are calculated from the model tests results conducted on similar soil profiles. Design charts were presented as an aid in design.

According to the theory presented in this paper, the failure mechanism of the upper layer is the same as if the footing was in a homogeneous deep sand layer and the influence of the layered soil is restricted to the difference in the bearing capacity factors, which were calculated experimentally from model tests. It is a simple method to overcome the complexity of finding the real failure mechanism, and it gives fairly accurate results. But the values of the bearing capacity factors depend on the kind of sand used in the tests, and they may change by

using different kind of sands taken from different places.

Georgiadis and Michalopoulos (1985) presented a numerical method for evaluating the bearing capacity of shallow foundations on layered soil, which may contain any combination of cohesive and non-cohesive layers. Several potential failure surfaces were analyzed and the minimum material factor for which the foundation is stable was determined. Comparisons between the results obtained with this method, a number of semi-empirical solutions for homogeneous and two-layered soil profiles, experiments and other numerical methods including finite elements, demonstrated the validity of the proposed method.

Semi-empirical methods for the evaluation of the bearing capacity of shallow foundations on two-layer systems are primarily based on the results of experimental investigations. Most of them are restricted to a number of limited cases, and cannot cover any limited soil profiles; moreover, the bearing capacity computed with the various semi-empirical formulae are usually scattered. In the case of more than two layers in a soil profile, the bearing capacity can be computed with a finite element analysis or numerical analysis.

Oda and Win (1990) investigated the ultimate bearing capacity of footings on a sand layer overlying a clay layer in order to study its influence on the ultimate bearing capacity of footings. Twelve tests were carried out on sand beds with an interstratified clay layer. For this purpose the thickness and the depth of the clay layer were variables. It was found experimentally that the clay layer reduces the bearing capacity of the footing even at a depth five times greater than the width of the footing. Thus, the author concluded that the plastic flow, which occurs in the lateral direction in a clay layer, exerts drag force on an upper sand layer, and this drag force results in the loss of bearing capacity.

It is obvious and experimentally proven that the presence of a thin clay layer even at a great depth reduces the bearing capacity of footings resting on granular soil.

Burd and Frydman (1996) presented an admirable discussion of the analysis of the bearing capacity of layered soils. The purpose of this discussion is two fold: First, a comparison is given between the results of independent numerical analyses performed by the discussers' and the authors' design charts. Second, the ideas presented in the paper are used as the basis

for a discussion of the analytical framework proposed by Hanna and Meyerhof (1980) for this type of problem.

A numerical study of bearing capacity of thin sand layers overlying soft clay deposits has been considered using two separate approaches. One set of results was obtained using a finite-element method; the other set was obtained using the finite-difference code FLAC. By comparing the results of the two methods, the authors found that, for the range of parameters considered, the kinematic approach may over-estimate the bearing capacity by a significant amount.

They also discuss the analytical procedures mainly the one proposed by Hanna and Meyerhof (1980), which was based on the equilibrium analysis of a granular soil below the footing. To calculate the bearing capacity of the system using this approach, it is necessary to estimate the value of shear force acting on the sides of this block of soil. This was achieved by introducing the coefficient of punching shear Ks, which is related to a set of parameters including the unit weight γ and the depth t of the sand layer. And these two parameters are not considered in the design charts presented by Hanna and Meyerhof; therefore, their design charts are only appropriate for the particular values of γ and t on which they are based, and cannot be relied upon for a range of values of sand unit weight, although the limit-equilibrium approach on which they are based appears to beacceptable.

Carlos Abou Farah (2004) investigated the ultimate bearing capacity of shallow foundations subjected to axial vertical loads and resting on soil consisting of two layers for the case of strong cohesionless soil overlying weak deposit. In this study, stress analysis was performed on the actual failure planes observed in the laboratory. Full mobilization of the shear strength on the failure planes was considered. New bearing capacity equation was derived as a function of the properties of the upper and lower soil layers, the thickness of the upper layer, the footing depth/width ratio and the angle of the failure surfaces with respect to thevertical.

Ming Zhu (2004) carried out parametric study to evaluate the ultimate bearing capacity of a rough strip footing resting on two-layer clay soil. Computations were performed by the commercial finite element analysis software ABAQUS. The computational results are compared with published lower bound and upper bound solutions by limit analysis. Parametric study was carried out to investigate the bearing capacity factor N_c^* as a function of H/B and c_1/c_2. Seven ratios of H/B were considered: 0.125, 0.25, 0.5, 0.75, 1.0, 1.25, and

2.0. Nine ratios of c_1/c_2 were considered: 5, 4, 3, 2, 1.5, 1, 0.8, 0.5, and 0.2. In total, 63 computations were performed.

For cases where the top layer is weaker than the bottom layer ($C_1/C_2 < 1$), N_C^* decreases as H/B increases. For cases where the top layer is stronger than the bottom layer ($C_1/C_2 > 1$), N_C^* increases as H/B increases. N_C^* approaches 5.146 for all cases, which indicates that the failure mechanism is limited in the top layer and the whole soil can be treated as a homogenous soil using the properties of the top soil only. According to Michalowski (2002), there exists a so-called critical depth where the strength of the bottom layer does not affect the bearing capacity. the critical depth is the depth H where the curve of N_C^* reaches 5.146. For strong-over-soft clay profile ($C_1/C_2 > 1$), the larger the ratio C_1/C_2 is, the larger the critical depth. Whereas, for soft-over-strong clay profile ($C_1/C_2 < 1$), the critical depth seems to be a constant around 0.75B. This observation is consistent with the finding by Michalowski(2002).

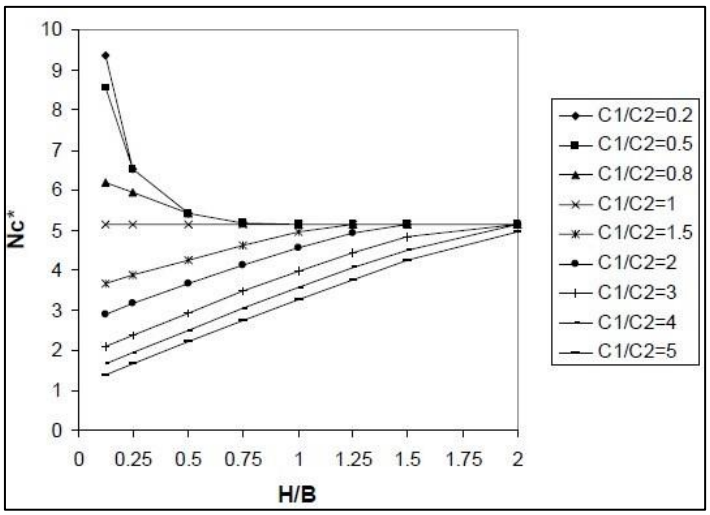

Fig 2.6 :- Bearing Capacity factors N_c^*, Ming Zhu(2004)

Zenon Szypcio and Katarzyna Dolzyk (2006) analyzed various methods for calculation of the bearing capacity of a layered subsoil. The values obtained are compared with the values calculated by means of PLAXIS Version 8, the latter being considered the correct ones. It is shown that Polish Standards and proposition modified by the authors are admissible to use only in the case of subsoil with a weak cohesionless lower layer, with small angle of friction. From the engineering point of view only the layer thickness H = 2B influences the subsoil bearing capacity. Accordingly to the Polish Standards the substitute foundation can be laid

only on the top of a very weak cohesionless lower layer. The simpler authors' modification of the Polish Standards proposition for that case is also correct. The most general, simple and correct calculation of the bearing capacity of layered subsoil is done based on the Terzaghi formula with average parameters of homogeneous subsoil. There is no big difference in the bearing capacity if we use a direct formula for calculating the average angle of friction or indirect formula. In this paper, the investigation was carried out only for strip and square foundations of the width B =1.0 m loaded symmetrically and vertically. In authors' opinion, similar conclusions are correct for other loaded foundations of different size andshape.

Ming Zhu and Radoslaw L. Michalowski (2010) presented a finite element analysis of square and rectangular footings over two-layer clay foundation soil. Bearing capacity results are shown for a limited range of parameters. While the bearing capacity is distinctly affected by both the ratio of the strengths of the two layers and the depth of the weak layer, the shape factors are only dependent on the depth ratio.

The bearing capacity of clay is reduced if a weaker layer of clay is present below a stronger crust. The limit load is affected by both the depth of the weaker layer and the ratio of the strengths of the two layers. However, the shape factor appears to be only weakly dependent on the depth, whereas it varies distinctly with a change in the strength ratio of the two layers.

Benmebarek and et. al(2012) estimated bearing capacity of the soil,using conventional bearing capacity theory based on the properties of the top layer, introduces significant inaccuracies if the thickness of the top layer is comparable to the width of the rigid footing placed on the soil surface. Saturated normally consolidated and lightly overconsolidated clays indicate that under undrained condition the cohesion of soil mass increases almost linearly with depth. In this paper, after reviewing previous works, numerical computations using the FLAC code (Fast Lagrangian Analyses of Continua) are reported to evaluate the two layered clays effect on the bearing capacity beneath rigid strip footing subject to axial static load. The results of the bearing capacity relating to the relative thickness of the top layer, the strength ratio of the soil two-layered clays and the rates of the increase of soil cohesion with depth are presented in. The obtained results are compared with previous published results available in the literature.

The results obtained have been presented in terms of a modified bearing capacity factor Nc^* in both tabular and graphical forms to facilitate their use in solving practical design problems. A number of conclusions may be drawn from this investigation:

• For a single layer profile, the footing roughness effect is more pronounced with the increase of cohesion with depth and comparison of the present solutions with published characteristics method solutions shows a good agreement.

• Nc^* is found to increase continuously with the rate of increase of cohesion with depth.

• The contrasting nature of the failure mechanisms in the cases of 'strong-over-soft' and 'soft-over strong' is clearly indicated by the present numerical computations using the FLAC code:

Verma et. Al (2013) conducted plate load test in a large tank to observe the load settlement behavior of plates of different sizes resting on layered granular soils. Tests were conducted on two layers of soils. Fine gravel layer overlain sand layer were tested using mild steel plates of square shapes. The effect of the placement of layers on the bearing capacity, settlement characteristics of footing, has been studied and an equation for predicting the bearing capacity of two layered granular soils is developed based on the plate load test data. The following conclusions were made:

1. In case of layered soils, for the same thickness and type of soils in top layer (fine gravel) and bottom layer (sand), the ultimate bearing capacity increases with the increase of size of square test plates and settlement decreases with increases the size of the square testplate.
2. In case of layered soils in which the top layer is courser (fine gravel) than the bottom layer (sand), the ultimate bearing capacity increases with the increase of the thickness of top layer (fine gravel) and settlement decreases in allcases.
3. The ultimate bearing capacity (q_u) of layered soil for L = 2 B is slightly equally than the corresponding value for homogenous Fine gravel and Ultimate bearing capacities (q_u) remain constant after the top layer of fine gravel is exceeding twice of the width of square test plate on layeredsoil.
4. In the case of layered soils, the ultimate bearing capacity in the combination of the layers affected by the load, an effective depth factor (X) is introduced. It is defined as 'the

multiplication factor which, when multiplying with the width of test plates give the total thickness of soils affected by the appliedload'.

5. Effected depth factor (X) is not constant in layered soil. Its value depends on the thickness of top layer and width of test plates. Its value varies from 1.000 to 2.213. Its value increases with increase in the thickness of top layer (finegravel).
6. The effected depth of layered soils are given by the equation, $D_{efl} = 0.73\ R_{T/B} + 0.64$ for $0.5 < T/B < 2.0$

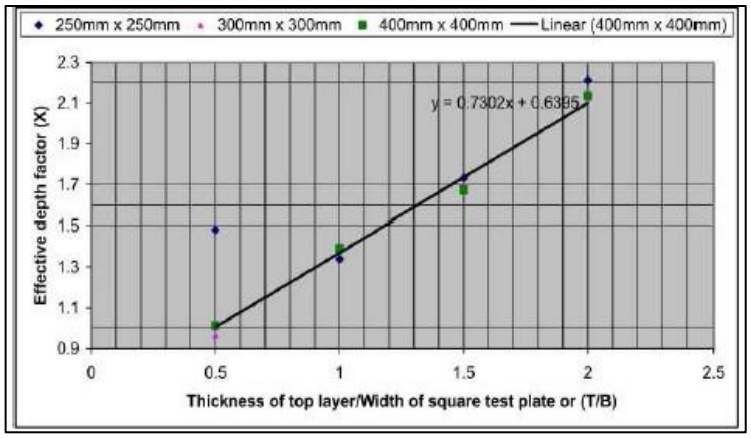

Fig 2.7 : Plot between Effective depth factor(X) and Thickness of top layer/Width of squaretest plate or (T/B) of Layered soils, Verma et. Al(2013)

Azam and Wang (2015) investigated that the ultimate bearing capacity of a shallow continuous footing supported by two-layer C-Phi soils using an elasto-plastic finite-element computer program. Three soils-a soft clay (silty clay), a stiff clay (kaolin), and a clayey sand (90 percent sand + 10 percent kaolin) were used to form representative soil layer combinations. The effect of top-layer thickness (H_1) on bearing capacity was investigated for each layer combination. Footing width (B) and depth of foundation (D_1) were kept constant at 3.0 ft (91.4 cm). The results of the analysis led to the formulation of a semiempirical bearing capacity equation that is simple in its application.

The results of the analysis indicate that when the top layer is a thin weak clay underlain by a stiff clay, the failure mode is predominantly a general shear failure involving both clay layers. But when the top layer is a thin stiff clay underlain by a weak clay, the plastic yield pattern suggests a predominantly punching shear failure of the top clay layer. For a thin sand layer underlain by a stiff clay, the yield patterns suggest a local shear failure limited to the sand

layer. For a thin layer of stiff clay underlain by sand, the failure mode is predominantly a punching shear failure of the top clay layer.

The thickness of top soil layer has a marked influence on the ultimate bearing capacity. The bearing capacity decreases steadily with increasing top-layer thickness when the top layer is weaker than the bottom layer, and vice versa. The bearing capacity attains a steady value at a specific top-layer thickness, depending on the strength properties of the two soils.

Mosadegh and Nikraz H (2015) applied finite element method (FEM) to calculate bearing capacity of a strip footing on one-layer and two-layer soil. To investigate the effect of various parameters on soil failure mechanism under the footing a commercial finite element software, ABAQUS, has been used. Soil profile contains two soil types including sand and clay. Soil behaviour is represented by the elasto-plastic Drucker-Prager model and footing material is assumed isotropic and linear elastic. For a homogenous soil profile, the effect of soil properties such as dilation angel, initial condition and footing roughness on soil failure mechanism under the footingare assessed. For a one-layer case, the bearing capacity also is calculated which has a good agreement with Terzaghi's equation. For a layered soil, soft-overstrong soil, the effect of layer thickness, soil shear strength and material property on bearing capacity value and failure mechanism of footing is investigated. It is concluded that the bearing capacity of footing decreases as the height of clayey soil increases whilst the displacement under footing increases. There is a critical depth where the stronger bottom layer does not affect ultimate bearing capacity and failure mechanism of footing.

Misir and Lama (2017) investigated bearing capacity of circular footings on a granular fill layer above a soft clay soil. The results of an extensive series of laboratory and field tests were used to define an empirical equation. This has been done by estimating the dependent variable (e.g. bearing capacity) based on the independent variables (e.g. granular fill layer thickness, soil and footing parameters and settlement ratio). A logarithmic model has been developed by using regression analysis to estimate the bearing capacity of a circular footing resting on granular fill at any settlement ratio, using all possible regression techniques based on 342 field test data, to select the significant subset of the predictors. The results indicate that the logarithmic model serves a simple and reliable tool to predict the bearing capacity of circular footings placed on a granular fill with different thicknesses above a soft clay soil.

And also, the validity of the developed formulation was verified with different plate load test results from literature.

From the laboratory and field test results, it is concluded that, the bearing capacity of the circular footing on granular fill layer over soft clay soil was increased up to 78% depending on the granular fill layer thicknesses for the different footing diameters. The statistical method in determining the bearing capacity of layered soil, for a desired settlement ratio in which the stiff soil is above the weak layer, provides realistic results for the parameters considered in this study.

Bera and Sasmal (2017) carried out model footing tests on layered soil. In the investigation top layer kept as granular soil such as sand and bottom layer clay. From the experimental results it is found that with increase in depth of top layer thickness (d) the ultimate bearing capacity of footing increases. The optimum value of depth of top layer thickness depends on relative density of sand. From the present experimental results a non linear power model has been developed to predict the ultimate bearing capacity of square footing on layered soil.

2.3 REVIEW BASED ON SEISMIC BEARING CAPACITY OF FOUNDATION :

Soubra(1996) calculated The seismic bearing capacity factors of shallow strip footings. The approach used is pseudo-static, where the seismic effects are considered by taking into account static inertia forces. The upper bound method of limit analysis is used. Two failure mechanisms, referred to as the M_1 and M_2 mechanisms, are considered for the calculation schemes. These mechanisms are non-symmetrical. M_1 consists of a log sandwich composed of a triangular active wedge, a log-spiral radial shear zone and a triangular passive wedge. M_2 consists of an arc sandwich composed of a triangular active wedge, a circular radial shear zone and a triangular passive wedge. The solutions obtained are rigorous upper-bound ones in the framework of the limit analysis theory for an associated flow rule Coulomb material. For the static case, the numerical results of the bearing capacity factors show that the M_1 mechanism gives the exact well known solutions of both the Nc_S and Nq_S factors. This is not the case with the M_2 mechanism. However, for the $N_{\gamma s}$ factor, the lowest upper-bound solutions are obtained from the M_1 mechanism for $\varphi > 30°$ and from the M_2 mechanism for $\varphi < 30°$. For the seismic case, the lowest upper-bound solutions of the seismic bearing capacity

factors obtained from both the M_1 and M_2 mechanisms are presented in the form of design charts for practical use in geotechnical engineering. These results are compared with other authors' results.

AI-Karni and Budhu (2001) presented the results of an experimental investigation on the response of model shallow footings to horizontal accelerations. The experiments were conducted on square and rectangular footings resting on or embedded in a dry sand and shaken in a shake box. The shake box was designed to subject the soil to simple shear conditions during shaking. Model footings, constructed from lead, were used to study the seismic bearing capacity. The influence of the magnitude and frequency of the horizontal accelerations, the static bearing capacity safety factor, the footing shape, the depth of embedment, and the relative density of the soil on the seismic bearing capacity were investigated. It is shown that the initial shear fluidization acceleration is the maximum acceleration sustainable by a shallow footing regardless of the static bearing capacity safety factor. Critical accelerations from limit equilibrium analyses do not compare favorably with the experimental results except when the change in angle of friction from cyclic densification was taken into account.

The results showed that the predictions of critical accelerations from recently proposed seismic bearing capacity equations are conservative when compared with the experimental results. The disagreement between the theoretical predictions and the experimental results stems from cyclic densification which significantly increased the angle of friction of the soil and the experimental difficulties in obtaining the desired angle of friction of the soil in the test setup.

MAEDA et. Al (2004) proposed a formula widely applicable for calculating bearing capacity of shallow foundations, which can evaluate both inclined load action of superstructure and inclined bearing stratum during earthquake. The formula is derived using seismic coefficient method and admissible velocity field method from upper bound theorem. Its applicability was verified by series of experiment. In practice, most bearing capacity formulas assume only the influence of load inclination. However, it was found from the newly proposed formula and experimental results that in case of strong earthquake most of the present formulas might have risk of over-evaluating the bearing capacity.

Results are summarized as follows.

1. A multi-application bearing capacity equation is proposed. It assumes a failure mechanism that considers inclinations of load and ground, and applies admissible velocity field method. Using this equation, evaluation of bearing capacity becomes possible, by considering the degree of inertia force acting on the superstructure and bearing stratum.

2. The applicability of the proposed equation is confirmed, since the decrease of bearing capacity coefficient according to the equation agrees with the test results from a two-dimensional model.

3. Based on two-dimensional bearing capacity model test results, the bearing capacity coefficient Nγ decreases according to inclinations of load and ground, similar to results from past studies. The rate of decrease becomes large as the inclination angle increases.

Choudhury and Rao(2006) The seismic bearing capacity factors for shallow strip footings embedded in sloping ground with general c-φ soil are found out by using the limit equilibrium method. The seismic forces are considered as pseudostatic forces acting both on the footing and on the soil below the footing. A composite failure surface involving planar and logspiral is considered in the analysis. A new methodology to establish minimum bearing capacity factors has been adopted by numerical iteration technique to determine the critical focus of the logspiral. Three different types of failure surfaces are considered depending on the embedment depth and ground inclinations. The seismic bearing capacity factors with respect to cohesion, surcharge and unit weight components viz. N_{cd}, N_{qd}, and $N_{\gamma d}$, respectively, are found out separately for various values of soil friction angles and seismic acceleration coefficients both in the horizontal and vertical directions, ground inclinations, and embedment depths.

Both the horizontal and vertical seismic accelerations reduce the bearing capacity factors drastically. Increase in ground slope and decrease in embedment depth results in a major decrease in seismic bearing capacity factors. Comparison with available solutions under static and seismic conditions shows that the present analysis leads to the minimum seismic bearing capacity factors with the search for critical focus of the logspiral with a critical failure surface.

HUANG and KANG(2008) investigated Seismic Bearing capacity of a rigid footing adjacent to a cohesionless slope. They used a Psuedo Static approach in conjunction with rigorous Janbu's slice method to derive analytical values of Seismic bearing capacity factors ($N\gamma$) and correction factors for the effect of inertia of soil mass and load inclinations for a rigid footing adjacent to cohesionless slopes. It is shown that both the bearing capacity factors and correction factors for the seismic bearing capacity of footings placed on level ground derived are comparable with those reported in the literature. Emperical equations regarding the effects of slope angles and load inclinations, expressed using generalised forms of those proposed in the literature, are also derived. It is also found that the emperical equations derived in the present study provide values of correction factors in good agreements with the analytical ones, indicating the validity of using these emperical equations for assessing the bearing capacity of rigid footings situated on the slope subjected to psuedo-Static seismic loading.

Shafiee and Jahanandish(2010) used the finite element method to estimate the seismic bearing capacity of strip footings for a wide range of friction angles and seismic coefficients. Curves relating seismic bearing capacity factors to earthquake acceleration are presented, and compared to available solutions in the literature. Furthermore, the effect of soil inertia on the seismic bearing capacity is investigated in the present paper. The results indicate that soil inertia plays a negligible role compared to the structural seismic load.

The results showed that seismic bearing capacity factors decreaseconsiderably with increase in seismic coefficient. Factor $N\gamma_E$ had the most significant decrease. Moreover, it was observed that the soil inertia does not have any significant impact on the seismic bearing capacity. It was also shown that the error of superposition principle in conventional bearing capacity equation is on the safe side. Furthermore, using superposition principle to compute bearing capacity for the seismic case is more conservative than static case.

CAPUTO et. Al (2011) carried out earthquake-induced reduction of the bearing capacity for a shallow strip foundation using two different approaches, both relying on the application of the method of characteristics, extended to the seismic loading condition through the pseudo-static approach. Empirical equations are available in the literature to compute corrective

coefficients of static bearing capacity factors that allow considering separately the effects of soil inertia and superstructure inertia. The corrective factors provided by such equations, however, are less conservative than those obtained in the present paper.

Two different approaches have been developed to solve plastic equilibrium equations, both based on the method of characteristics. Preliminarily, the results obtained using both approaches have been checked against benchmark solutions in static conditions, and excellent agreement has been found. In pseudostatic conditions, corrective coefficients of the Nγ factor have been obtained accounting for kinematic and inertial effects separately and resulted to be more conservative than those provided by simple approximate expressions commonly used in routine analyses.

Castelli and Motta (2012) stated due to seismic loading, foundations may experience a reduction in bearing capacity and increase in settlement. Two sources of loading must be taken into consideration: "inertial" loading caused by the lateral forces imposed on the superstructure and "kinematic" loading caused by the ground movements developed during the earthquake.

Part 5 of Eurocode 8 (2003) states that foundations shall be designed for the following two loading conditions :

a. inertia forces on the superstructure transmitted on the foundations in the form of axial, horizontal forces and moment ;

b. soil deformations arising from the passage of seismic waves.

With the aim to investigate the influence of these factors on the seismic stability of a shallow foundation, a model based on the limit equilibrium method has been developed. A pseudo-static model to account for reduction in bearing capacity due to earthquake loading is presented. In this model the loading condition consists in normal and tangential forces on the foundation and inertial forces into the soil. An upper bound solution of the limit load of the shallow foundation is found. Results of the proposed analysis are given in terms of the ratios between seismic and static bearing capacity factors Nc^*/Nc , Nq^*/Nq and N_γ^*/N_γ. Results are also compared with those deduced by other authors using different methods of analysis.

Seismic bearing capacity factors with respect to cohesion, surcharge and unit weight components have been computed for a wide range of variation in parameters such as soil

friction angle , horizontal and vertical seismic coefficients (k_h and k_v). An "upper bound" approach of the limit load was adopted to evaluate the seismic reduction factors to take into account the embedment depth of the footing and the inertia of the soil mass, as well as, the bearing capacity ratio for structure inertia only and the bearing capacity ratio for soil mass inertia only.

Fazeli and Ghareh(2012) evaluated soil bearing capacity coefficients under earthquake load has been carried out using finite elements software Plaxis and the obtained results have been compared with those from other published studies. Moreover, the effect of the inertia of the underpinning soil on the soil bearing capacity coefficients was modeled in the pseudo- static mode and the results indicated that bearing capacity coefficients obtained from pseudo-static gave good agreement with other methods. However, comparison of these two results revealed that the results obtained from numerical modeling are more conservative and are on the safety side. Finally, since the pseudo-static load is not characterized as an appropriate alternative for the earthquake load; the effect of underpinning soil on the manner of transferring the earthquake waves until reaching the foundation bed has been also investigated.

The results of the present study can be summarized as follows:

(1) PLAXIS finite element software models the soil beneath foundation on the basis of layer type, acceleration, damping and magnification of earthquake waves passing from depth to the surface of earth.

(2) This software is capable to consider the inertia effect of soil mass to estimate bearing capacity and its parameters under pseudo static conditions.

(3) The reducing rate of bearing capacity because of the earthquake is more sensible when the inertia effect of soil is considered.

(4) Seismic modeling of soil bearing capacity by pseudo static load fails to consider the effect of parameters such as soil compaction, instantaneous increase in pore water and strength parameters of soil, i.e., cohesion and internal friction angle during earthquake

Chowdhury (2015) obtained Seismic bearing capacity of shallow strip footings in soil has been obtained in the form of pseudo-static seismic bearing capacity factors N_{cd}, Nqd and Nγd, denoting the cohesion, surcharge and unit weight components, respectively, by an extensive

numerical iteration technique. Limit equilibrium method of analysis with composite failure surface is assumed. The validity of the principle of superposition is examined. Effects of both the horizontal and vertical seismic acceleration coefficients have been found to always reduce the ultimate bearing capacity significantly. Results obtained by the present method of analysis are compared with the available results and are found to be the least in the seismic case.

Pane et. Al (2015) followed pseudo-static approach, finite difference (FDM) numerical analyses have been performed aimed at evaluating the seismic effects on the ultimate bearing capacity of shallow strip foundations. In the specialised literature, such seismic effects are usually divided in two components, namely, a structure inertia and a soil inertia, which can be either considered together, or separately addressed and then superposed. The good agreement found between the numerical and the analytical approaches is pointed out, thus providing further evidence of the reliability of some available and widespread solutions. The possibility of superposition of the two inertia effects is investigated. It is found that in some cases the soil inertia may play a significant role in the seismic capacity of the system, and that simple one-constant equations can be readily used in foundation design to estimate the reduction in bearing capacity (namely, factors e_i, e_k) deriving from the two inertia effects.
The coupling effect of structure-inertia (e_i) and soil-inertia (e_k) is not essential; in fact, the overall reduction of capacity that has been obtained considering the simultaneous occurrence of the two inertias is almost coincident, for all practical purposes, to the one obtained by separately evaluating ei, ek and then computing their overall effect by superposition of effects (e_i & e_k); From the results, it appears reasonable and convenient to quantify the two inertial effects in a separate manner. By so doing, the relative importance of the two inertias can be easily brought to light and quantified; in addition, this approach makes it easier to face the more general situations in which the structure-inertia seismic coefficient differs from the soil-inertia one (k_h,i = k_h,k).

Yadav and Jawaid(2016) stated that the problem of the seismic bearing capacity of shallow foundations has been solved indirectly, either due an increase of the static allowable soil pressures related to the probability of occurrence of the design earthquake or by adopting an equivalent pseudo-static approach. This paper presents a parametric comparative analysis of different methods for estimating seismic bearing capacity of shallow strip foundations.

Analytical methods, developed in the framework of both limit equilibrium and limit analysis theories, and also simplified design procedures typically used in practice were considered. The results obtained show an important decrease of the bearing foundation capacity with increasing of the maximum earthquake acceleration, which highlights the need to obtain a measure of the reliability associated with both calculation methods and safety factors commonly used for seismic design.

Chattopadhyay et. Al (2017) proposed to study changes of allowable bearing capacity during earthquake for strip footing on sandy soil for various ranges of width of foundation (B), angle of shearing resistance (Φ) of supporting soil and intensity of earthquake from different available theories to check the relativities of such theories. The majority of available solutions in the literature are analytical. Solutions for dynamic bearing capacity for identical foundation were obtained and comparison were made to seek relative differences between the results from such different theories for varying seismic condition.

Detailed examination regarding available methods to find dynamic bearing capacity of strip footings on cohesionless soils under seismic condition has been made in this paper. An examination was made to find the predicted values of dynamic bearing capacity from allowable theories advanced by recent researchers under varying width of strip footing and different soil properties and seismic condition. For the purpose of comparison bench mark solution for dynamic bearing capacity was taken those from Richard et.al (1993) which was the most important publication within last two decades which indicated large scale research activity in this domain. However, from all the comparisons it is seen that Richard et.al. theory gives higher values may be due to the model chosen by Richard et.al (two wedge below foundation at failure condition). But in pseudo-dynamic condition Saha & Ghosh theory gives much lower values compared to other theories.

Saha et. Al (2018) presents an upper-bound solution for bearing capacity of shallow strip footing considering composite failure mechanisms by the pseudodynamic approach. A recently developed hybrid symbiosis organisms search (HSOS) algorithm has been used to solve this problem. In the HSOS method, the exploration capability of SQI and the exploitation potential of SOS have been combined to increase the robustness of the algorithm. Numerical analysis is also done using dynamic modules of PLAXIS-8.6v for the validation of

this analytical solution.The results obtained from the present analysis using HSOS are thoroughly compared with the existing available literature and also with the other optimization techniques.

Using the pseudodynamic approach, the effect of the shear wave and primary wave velocities traveling through the soil layer and the time and phase difference along with the horizontal and vertical seismic accelerations are used to evaluate the seismic bearing capacity of the shallow strip footing. A composite failure mechanism which includes both planer and log-spiral zone is considered here to develop this mathematical model for the shallow strip footing resting on c-φ soil. The effect of various parameters such as soil friction angle (φ), seismic accelerations (k_h and k_v), cohesion factor ($2C/\gamma B_0$), and depth factor (D_f/B_0) is studied here. It is seen that the pseudodynamic bearing capacity coefficient ($N\gamma e$) increases with the increase in φ, $2C/\gamma B_0$, and $D_f/B0$, but it decreases with the increase in horizontal and vertical seismic accelerations (k_h and k_v).

Accordingly, Research gap and motivation of work has been discussed in chapter 01 and objective, scope of the present study as obtained from research gap is also discussed in chapter 01.

CHAPTER 3: MATERIALS AND METHODOLOGY

3.0 GENERAL

In this chapter properties of the materials such as subsoil layer and footing is adopted and program of finite element modelling is discussed.

3.1 MATERIAL PROPERTIES

Materials that have been used in PLAXIS 2D for finite element modeling are as follows:

3.1.1 Soil

The present study deals with the ultimate bearing capacity of shallow footings placed on layered cohesionless soil where cohesionless soil is having very small cohesion (very small value of cohesion as 1 kN/m^2 is used to eliminate errors in plaxis) . The properties of soil are presented in the table below:

Table 3.1:- Properties of Layered Soil taken as problem defination

Soil Type	γ (kN/m^3)	Young's Modulus,E (kN/m^2)	Poisson Ratio (μ)	Cohesion, C (kN/m^2)	Friction Angle (ϕ)
Top Loose Sand	18	12500	0.35	1	28
Bottom Medium Dense Sand	18.8	15000	0.35	1	31

3.1.2 FOOTING:

The foundation here is very flexible and very rough (no soil sliding in their base) with following properties:

Table 3.2:- Property of the Foundation

Footing Legend	Footing Type	Footing Dimension	EI (kN/ m^2)	EA (kN)	Equivalent Thickness (m)
F1	STRIP	2 m	$5*10^6$	8500	0.143
F2	STRIP	3 m	$5*10^6$	8500	0.143
F3	CIRCULAR	2 m	$5*10^6$	8500	0.143
F4	CIRCULAR	3m	$5*10^6$	8500	0.143

3.2 PROGRAM OF FINITE ELEMENT MODELLING IN PLAXIS 2D :

To determine the static bearing capacity of shallow foundations on layered cohesionless soils and to carry out a parametric study to understand the influence of different parameters like footing width, thickness of different layers etc. on ultimate bearing capacity of shallow footings total 36 finite element modeling has been carried out in PLAXIS 2D Foundation:

Schematic diagram of the problem used in PLAXIS is presented here :

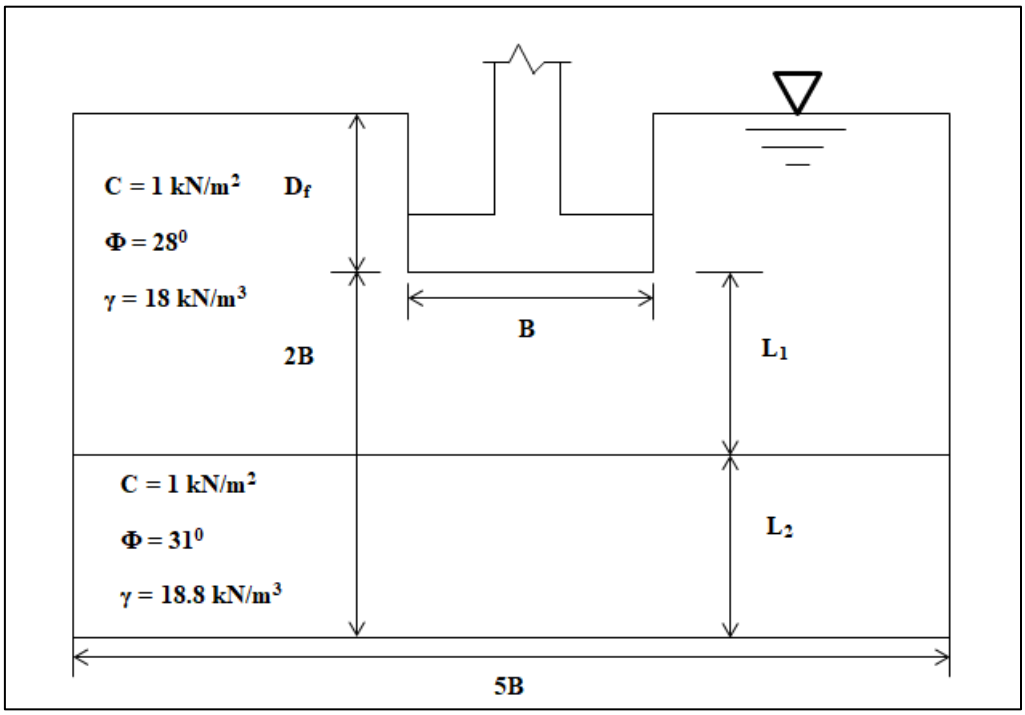

Fig 3.1 :- Schematic Diagram of the Problem

Program of the finite element programming in Plaxis 2D is presented in tabular format :

Table 3.3: Program of Finite element Modelling

Model Serial No	Type of Footing	Width of Footing (m)	D_f/B	L_1/L_2
1	Strip (F1)	2	0.5	1/3
2	Strip (F1)	2	0.5	1
3	Strip (F1)	2	0.5	3
4	Strip (F1)	2	1	1/3
5	Strip (F1)	2	1	1
6	Strip (F1)	2	1	3
7	Strip (F1)	2	1.5	1/3
8	Strip (F1)	2	1.5	1
9	Strip (F1)	2	1.5	3
10	Strip (F2)	3	0.5	1/3
11	Strip (F2)	3	0.5	1
12	Strip (F2)	3	0.5	3
13	Strip (F2)	3	1	1/3
14	Strip (F2)	3	1	1
15	Strip (F2)	3	1	3
16	Strip (F2)	3	1.5	1/3
17	Strip (F2)	3	1.5	1
18	Strip (F2)	3	1.5	3
19	Circular (F3)	2	0.5	1/3
20	Circular (F3)	2	0.5	1
21	Circular (F3)	2	0.5	3
22	Circular (F3)	2	1	1/3
23	Circular (F3)	2	1	1
24	Circular (F3)	2	1	3
25	Circular (F3)	2	1.5	1/3
26	Circular (F3)	2	1.5	1

27	Circular (F3)	2	1.5	3
28	Circular (F4)	3	0.5	1/3
29	Circular (F4)	3	0.5	1
30	Circular (F4)	3	0.5	3
31	Circular (F4)	3	1	1/3
32	Circular (F4)	3	1	1
33	Circular (F4)	3	1	3
34	Circular (F4)	3	1.5	1/3
35	Circular (F4)	3	1.5	1
36	Circular (F4)	3	1.5	3

CHAPTER 4 : NUMERICAL STUDY BY FINITE ELEMENT METHOD IN PLAXIS 2D

4.0 GENERAL

Numerical analysis is the study of algorithms that use numerical approximation(as opposed to general symbolic manipulations) for the problems of mathematical analysis (as distinguished from discrete mathematics).The overall goal of the field of numerical analysis is the design and analysis of techniques to give approximate but accurate solutions to hard problems. Common methods of numerical study used in the analysis of bearing capacity of shallow footing include the finite difference method, finite element methods etc.

In the finite element method a continuum is divided into a number of elements. Each element consists of a number of nodes. Each node has a number of degrees of freedom that correspond to discrete values of the unknowns in the boundary value problem to be solved. Analyses were performed with several trail meshes with increasing mesh refinement until the displacement changes very minimal with more refinement.

Now-a-days finite element analysis has wide-spread applications in Geotechnical Engineering. There are various FEM Software packages available such as PLAXIS, ABAQUS, GEOSTUDIO, FLAC etc. These FEM S/W Packages are worldwide used for numerical modeling and analysis of any geotechnical problem and are popular for their robust and accurate simulation techniques. In the present study finite element analysis has been carried out using PLAXIS 2D software.

4.1 FINITE ELEMENT METHOD

It is an approximate numerical solution technique in which continuous system is discretized into many small and simple pieces called finite elements. For each element it is necessary to make an assumption as to how the primary variables, such as displacement, are distributed in terms of geometrical position. Then a set of simultaneous equations are developed for describing the constitutive or other behaviour of each element in terms of discrete nodal point values of the primary variable. Each of these elements is then combined using proper compatibility relations between them and global set of simultaneous equations is obtained. Then the applications of load and boundary conditions are imposed to the global set of

simultaneous equations. These equations are solved simultaneously or implicitly in a personal computer. Solutions of these equations provide the approximate results or prediction of behavior of the physical system that has been modeled. A short overview of the finite element is provided below.

At first, body to be analyzed is discretized into finite elements which can be one dimensional, two dimensional or three dimensional depending on the body to be discretized and the need of the user. Within an element the displacement field u is obtained from the discrete nodal values in a vector ν using interpolation functions assembled in matrix N :

$$\underline{\boldsymbol{u}} = \underline{\underline{\boldsymbol{N}}}\,\underline{\boldsymbol{\nu}} \qquad \text{……...(4.1)}$$

The interpolation functions in matrix N are often denoted as shape functions. The shape function depends entirely on the type of the element considered and its geometry.

The relation between strain and displacement field vector can be formulated as:

$$\underline{\boldsymbol{\varepsilon}} = \underline{\underline{\boldsymbol{L}}}\,\underline{\boldsymbol{u}} \qquad \text{……(4.2)}$$

This equation expresses the six strain components, assembled in vector ε, as the spatial derivatives of the three displacement components, assembled in vector u, using the differential operator *L*.

Substitution of Eq.4.1 in the relation gives:

$$\underline{\boldsymbol{\varepsilon}} = \underline{\underline{\mathbf{L}}}\,\underline{\underline{\mathbf{N}}}\,\underline{\boldsymbol{\nu}} = \underline{\mathbf{B}}\,\underline{\boldsymbol{\nu}} \qquad \text{……..(4.3)}$$

In this relation B is the strain displacement matrix, which contains information of geometry of the element.The stress vector is then estimated from the strain vector by multiplying with constitutive matrix as

$$\boldsymbol{S} = \boldsymbol{D^e B \nu} \qquad \text{……..(4.4)}$$

Finite elements obtained by discretization of a continuum are formulated in general and systematic way. The stiffness matrix and load vectors of an element can be formulated by Rayleigh-Ritz or variational principle and Galerkin weighted residual methods. Consequently the body is reduced into a basic matrix equation form as:

$$\mathbf{[F]=[K][\,v]} \qquad \text{……..(4.5)}$$

$$\textbf{Here, } \mathbf{F = f_b + f_S + f_i} \qquad \text{……..(4.6)}$$

Where $\boldsymbol{f_b}$ is the body force, $\boldsymbol{f_S}$ is the surface traction force vector and $\boldsymbol{f_i}$ concentrated or internal force vector.

The matrix K defines the stiffness of the element and its basic form can be expressed as:-

$$\underline{\underline{K}} = \int \underline{\underline{B^T}}\ \underline{\underline{D^e}}\ \underline{\underline{B}}\ dV \qquad \text{.....(4.7)}$$

The stiffness matrix is evaluated using any suitable numerical integration scheme.

Once the element stiffness matrices are formulated they are assembled into global stiffness matrix to generate a set of simultaneous equations of all degree of freedom. For 3D analysis the dimension of the global stiffness matrix is **2n X 2n**, n being number of nodes of the model. In mathematical form, the globalsimultaneous equations are written as:

$$\mathbf{F^g = K^g U^g} \qquad \text{.....(4.8)}$$

Where:

$\mathbf{K^g}$= is the global stiffness matrix

$\mathbf{U^g}$= is the global displacement vector $\{ U_1V_1 \ldots U_2V_2 \}^T$

$\mathbf{F^g}$ = is the global force vector $\{ F_{1x}F_{1y} \ldots F_{nx}\ F_{ny} \}^T$

Once the global displacement vector is evaluated nodal displacement vector is extracted separately. Then with the help of equations above we can calculate the strain and stress respectively.

4.2 MODELLING BY PLAXIS

4.2.1 Basic Aspects

In the present study finite element analysis has been carried out using PLAXIS 2D software. It is a two-dimensional finite element program especially developed for the analysis of foundation structures. It combines simple graphical input procedures, which allows the user to automatically generate complex finite element models, with advanced output facilities and robust calculation procedures. PLAXIS 2D is a special purpose two-dimensional finite element computer program used to perform deformation and stability analyses for various types of geotechnical applications. Real situations may be modelled either by a plane strain or an axisymmetric model. The program uses a convenient graphical user interface that enables users to quickly generate a geometry model and finite element mesh based on a representative vertical cross-section of the situation at hand PLAXIS 2D program consists of four basic components, namely **Input, Calculation, Output and Curves.**

- **Input :-**

  In the Input program the boundary conditions, problem geometry with appropriate material properties are defined. The problem geometry is the representation of a real three-dimensional problem into two-dimensional problem.**(Plane Strain & Axisymmetry).**

  A **Plane strain** model is used for geometries with a (more or less) uniform cross section and corresponding stress state and loading scheme over a certain length perpendicular to the cross section (z-direction). Displacements and strains in z-direction are assumed to be zero. However, normal stresses in z- direction are fully taken intoaccount.

  An **Axisymmetric model** is used for circular structures with a (more or less) uniform radial cross section and loading scheme around the central axis, where the deformation and stress state are assumed to be identical in any radial direction. Note that for axisymmetric problems the x-coordinate represents the radius and the y-coordinate corresponds to the axial line of symmetry. Negative x-coordinates cannot be used.

  The selection of Plane strain or Axisymmetric results in a two dimensional finite element model with only two translational degrees of freedom per node (x- and y-direction).

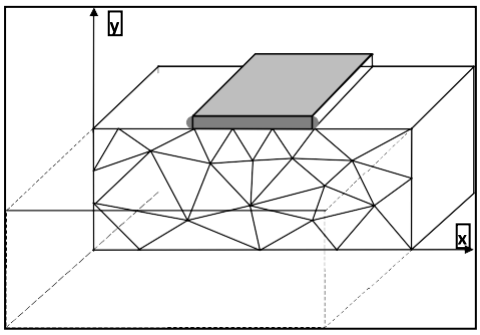

Fig 4.1 :- Plain Strain Model

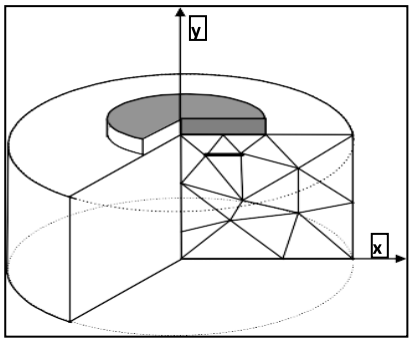

Fig 4.2 :-Axisymetric Model

The user may select either **6-node or 15-node** triangular elements to model soil layers and other volume clusters. The 15-node triangle is the default element. It provides a fourth order interpolation for displacements and the numerical integration involves twelve Gauss points (stress points). For the 6-node triangle the order of interpolation is two and the numerical integration involves three Gauss points.The type of element for structural elements and interfaces is automatically taken to be compatible with the soil element type as selected here.

The **15-node triangle** is a very accurate element that has produced high quality stress results for difficult problems, as for example in collapse calculations for incompressible soils . The use of 15-node triangles leads to relatively high memory consumption and relatively slow calculation and operation performance. Therefore a more simple type of elements is also available.

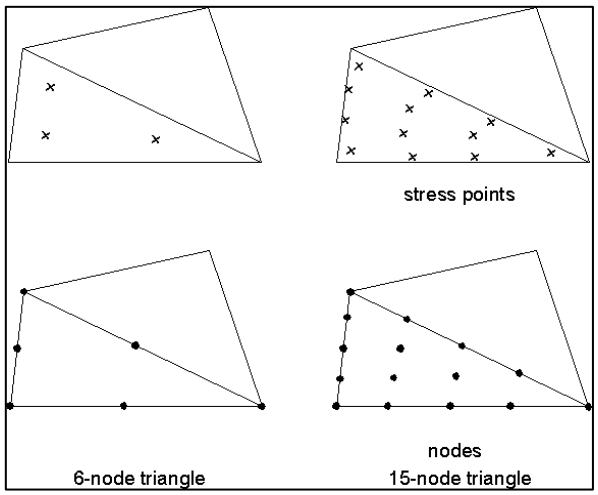

Fig 4.3 :- 6 noded & 15 noded traingular finite element

The **6-node** triangle is a fairly accurate element that gives good results in standard deformation analyses, provided that a sufficient number of elements are used. However, care should be taken with axisymmetric models or in situations where (possible) failure plays a role, such as a bearing capacity calculation or a safety analysis by means of phi-c reduction. Failure loads or safety factors are generally overpredicted using 6-noded elements. In those cases the use of 15-node elements is preferred.One 15-node element can be thought of a composition of four 6-node elements, since the total number of nodes and stress points is equal.

When the geometry model is fully defined and material properties are assigned to all clusters and structural objects, the geometry has to be divided into finite elements in order to perform finite element calculations. A composition offinite elements is called a mesh. The basic type of element in a mesh is the 15-node triangular element or the 6-node triangular element . The generation of the mesh is based on a robust triangulation procedure, which results in

'unstructured' meshes. These meshes may look disorderly, but the numerical performance of such meshes is usually better than for regular (structured) meshes. Distinction is made between five levels of global coarseness: Very coarse, Coarse, Medium, Fine, Very fine. The mesh element size can be adjusted by using a general mesh size varying from very coarse to very fine and also by using line, cluster and point refinements. Very fines meshes should be avoided in order to reduce the number of elements, thus to reduce the memory consumption and calculation time. The program does not allow entering a new structural element or a new soil cluster after the mesh is generated. If a new element or cluster is added to the geometry model, the mesh generation should be repeated with the new input.

Once the geometry model has been created and the finite element mesh has been generated, the initial stress state and the initial configuration must be specified. This is done in the initial conditions part of the input program. The initial conditions consist of two different modes: One mode for the generation of initial water pressures (water conditions mode) and one mode for the specification of the initial geometry configuration and the generation of the initial effective stress field (geometry configuration mode).

After defining the model geometry and generation of 3D mesh, initial stresses are applied by using either K0-procedure or gravity loading. The initial stresses in the soil are affected by the weight of the soil and history of the soil formation. Stress state is characterized by vertical and horizontal stresses. Initial vertical stress depends on the weight of the soil and pore pressures; whereas initial horizontal stresses are related to the vertical stresses multiplied by the coefficient of lateral earth pressure at rest. The K0-procedure may only be used for horizontally layered geometrics with a horizontal ground surface and, if applicable, a horizontal phreatic level. In the present study the K0-procedure has been used.

In this analysis the effect of ground water table is taken into account. Iinitial stress would have been calculated by effective stress consideration.

$$\overline{\sigma}_h = K_0 . \overline{\sigma}_v \qquad \text{……(4.9)}$$

where Ko is based on jacky's formula (1944) which is written as:

$$K_0 = 1 - \sin\varphi \qquad \text{……..(4.10)}$$

- **Calculation :-**

After the generation of a finite element model, the actual finite element calculations can be executed. Therefore it is necessary to define which types of calculations are to be performed

and which types of loadings or construction stages are to be activated during the calculations. The Calculations program considers only deformation analyses and distinguishes between a Plastic calculation, a Consolidation analysis, Phi-c reduction (safety analysis) and a Dynamic calculation. The first three types of calculations (Plastic, Consolidation, Phi-c reduction) optionally allow for the effects of large displacements being taken into account. This is termed Updated mesh, which is available as an advanced option. In the engineering practice, a project is divided into project phases. Similarly, a calculation process in PLAXIS is also divided into calculation phases. Examples of calculation phases are the activation of a particular loading at a certain time, the simulation of a construction stage, the introduction of a consolidation period, the calculation of a safety factor, etc. Each calculation phase is generally divided into a number of calculation steps. This is necessary because the non-linear behaviour of the soil requires loadings to be applied in small proportions (called load steps). In most cases, however, it is sufficient to specify the situation that has to be reached at the end of a calculation phase. Robust and automatic procedures in PLAXIS will take care of the sub-division into appropriate load steps.

Since staged construction is performed using the Load advancement ultimate level procedure, it is controlled by a total multiplier (ΣMstage). This multiplier generally starts at zero and is expected to reach the ultimate level of 1.0 at the end of the calculation phase. In some special situations, however, it might be necessary to split the staged construction process into more than one calculation phase and to specify an intermediate value of ΣMstage.

- **Output :-**

  The main output quantities of a finite element calculation are the displacements at the nodes and the stresses at the stress points. In addition, when a finite element model involves structural elements, structural forces are calculated in these elements. An extensive range of facilities such ascalculation total displacements, vertical & Horizontal displacements, Total Stress, effective stress, total strain exist within PLAXIS to display the results of a finite element analysis.

- **Curve :-**

  This icon represents the Curves program. The Curves program contains all facilities to generate load-displacemen tcurves,stress paths ands tress-strain diagrams. Load-displacement curves can be used to visualise the relationship between the applied loading and the resulting displacement of a certain point in the geometry. In general, the x-axis relates to the

displacement of a particular node (Displacement), and the y-axis contains data relating to load level (Multipliers). Other types of curves can also be generated.

4.2.2 Mohr-Coulomb Model

Soil tends to behave in a highly non-linear way under load. This non-linear stress-strain behavior can be modeled at several levels of sophistication. Clearly, the number of model parameters increases with the level of sophistication. The well-known Mohr-Coulomb model can be considered as a first order approximation of real soil behavior. This elastic - perfectly plastic model requires five basic input parameters, namely Young's Modulus (E), Poisson's Ratio (ν), Cohesion (C), Friction Angle (Φ) and Dilatancy Angle (ψ). For each layer one estimates a constant average stiffness. Due to this constant stiffness computations tend to be relatively fast and one obtains a first impression of deformations. Besides the five model parameters mentioned above, initial soil conditions play an essential role in most soil deformation problems. Initial horizontal soil stresses have to be generated by selecting proper K_0-values. PLAXIS also supports some advanced soil models such as Hardening-Soil Model which involves compression hardening to simulate irreversible compaction of soil under primary compaction. Therefore, in contrast to Mohr-Coulomb model, the Hardening-Soil model account for stress-dependency of stiffness moduli. All soils exhibit some creep and primary compression is thus followed by a certain amount of secondary compression especially in very soft soil. The Hardening-Soil model does not account for viscous effects i.e. creep and stress relaxation where Soft-Soil-Creep (SSC) model plays an advanced role. It is advised by the PLAXIS Engineering forum to use the Mohr-Coulomb model for a relatively quick and simple first analysis of the problem considered. When good soil data is lacking, there is no use in further more advanced analyses. In the present study Mohr-Coulomb model has been used with the aforementioned five basic soil parameters to calculate the complete $\sigma - \varepsilon$ behavior.

Plasticity is associated with the development of irreversible strains. In order to evaluate whether or not plasticity occurs in a calculation, a yield function, f, is introduced as a function of stress and strain. A yield function can often be presented as a surface in principal stress space. A perfectly-plastic model is a constitutive model with a fixed yield surface, i.e. a yield surface that is fully defined by model parameters and not affected by (plastic) straining. For stress states represented by points within the yield surface, the behavior is purely elastic

and all strains are reversible.

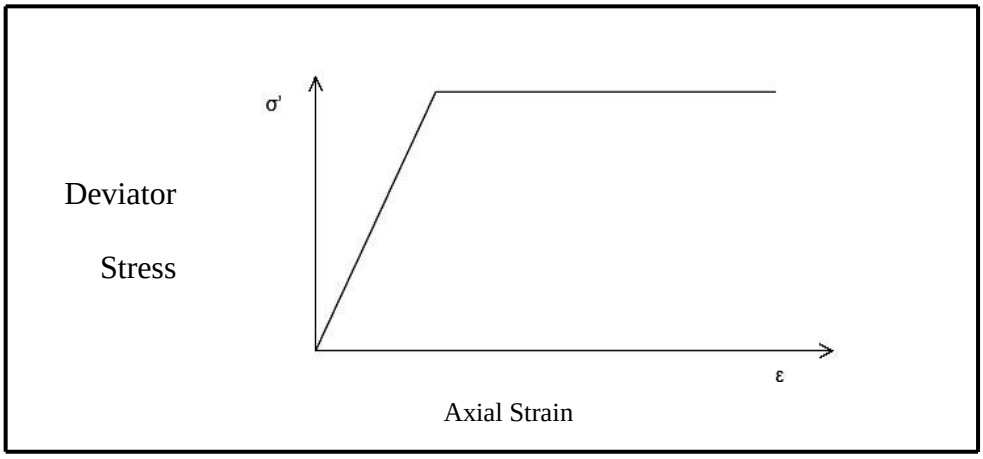

Fig 4.4 :- Linearly elastic perfectly plastic stress strain relationship

4.2.3 PLAXIS 3D FORMULATION

4.2.3.1 General defination of stress

Stress is a tensor which can be represented by a matrix in Cartesian coordinates:

$$\underline{\underline{\boldsymbol{\sigma}}} = \begin{bmatrix} \boldsymbol{\sigma_{xx}} & \boldsymbol{\sigma_{xy}} & \boldsymbol{\sigma_{xz}} \\ \boldsymbol{\sigma_{yx}} & \boldsymbol{\sigma_{yy}} & \boldsymbol{\sigma_{yz}} \\ \boldsymbol{\sigma_{zx}} & \boldsymbol{\sigma_{zy}} & \boldsymbol{\sigma_{zz}} \end{bmatrix} \qquad \text{.....(4.11)}$$

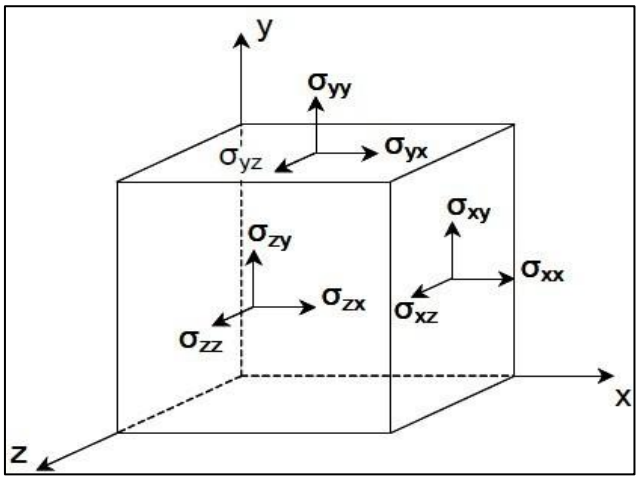

Fig 4.5 :- General three-dimensional coordinate system and sign convention for stresses

In the standard deformation theory, the stress tensor is symmetric such that $\sigma_{xy} = \sigma_{yx}$, $\sigma_{yz} = \sigma_{zy}$ and $\sigma_{zx} = \sigma_{xz}$. In this situation, stresses are often written in vector notation, which involve only six different components.

$$\boldsymbol{\sigma} = \left(\boldsymbol{\sigma_{xx}\sigma_{yy}\sigma_{zz}\sigma_{xy}\sigma_{yz}\sigma_{zx}}\right)^{\boldsymbol{T}} \qquad \text{……..(4.12)}$$

In plane strain condition, however,

$$\boldsymbol{\sigma_{xz} = \sigma_{yz} = 0} \qquad \text{……..(4.13)}$$

According to Terzaghi's principle, stresses in the soil are divided into effective stresses σ' and pore pressures σ_w.

$$\boldsymbol{\sigma = \underline{\sigma}' + \underline{\sigma}_w} \qquad \text{……..(4.14)}$$

Water is considered not to sustain any shear stresses. As a result, effective shear stresses are equal to total shear stresses. Positive normal stress components are considered to represent tension, whereas negative stress components indicate pressure or compression.

Material models for soil and rock are generally expressed as a relationship between infinitesimal increments of effective stress and infinitesimal increments of strain. In such a relationship, infinite increments of effective stress are represented by stress rates (with a dot above the stress symbol):

$$\dot{\boldsymbol{\sigma}}' = \left(\dot{\boldsymbol{\sigma}}'_{\boldsymbol{xx}}\dot{\boldsymbol{\sigma}}'_{\boldsymbol{yy}}\dot{\boldsymbol{\sigma}}'_{\boldsymbol{zz}}\dot{\boldsymbol{\sigma}}_{\boldsymbol{xy}}\dot{\boldsymbol{\sigma}}_{\boldsymbol{yz}}\dot{\boldsymbol{\sigma}}_{\boldsymbol{zx}}\right)^{\boldsymbol{T}} \qquad \text{……..(4.15)}$$

It is often useful to use principal stresses rather than Cartesian stress components when formulating material models. Principal stresses are the stresses in such a coordinate system direction that all shear stress components are zero. Principal stresses are, in fact, the eigenvalues of the stress tensor. Principal effective stresses can be determined in the following way :

$$\boldsymbol{det\left(\underline{\sigma}' - \sigma'\underline{I}\right) = 0} \qquad \text{……..(4.16)}$$

Where $\underline{I}$ is the identity matrix. The equation gives three solutions for σ' , i.e the principal effective str (σ'_1, σ'_2, σ'_3). In PLAXIS the principal effective stresses are arranged in algebraic order

$$\boldsymbol{\sigma'_1 \leq \sigma'_2 \leq \sigma'_3} \qquad \text{……..(4.17)}$$

Hence, σ'_1 is the largest compressive principal stress and σ'_3 is the smallest compressive principal stress. Models are often presented with reference to the principal stress space as

indicated in previous figure.

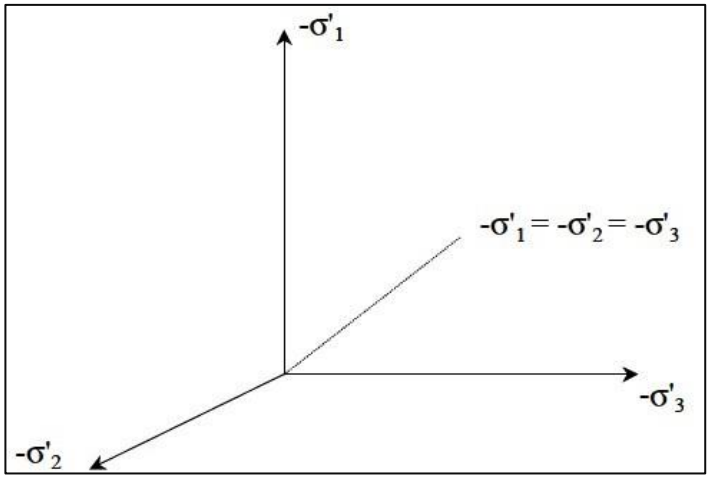

Fig 4.6 :- Principal stress space

In addition to principal stresses it is also useful to define invariants of stress, which are stress measures thatare independent of the orientation of the coordinate system. Two useful stress invariants are:

$$\boldsymbol{p'} = -\frac{\mathbf{1}}{\mathbf{3}}\left(\boldsymbol{\sigma'_{xx}} + \boldsymbol{\sigma'_{yy}} + \boldsymbol{\sigma'_{zz}}\right) = -\frac{\mathbf{1}}{\mathbf{3}}\left(\boldsymbol{\sigma'_1} + \boldsymbol{\sigma'_2} + \boldsymbol{\sigma'_3}\right) \quad \ldots\ldots(4.18)$$

$$\boldsymbol{q} = \sqrt{\frac{\mathbf{1}}{\mathbf{2}}\left(\left(\boldsymbol{\sigma'_{xx}} - \boldsymbol{\sigma'_{yy}}\right)^{\mathbf{2}} + \left(\boldsymbol{\sigma'_{yy}} - \boldsymbol{\sigma'_{zz}}\right)^{\mathbf{2}} + \left(\boldsymbol{\sigma'_{zz}} - \boldsymbol{\sigma'_{xx}}\right)^{\mathbf{2}} + \mathbf{6}\left(\boldsymbol{\sigma_{xy}}^{\mathbf{2}} + \boldsymbol{\sigma_{yz}}^{\mathbf{2}} + \boldsymbol{\sigma_{zx}}^{\mathbf{2}}\right)\right)} \ldots(4.19)$$

Where p' is isotropic effective stress or mean effective stress and *q* is the equivalent shear stress. p' is positive for compression in contrast to other stress measures.

Principal effective stresses can be written in terms of the invariants:

$$-\boldsymbol{\sigma'_1} = \boldsymbol{p'} + \frac{\mathbf{2}}{\mathbf{3}}\boldsymbol{q}\ \sin\left(\boldsymbol{\theta} - \frac{\mathbf{2}}{\mathbf{3}}\boldsymbol{\pi}\right) \quad \ldots\ldots\ldots\ldots(4.20)$$

$$-\boldsymbol{\sigma'_2} = \boldsymbol{p'} + \frac{\mathbf{2}}{\mathbf{3}}\boldsymbol{q}\ \sin(\boldsymbol{\theta}) \quad \ldots\ldots\ldots\ldots(4.21)$$

$$-\boldsymbol{\sigma'_3} = \boldsymbol{p'} + \frac{\mathbf{2}}{\mathbf{3}}\boldsymbol{q}\ \sin\left(\boldsymbol{\theta} + \frac{\mathbf{2}}{\mathbf{3}}\boldsymbol{\pi}\right) \quad \ldots\ldots\ldots\ldots(4.22)$$

In which θ is referred to as Lode's angel (a third invariant), which is defined as

$$\boldsymbol{\theta} = \frac{\mathbf{1}}{\mathbf{3}}\boldsymbol{arc}\,\mathbf{sin}\left(\frac{\mathbf{27}}{\mathbf{3}}\frac{\boldsymbol{J_3}}{\boldsymbol{q^3}}\right) \qquad \text{…….(4.23)}$$

With,

$$\boldsymbol{J_3} = (\boldsymbol{\sigma'_{xx}} - \boldsymbol{p'})(\boldsymbol{\sigma'_{yy}} - \boldsymbol{p'})(\boldsymbol{\sigma'_{zz}} - \boldsymbol{p'}) + (\boldsymbol{\sigma'_{xx}} - \boldsymbol{p'})\boldsymbol{\sigma_{yz}}^2 + (\boldsymbol{\sigma'_{yy}} - \boldsymbol{p'})\boldsymbol{\sigma_{zx}}^2 + (\boldsymbol{\sigma'_{zz-}}\boldsymbol{p'})\boldsymbol{\sigma_{xy}}^2 + \mathbf{2}\boldsymbol{\sigma_{xy}}\boldsymbol{\sigma_{yz}}\boldsymbol{\sigma_{zx}} \qquad \text{……..(4.24)}$$

4.2.3.2 General defination of strain

Strain is a tensor which can be represented by a matrix with Cartesian coordinates as:

$$\underline{\underline{\boldsymbol{\varepsilon}}} = \begin{bmatrix} \boldsymbol{\varepsilon_{xx}} & \boldsymbol{\varepsilon_{xy}} & \boldsymbol{\epsilon_{xz}} \\ \boldsymbol{\varepsilon_{yx}} & \boldsymbol{\varepsilon_{yy}} & \boldsymbol{\varepsilon_{yz}} \\ \boldsymbol{\varepsilon_{zx}} & \boldsymbol{\varepsilon_{zy}} & \boldsymbol{\varepsilon_{zz}} \end{bmatrix} \qquad \text{……(4.25)}$$

According to the small deformation theory, only the sum of complementing Cartesian shear strain components ε_{ij} and ε_{ji} result in shear stress. This sum is denoted as the shear strain γ. Hence, instead of ε_{xy}, ε_{yx}, ε_{yz}, ε_{zy}, ε_{zx} and ε_{xz} the shear strain components γ_{xy}, γ_{yz} and γ_{zx} are used respectively. Under the above conditions, strains are often written in vector notation, which involve only six different components

$$\boldsymbol{\varepsilon_{xx}} = \frac{\boldsymbol{\partial u_x}}{\boldsymbol{\partial x}}\ ;\ \boldsymbol{\varepsilon_{yy}} = \frac{\boldsymbol{\partial u_y}}{\boldsymbol{\partial y}}\ \mathbf{;}\ \boldsymbol{\varepsilon_{zz}} = \frac{\boldsymbol{\partial u_z}}{\boldsymbol{\partial z}} \qquad \text{……(4.26)}$$

$$\boldsymbol{\gamma_{xy}} = \boldsymbol{\varepsilon_{xy}} + \boldsymbol{\varepsilon_{yx}} = \frac{\boldsymbol{\partial u_x}}{\boldsymbol{\partial y}} + \frac{\boldsymbol{\partial u_y}}{\boldsymbol{\partial x}} \qquad \text{……(4.27)}$$

$$\boldsymbol{\gamma_{yz}} = \boldsymbol{\varepsilon_{yz}} + \boldsymbol{\varepsilon_{zy}} = \frac{\boldsymbol{\partial u_y}}{\boldsymbol{\partial z}} + \frac{\boldsymbol{\partial u_z}}{\boldsymbol{\partial y}} \qquad \text{……(4.28)}$$

$$\boldsymbol{\gamma_{zx}} = \boldsymbol{\varepsilon_{zx}} + \boldsymbol{\varepsilon_{xz}} = \frac{\boldsymbol{\partial u_z}}{\boldsymbol{\partial x}} + \frac{\boldsymbol{\partial u_x}}{\boldsymbol{\partial z}} \qquad \text{……(4.29)}$$

$$\underline{\boldsymbol{\varepsilon}} = \left(\boldsymbol{\varepsilon_{xx}}\boldsymbol{\varepsilon_{yy}}\boldsymbol{\varepsilon_{zz}}\boldsymbol{\gamma_{xy}}\boldsymbol{\gamma_{yz}}\boldsymbol{\gamma_{zx}}\right)^{\boldsymbol{T}} \qquad \text{……(4.30)}$$

Similarly as for stresses, positive normal strain components refer to extension, whereas negative normal strain components indicate compression.

In the formulation of material models, where infinitesimal increments of strain are considered, these increments are represented by strain rates (with a dot above the strain symbol).

$$\underline{\dot{\boldsymbol{\varepsilon}}} = \left(\dot{\boldsymbol{\varepsilon}}_{\boldsymbol{xx}}\dot{\boldsymbol{\varepsilon}}_{\boldsymbol{yy}}\dot{\boldsymbol{\varepsilon}}_{\boldsymbol{zz}}\dot{\boldsymbol{\gamma}}_{\boldsymbol{xy}}\boldsymbol{\gamma}_{\boldsymbol{yz}}\dot{\boldsymbol{\gamma}}_{\boldsymbol{zx}}\right)^{\boldsymbol{T}} \qquad \text{……..(4.31)}$$

for plane strain conditions, as considered in PLAXIS version 8,

$$\boldsymbol{\varepsilon_{zz} = \gamma_{xz} = \gamma_{yz}} \quad \text{.....(4.32)}$$

whereas for axisymmetric conditions,

$$\boldsymbol{\varepsilon_{zz} = \frac{U_x}{r}} \text{ and } \boldsymbol{\gamma_{xz} = \gamma_{yz}} \quad \text{.....(4.33)}$$

In analogy to the invariants of stress, it is also useful to define invariants of strain. A strain invariant that is often used is the volumetric strain, ε_v, which is defined as the sum of all normal strain components:

$$\underline{\boldsymbol{\varepsilon}} = \left(\boldsymbol{\varepsilon_{xx}\varepsilon_{yy}\varepsilon_{zz}\gamma_{xy}\gamma_{yz}\gamma_{zx}}\right)^{\boldsymbol{T}} \quad \text{.....(4.34)}$$

For elastoplastic models, as used in PLAXIS program, strains are decomposed into elastic and plastic components:

$$\underline{\boldsymbol{\varepsilon}} = \underline{\boldsymbol{\varepsilon}}^{\boldsymbol{e}} + \underline{\boldsymbol{\varepsilon}}^{\boldsymbol{p}} \quad \text{.....(4.35)}$$

4.2.3.3 Basic equations of continuum deformation

The static equilibrium of a continuum can be formulated as:

$$\underline{\underline{\boldsymbol{L}}}^{\boldsymbol{T}}\underline{\boldsymbol{\sigma}} + \underline{\boldsymbol{p}} = \underline{\boldsymbol{O}} \quad \text{.....(4.36)}$$

This equation relates the spatial derivatives of the six stress components of the six stress components, assembled in vector σ, to the three components of the body forces, assembled in vector p . L^T is the transpose of a differential operator, defined as:

$$\boldsymbol{L^T} = \begin{bmatrix} \frac{\partial}{\partial x} & 0 & 0 & \frac{\partial}{\partial y} & 0 & \frac{\partial}{\partial z} \\ 0 & \frac{\partial}{\partial y} & 0 & \frac{\partial}{\partial x} & \frac{\partial}{\partial z} & 0 \\ 0 & 0 & \frac{\partial}{\partial z} & 0 & \frac{\partial}{\partial y} & \frac{\partial}{\partial x} \end{bmatrix} \quad \text{.....(4.37)}$$

In addition to the equilibrium equation, the kinematic equation can be formulated as:

$$\underline{\boldsymbol{\varepsilon}} = \underline{\underline{\boldsymbol{L}}}\,\underline{\boldsymbol{u}} \quad \text{.....(4.38)}$$

This equation expresses the six strain components, assembled in vector ε, as the spatial derivatives of the three displacement components, assembled in vector u using the previously defined differential operator L. The link between equations is formed by a constitutive relation i.e. relation between ratesof stress and strain:

$$\dot{\underline{\boldsymbol{\sigma}}} = \underline{\underline{\boldsymbol{M}}}\,\dot{\underline{\boldsymbol{\varepsilon}}} \quad \text{.....(4.39)}$$

The combination of equations lead to a second order partial differential equation in the displacements u

However, instead of a direct combination, the equilibrium equation is reformulated in a weak form according to Galerkin's variation principle (see among others Zienkiewicz, 1967):

$$\int \boldsymbol{\delta}\, \underline{\boldsymbol{u}}^{\boldsymbol{T}} \left(\underline{\underline{\boldsymbol{L}}}^{\boldsymbol{T}} \boldsymbol{\sigma} + \underline{\boldsymbol{p}} \right) \boldsymbol{dV} = \mathbf{0} \qquad \text{……..(4.40)}$$

In this formulation $\delta\underline{u}$ represents a kinematically admissible variation of displacements. Applying Green's theorem for partial integration to the first term in equation leads to:

$$\int \boldsymbol{\delta}\, \underline{\boldsymbol{\varepsilon}}^{\boldsymbol{T}} \underline{\boldsymbol{\sigma}}\, \boldsymbol{dV} = \int \boldsymbol{\delta}\, \underline{\boldsymbol{u}}^{\boldsymbol{T}} \underline{\boldsymbol{p}}\, \boldsymbol{dV} + \int \boldsymbol{\delta}\, \underline{\boldsymbol{u}}^{\boldsymbol{T}} \underline{\boldsymbol{t}}\, \boldsymbol{dS} \qquad \text{……..(4.41)}$$

This introduces a boundary integral in which the boundary traction appears. The three components of the boundary traction are assembled in the vector t. Equation (4.41) is referred to as the virtual work equation. The development of the stress state $\underline{\sigma}$ can be regarded as an incremental process:

$$\underline{\boldsymbol{\sigma}}^{\boldsymbol{i}} = \underline{\boldsymbol{\sigma}}^{\boldsymbol{i-1}} + \Delta\underline{\boldsymbol{\sigma}} \qquad \Delta\underline{\boldsymbol{\sigma}} = \int \underline{\dot{\boldsymbol{\sigma}}}\, \boldsymbol{dt} \qquad \text{……...(4.42)}$$

In this relation $\underline{\sigma}^{i}$ represents the actual state of stress which is unknown and σ^{i-1} represents the previous state of stress which is known. The stress increment $\Delta\underline{\sigma}$ increment is the stress rate integrated over a small time.

the unknown stresses σ^{i} can be eliminated using equation.

$$\int \boldsymbol{\delta}\, \underline{\boldsymbol{\varepsilon}}^{\boldsymbol{T}}\, \Delta\boldsymbol{\sigma}\, \boldsymbol{dV} = \int \boldsymbol{\delta}\, \underline{\boldsymbol{u}}^{\boldsymbol{T}} \boldsymbol{p}^{\boldsymbol{i}} \boldsymbol{dV} + \int \boldsymbol{\delta}\, \boldsymbol{u}^{\boldsymbol{T}} \boldsymbol{t}^{\boldsymbol{i}}\, \boldsymbol{dS} - \int \boldsymbol{\delta}\, \underline{\boldsymbol{\varepsilon}}^{\boldsymbol{T}} \boldsymbol{\sigma}^{\boldsymbol{i-1}} \boldsymbol{dV} \quad \text{...(4.43)}$$

4.2.3.4 Finite element discretization

According to finite element method a continuum is divided into a number of (volume) elements. Each element consists of a number of nodes. Each node has a number of degrees of freedom that correspond to discrete values of the unknowns in the boundary value problem to be solved. In the present case of deformation theory the degrees of freedom correspond to the displacement components. Within an element the displacement field $\underline{u}$ is obtained from the discrete nodal values in a vector $\underline{v}$ using interpolation functions assembled in matrix N :

$$\underline{\boldsymbol{u}} = \underline{\underline{\boldsymbol{N}}}\, \boldsymbol{v} \qquad \text{……...(4.44)}$$

The interpolation functions in matrix N are often denoted as shape functions. Substitution of this equation in the kinematic relation gives:

$$\underline{\boldsymbol{\varepsilon}} = \underline{\underline{\boldsymbol{L}}}\, \underline{\underline{\boldsymbol{N}}}\, \underline{\boldsymbol{v}} = \underline{\underline{\boldsymbol{B}}}\, \underline{\boldsymbol{v}} \qquad \text{……..(4.45)}$$

In this relation $\underline{B}$ is the strain interpolation matrix, which contains the spatial derivatives of the interpolation functions. Above Equations can be used in variational, incremental and rate form as well.

Equation (4.45) can now be reformulated in discretized form as:

$$\int \left(\underline{\underline{B}}\,\delta\underline{v}\right)^T \Delta\underline{\sigma}\, dV = \int \left(N\,\delta\underline{v}\right)^T \underline{p}^i dV + \int \left(\underline{\underline{N}}\,\delta\underline{v}\right)^T \underline{t}^i dS - \int \left(\underline{\underline{B}}\,\delta\underline{v}\right)^T \underline{\sigma}^{i-1}\, dV \quad \text{…….(4.46)}$$

The discrete displacements can be placed outside the integral :

$$\delta\,\underline{v}^T \int \underline{\underline{B}}^T \Delta\underline{\sigma}\, dV = \delta\,\underline{v}^T \int \underline{\underline{N}}^T \underline{p}^i\, dV + \delta\,\underline{v}^T \int \underline{\underline{N}}^T \underline{t}^t\, dS - \delta\,\underline{v}^T \int \underline{\underline{B}}^T \underline{\sigma}^{i-1} dV \quad \text{…...(4.47)}$$

Provided that equation holds for any kinematically admissible displacement variation $\delta\mathbf{v}^T$, the equation can be written as :

$$\int \underline{\underline{B}}^T \Delta\underline{\sigma}\, dV = \int \underline{\underline{N}}^T \underline{p}^i\, dV + \int \underline{\underline{N}}^T \underline{t}^t\, dS - \int \underline{\underline{B}}^T \underline{\sigma}^{i-1} dV \quad \text{…...(4.48)}$$

The above equation is the elaborated equilibrium condition in discretized form.

The first term on the right- hand side together with the second term represent the current external force vector and the last term represents the internal reaction vector from the previous step. A difference between the external force vector and the internal reaction vector should be balanced by a stress increment $\Delta\underline{\sigma}$.

The relation between stress increments and strain increments is usually non-linear. As a result, strain increments can generally not be calculated directly, and global iterative procedures are required to satisfy the equilibrium condition for all material points.

4.2.3.5 Implicit integration of differential plasticity models

The stress increments $\Delta\underline{\sigma}$ obtained by integration of the stress rates according to the equation.For differential plasticity models the stress increments can generally be written as:

$$\Delta\underline{\sigma} = \underline{\underline{D}}^e\left(\Delta\underline{\varepsilon} - \Delta\underline{\varepsilon}^p\right) \quad \text{……(4.49)}$$

In this equation D^e represnts the elastic material matrix for the current stress element. The stress increments $\Delta\underline{\varepsilon}$ are obtained from the displacement increments $\Delta\underline{v}$ using the strain interpolation matrix B, similar to Previous equation.

For elastic material behavior, the plastic strain increment $\Delta\underline{\varepsilon}^p$ is zero. For plastic material behavior, the plastic strain increment can be written, according to Vermeer (1979), as

$$\Delta\underline{\varepsilon}^p = \Delta\lambda\left[(1-\omega)\left(\frac{\partial g}{\partial\underline{\sigma}}\right)^{i-1} + \omega\left(\frac{\partial g}{\partial\underline{\sigma}}\right)^{i}\right] \quad \text{…….(4.50)}$$

In this equation $\Delta\lambda$ is the increment of the plastic multiplier and ω is a parameter indicating the type of time integration. For $\omega = 0$ the integration is called explicit and for $\omega = 1$ the

integration is called implicit. Vermeer (1979) has shown that the use of implicit integration (ω = 1) has some major advantages, as it overcomes the requirement to update the stress to the yield surface in the case of a transition from elastic to elastoplastic behavior. Moreover, it can be proven that implicit integration, under certain conditions, leads to a symmetric and positive differentialmatrix $\frac{\partial \underline{\varepsilon}}{\partial \underline{\sigma}}$ Which has a positive influence on iterative procedures.

Hence, for ω = 1 equation reduces to

$$\Delta \boldsymbol{\varepsilon^p} = \Delta \boldsymbol{\lambda} \left(\frac{\partial \boldsymbol{g}}{\partial \underline{\boldsymbol{\sigma}}}\right)^{\boldsymbol{i}} . \qquad \text{……..(4.51)}$$

Substitution of equation and successively into equation gives

$$\underline{\boldsymbol{\sigma}}^{\boldsymbol{i}} = \underline{\boldsymbol{\sigma}}^{\boldsymbol{tr}} - \Delta \boldsymbol{\lambda}\, \underline{\underline{\boldsymbol{D}}}^{\boldsymbol{e}} \left(\frac{\partial \boldsymbol{g}}{\partial \underline{\boldsymbol{\sigma}}}\right)^{\boldsymbol{i}} \text{ with } \underline{\boldsymbol{\sigma}}^{\boldsymbol{tr}} = \underline{\boldsymbol{\sigma}}^{\boldsymbol{i-1}} + \underline{\underline{\boldsymbol{D}}}^{\boldsymbol{e}} \Delta \underline{\boldsymbol{\varepsilon}} \quad \text{…….(4.52)}$$

In this relation σ^{tr} is an auxiliary stress vector, referred to as the elastic stresses or trial stresses, which is the new stress state when considering purely linear elastic materialbehavior. The increment of the plastic multiplier $\boldsymbol{\Delta\lambda}$**,** as used in equation (4.52), can be solved from the condition that the new stress state has to satisfy the yield condition:

$$\boldsymbol{f}\left(\underline{\boldsymbol{\sigma}}^{\boldsymbol{i}}\right) = \boldsymbol{0} \qquad \text{…….(4.53)}$$

For perfectly-plastic and linear hardening models the increment of the plastic multiplier can be written as:

$$\Delta \boldsymbol{\lambda} = \frac{\boldsymbol{f}(\underline{\boldsymbol{\sigma}}^{\boldsymbol{tr}})}{\boldsymbol{d+h}} \qquad \text{……(4.54)}$$

Where:

$$\boldsymbol{d} = \left(\frac{\partial \boldsymbol{f}}{\partial \underline{\boldsymbol{\sigma}}}\right)^{\underline{\boldsymbol{\sigma}}^{\boldsymbol{tr}}} \boldsymbol{D^e} \left(\frac{\partial \boldsymbol{g}}{\partial \underline{\boldsymbol{\sigma}}}\right)^{\boldsymbol{i}} \qquad \text{…….(4.55)}$$

The symbol h denotes the hardening parameter, which is zero for perfectly-plastic models and constant for linear hardening models. In the latter case the new stress state can be formulated as:

$$\underline{\boldsymbol{\sigma}}^{\boldsymbol{i}} = \underline{\boldsymbol{\sigma}}^{\boldsymbol{tr}} - \frac{\langle \boldsymbol{f}(\underline{\boldsymbol{\sigma}}^{\boldsymbol{tr}}) \rangle}{\boldsymbol{d+h}} \underline{\underline{\boldsymbol{D}}}^{\boldsymbol{e}} \left(\frac{\partial \boldsymbol{g}}{\partial \underline{\boldsymbol{\sigma}}}\right)^{\boldsymbol{i}} \qquad \text{……(4.56)}$$

$\langle\ \rangle$ - brackets are referred to as McCauley brackets, which have the following convention :

$$\langle \boldsymbol{x} \rangle = \boldsymbol{0} \text{ for: } x \leq 0 \quad \text{and:} \quad \langle x \rangle = x \ for: \ x > 0$$

4.2.3.6 Global iterative procedure

Substitutionoftherelationshipbetweenincrementsofstressandincrementsofstrain, $\Delta\underline{\sigma} = \underline{\underline{M}}\ \Delta\underline{\varepsilon}$, into the equilibrium equation leads to:

$$\underline{\underline{\boldsymbol{K}}}\ \Delta\underline{\boldsymbol{v}}^{\boldsymbol{i}} = \underline{\boldsymbol{f}}^{\boldsymbol{i}}_{\ \boldsymbol{ex}} - \underline{\boldsymbol{f}}^{\boldsymbol{i-1}}_{\ \boldsymbol{in}} \qquad \text{……..(4.57)}$$

In this equation $\underline{\underline{K}}^i$ is a stiffness matrix, $\Delta\underline{v}^i$ is the incremental displacement vector, f_{ex} is the external force and $\underline{f}_{in}$ is the internal reaction vector. The superscript *i* refers to the step number. However, because the relation between stress increments and strain increments is generally non-linear, the stiffness matrix cannot be formulated exactly beforehand. Hence, a global iterative procedure is required to satisfy both the equilibrium condition and the consecutive relation. The global iteration process can be written as:

$$\underline{\underline{\boldsymbol{K}}}^{\boldsymbol{j}}\ \boldsymbol{\delta}\underline{\boldsymbol{v}}^{\boldsymbol{j}} = \underline{\boldsymbol{f}}^{\boldsymbol{i}}_{\ \boldsymbol{ex}} - \underline{\boldsymbol{f}}^{\boldsymbol{j-1}}_{\ \boldsymbol{in}} \qquad \text{……(4.58)}$$

The superscript *j* refers to the iteration number .$\Delta\underline{v}$is a vector containing sub-incremental displacements,which contribute to the displacement increments of step *i*:

$$\Delta\underline{\boldsymbol{v}}^{\boldsymbol{i}} = \sum_{\boldsymbol{j=1}}^{\boldsymbol{n}} \boldsymbol{\delta}\underline{\boldsymbol{v}}^{\boldsymbol{j}} \qquad \text{……(4.59)}$$

Where n is the number of iterations within step i. The stiffness matrix K as used in equation, represents the material behavior in an approximated manner. The more accurate the stiffness matrix, the fewer iterations are required to obtain equilibrium within a certain tolerance.

In its Simplest form K represents a linear elastic response. In this case the stiffness matrix can be formulated as :

$$\underline{\underline{\boldsymbol{K}}} = \int \underline{\underline{\boldsymbol{B}}}^{\boldsymbol{T}}\ \underline{\underline{\boldsymbol{D}}}^{\boldsymbol{e}}\ \underline{\underline{\boldsymbol{B}}}\ \boldsymbol{dV} \qquad \textbf{(}\text{elastic Stiffness Matrix}\textbf{)} \qquad \text{…...(4.60)}$$

Where D^e is the elastic material matrix according to Hooke's Law and B is the strain interpolation matrix. The use of an elastic stiffness matrix gives a robust iterative procedure as long as the material stiffness does not increase, even when using non-associated plasticity models. Special techniques such as arc-length control (Riks, 1979), over-relaxation and extrapolation (Vermeer & Van Langen, 1989) can be used to improve the iteration process. Moreover, the automatic step size procedure, as introduced by Van Langen and Vermeer (1990), can be used to improve the practical applicability. For material models with linear behavior in the elastic domain, such as the standard Mohr-Coulomb model, the use of an elastic stiffness matrix is particularly favourable, as the stiffness matrix needs only be formed and decomposed before the first calculation step. The calculation procedure is summarized below.

Finite element calculation process based on the elastic stiffness matrix

Read input data		
Form stiffness matrix		$\underline{\underline{K}} = \int \underline{\underline{B}}^T \ \underline{\underline{D}}^e \ \underline{\underline{B}} \, dV$
New step		$i \rightarrow i+1$
Form new load vector		$\underline{f}_{ex}^{i} = \underline{f}_{ex}^{i-1} + \Delta \underline{f}_{ex}$
Form reaction vector		$\underline{f}_{in} = \int \underline{\underline{B}}^T \underline{\sigma}_c^{i-1} dV$
Calculate unbalance		$\Delta \underline{f} = \underline{f}_{ex}^{i} - \underline{f}_{in}$
Reset displacement increment		$\Delta \underline{v} = 0$
New iteration		$j \rightarrow j+1$
Solve displacements		$\delta \underline{v} = \underline{\underline{K}}^{-1} \Delta \underline{f}$
Update displacement increments		$\Delta \underline{v}^{j} = \Delta \underline{v}^{j-1} + \delta \underline{v}$
Calculate strain increments		$\Delta \underline{\varepsilon} = \underline{\underline{B}} \Delta \underline{v} \ ; \ \ \delta \underline{\varepsilon} = \underline{\underline{B}} \delta \underline{v}$
Calculate stresses:	Elastic	$\underline{\sigma}^{tr} = \underline{\sigma}_c^{i-1} + \underline{\underline{D}}^e \Delta \underline{\varepsilon}$
	Equilibrium	$\underline{\sigma}^{eq} = \underline{\sigma}_c^{i,j-1} + \underline{\underline{D}}^e \delta \underline{\varepsilon}$
	Constitutive	$\underline{\sigma}_c^{i,j} = \underline{\sigma}^{tr} - \dfrac{\langle f(\underline{\sigma}^{tr}) \rangle}{d} \underline{\underline{D}}^e \dfrac{\partial g}{\partial \underline{\sigma}}$
Form reaction vector		$\underline{f}_{in} = \int \underline{\underline{B}}^T \underline{\sigma}_c^{i,j} dV$
Calculate unbalance		$\Delta \underline{f} = \underline{f}_{ex}^{i} - \underline{f}_{in}$
Calculate error		$e = \dfrac{\lvert \Delta \underline{f} \rvert}{\lvert \underline{f}_{ex}^{i} \rvert}$
Accuracy check		if $e > e_{tolerated} \rightarrow$ new iteration
Update displacements		$\underline{v}^{i} = \underline{v}^{i-1} + \Delta \underline{v}$
Write output data (results)		
If not finished → new step		
Finish		

Fig 4.7 :- Reference of Symbols used in Plaxis and Finite element calculation process based on the elastic stiffness matrix

4.2.3.7 Formulation of the mohr-columb model

The Mohr-Coulomb yield condition is an extension of Coulomb's friction law to general states of stress. In fact, this condition ensures that Coulomb's friction law is obeyed in any plane within a material element.The full Mohr-Coulomb yield condition consists of six yield

functions when formulated in terms of principal stresses:

$$f_{1a} = \frac{1}{2}(\sigma'_2 - \sigma'_3) + \frac{1}{2}(\sigma'_2 + \sigma'_3)\sin\psi - c\cos\psi \leq 0 \quad \text{……..(4.61)}$$

$$f_{1b} = \frac{1}{2}(\sigma'_3 - \sigma'_2) + \frac{1}{2}(\sigma'_3 + \sigma'_2)\sin\psi - c\cos\psi \leq 0 \quad \text{……..(4.62)}$$

$$f_{2a} = \frac{1}{2}(\sigma'_3 - \sigma'_1) + \frac{1}{2}(\sigma'_3 + \sigma'_1)\sin\psi - c\cos\psi \leq 0 \quad \text{……..(4.63)}$$

$$f_{2b} = \frac{1}{2}(\sigma'_1 - \sigma'_3) + \frac{1}{2}(\sigma'_1 + \sigma'_3)\sin\psi - c\cos\psi \leq 0 \quad \text{……..(4.64)}$$

$$f_{3a} = \frac{1}{2}(\sigma'_1 - \sigma'_2) + \frac{1}{2}(\sigma'_1 + \sigma'_2)\sin\psi - c\cos\psi \leq 0 \quad \text{……..(4.65)}$$

$$f_{3b} = \frac{1}{2}(\sigma'_2 - \sigma'_1) + \frac{1}{2}(\sigma'_2 + \sigma'_1)\sin\psi - c\cos\psi \leq 0 \quad \text{……..(4.66)}$$

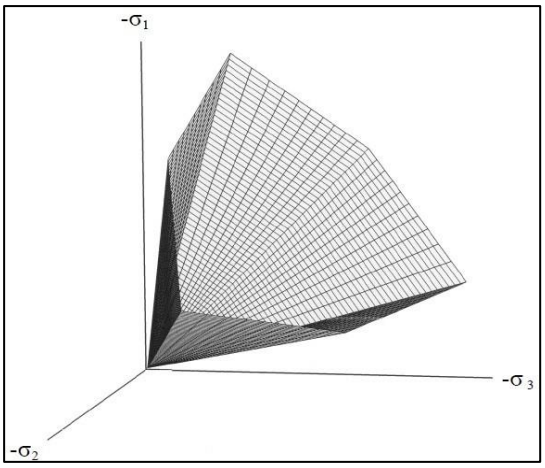

Fig 4.8 :- The Mohr-Coulomb Yield Surface in Principal Stress Space (c=0)

The two plastic model parameters appearing in the yield functions are the well-known friction angle Φ and the cohesion C. These yield functions together represent a hexagonal cone in principal stress space as shown in figure

In addition to the yield functions, six plastic potential functions are defined for the Mohr-Coulomb model:

$$g_{1a} = \frac{1}{2}(\sigma'_2 - \sigma'_3) + \frac{1}{2}(\sigma'_2 + \sigma'_3)\sin\psi \quad \text{……(4.67)}$$

$$g_{1b} = \frac{1}{2}(\sigma'_3 - \sigma'_2) + \frac{1}{2}(\sigma'_3 + \sigma'_2)\sin\psi \quad \text{……...(4.68)}$$

$$g_{2a} = \frac{1}{2}(\sigma'_3 - \sigma'_1) + \frac{1}{2}(\sigma'_3 + \sigma'_1)\sin\psi \quad \text{……...(4.69)}$$

$$g_{2a} = \frac{1}{2}(\sigma'_1 - \sigma'_3) + \frac{1}{2}(\sigma'_1 + \sigma'_3)\sin\psi \quad \text{.....(4.70)}$$

$$g_{3a} = \frac{1}{2}(\sigma'_1 - \sigma'_2) + \frac{1}{2}(\sigma'_1 + \sigma'_2)\sin\psi \quad \text{.....(4.71)}$$

$$g_{3b} = \frac{1}{2}(\sigma'_2 - \sigma'_1) + \frac{1}{2}(\sigma'_2 + \sigma'_1)\sin\psi \quad \text{.....(4.72)}$$

The plastic potential functions contain a third plasticity parameter, the dilatancy angle ψ. This parameter is required to model positive plastic volumetric strain increments (dilatancy) as actually observed for dense soils.

When implementing the Mohr-Coulomb model for general stress states, special treatment is required for the intersection of two yield surfaces. Some programs use a smooth transition from one yield surface to another, i.e. the rounding-off of the corners (Smith & Griffith, 1982). In PLAXIS, however, the exact form of the full Mohr-Coulomb model is implemented, using a sharp transition from one yield surface to another (Koiter, 1960; Van Langen & Vermeer,1990).

For C > 0, the standard Mohr-Coulomb criterion allows for tension. In fact, allowable tensile stresses increase with cohesion. In reality, soil can sustain none or or very small tensile stresses.

This behavior can be included in a PLAXIS analysis by specifying a tension cut-off. In this case, the Mohr circles with positive principal stresses are not allowed. The tension cut-off introduces three additional yield functions,defined as:

$$f_4 = \sigma'_1 - \sigma'_t \leq 0 \quad \text{.....(4.73)}$$

$$f_5 = \sigma'_2 - \sigma_t \leq 0 \quad \text{.....(4.74)}$$

$$f_6 = \sigma_3 - \sigma_t \leq 0 \quad \text{.....(4.75)}$$

When this tension cut-off procedure is used, the allowable tensile stress, σt, is, by default, taken equal to zero. For these three yield functions an associated flow rule is adopted. For stress states within the yield surface, the behavior is elastic and obeys Hooke's Law for isotropic linear elasticity. Hence, besides the plasticity parameters C, Φ and ψ, input is required on the elastic Young's modulus *E* and Poisson's ratio *v*.

4.2.4 Use of Plaxis in this Study

In the present investigation attempt has been made to study the bearing capacity of shallow footings (e.g. square, rectangular and strip footings) resting on layered cohesive soils using numerical modeling and analysis in finite element software package PLAXIS 3D. The following figures show input procedures, mesh generation and output curves of a PLAXIS model involved in the present study.

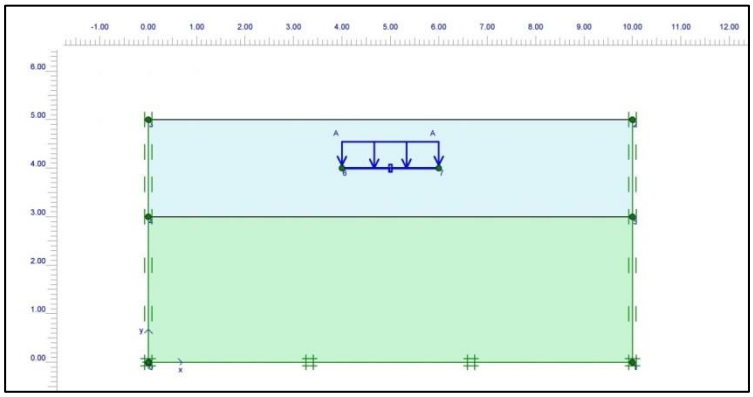

Fig 4.9 :- Input of Modelling in Plaxis

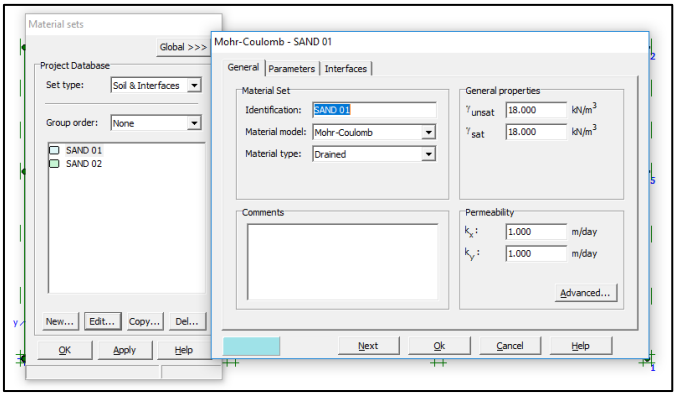

Fig 4.10 :- Defination of material properties in Plaxis

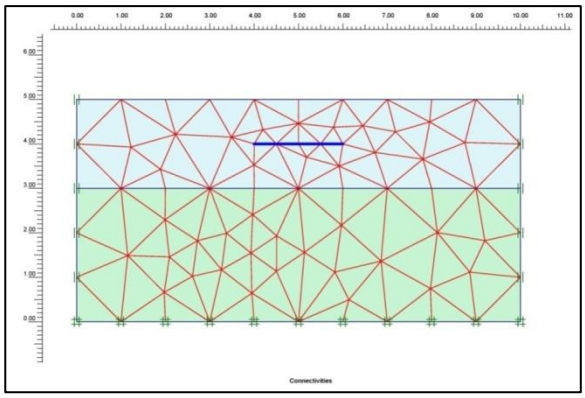

Fig 4.11 :- Distribution of nodes & finite element mesh in Plaxis

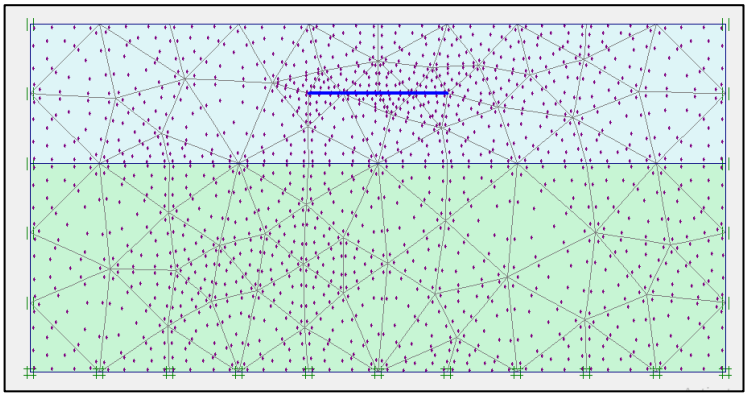

Fig 4.12 :- Distribution of gausian Stress Points in Plaxis

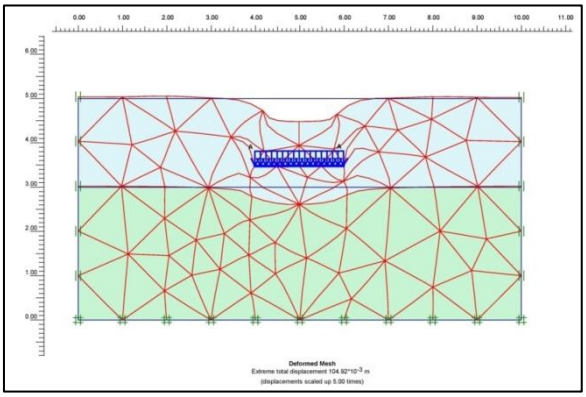

Fig 4.13 :- Output deformed mesh & total displacement in plaxis

Performing staged construction by increasing load with each step increment until failure and extracting settlement contour at the founding level as presented above a pressure-settlement

curve can be attained to ultimately evaluate the bearing capacity for that set of soil parameters and foundation system. Such pressure-settlement curve and its tabular presentation are given below. For this particular case the ultimate bearing capacity value using the double tangent method is found as 265 KN/m^2.

Table 4.1:- Pressure vs Disp Co-Ordinate

Pressure (kN/m^2)	Disp (mm)
0.00	0.00
51.63	8.57
102.16	20.60
149.52	32.63
257.45	62.61
300.84	75.81
355.40	103.35
355.29	103.59

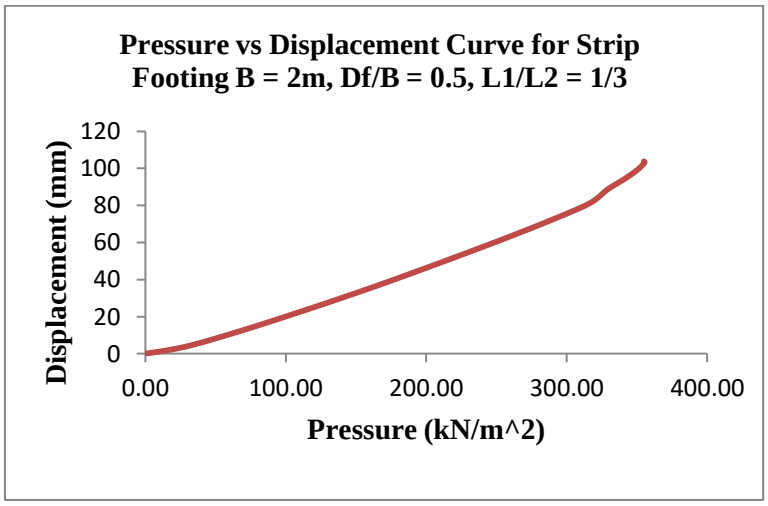

Fig 4.14 :- Pr vs Settlement Curve

CHAPTER 5: PRESENTATION OF NUMERICAL RESULTS

5.0 GENERAL

To carry out a parametric study to understand the influence of different parameters like footing width, thickness of different layers etc. on ultimate bearing capacity of shallow footings, total 36 finite element modeling has been analyzed in PLAXIS 2D. The corresponding pressure-settlement characteristics of each individual model have been studied to evaluate the ultimate bearing capacity.

5.1 MODEL -1 (Strip Footing, B = 2m, $D_f/B = 0.5$, $L_1/L_2 = 1/3$)

The following figures obtained as PLAXIS output represent settlement values (at center point just beneath the footing) for each individual stage/step:

- **Input :**

In the input stage, first of all geometry model is drawn and boundary condition is assigned. Plate is used as footing element. Layered subsoil properties are assigned in material properties section.

And finally Distributed load is assigned. Intial condition is defined here & water presure is applied

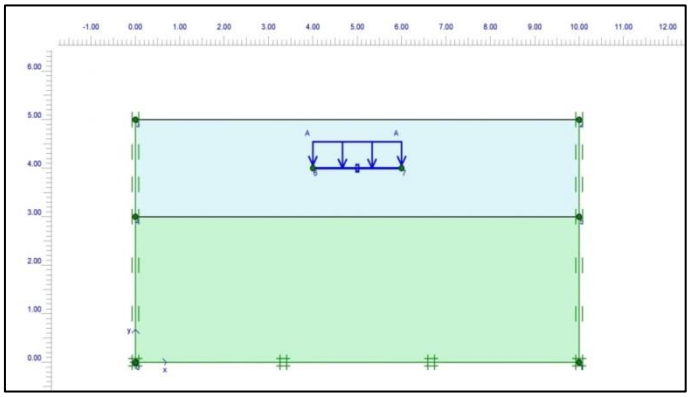

Fig 5.1 :- Input of Model-1

- **Mesh Generation :**

After creating the geometry model and putting initial conditions, a finite element mesh is generated. Mesh can be of very fine to coarse, depending upon the requirement. Besides local refinement is done near the foundation to avoid stress concentration beneath foundation.

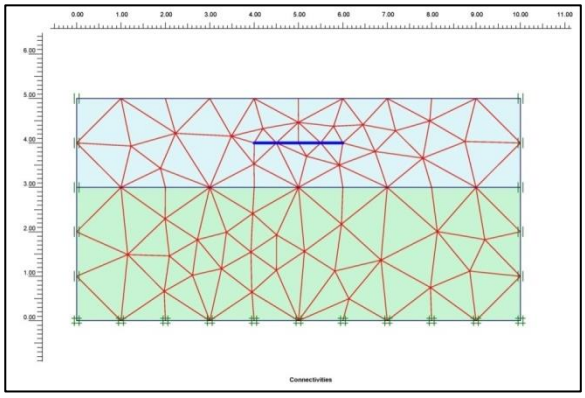

Fig 5.2 :- Finite Element mesh Configuration of Model-1

- **Output :**

After all the calculation phases are over, in the output window total displacement, vertical displacement, horizontal displacement, total stress, effective stress and other parameters can be calculated and final geometry of the model is presented after the application of several construction phases such as Loading and several other conditions.

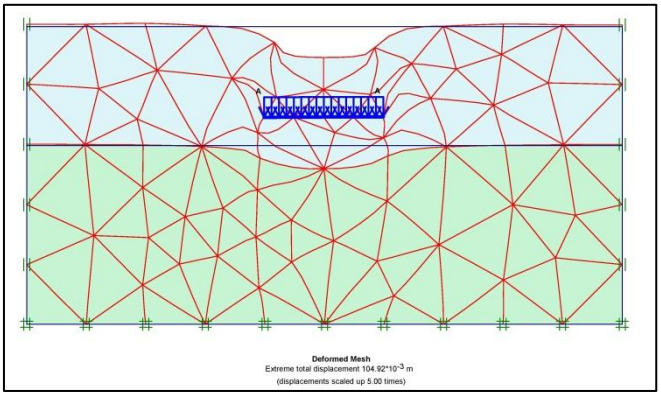

Fig 5.3 :- Final output deformed mesh of Model-1

- **Pressure vs Settlement Co-ordinate & Plotting in graph** :

After all the Calculation phases are over, Pressure vs Settlement Co-ordinates is obtained in terms of multiplier (ΣMstage) vs Displacement at a predetermined node at the center of the footing just below the footing. Multiplier is multiplied with corresponding input prescribed load to get the actual pressure and corresponding vertical displacement for various stages & steps of load increment at the above mentioned node is obtained. Finally the Ordinates are plotted in graph and double tangent method is applied to determine bearing capacity.

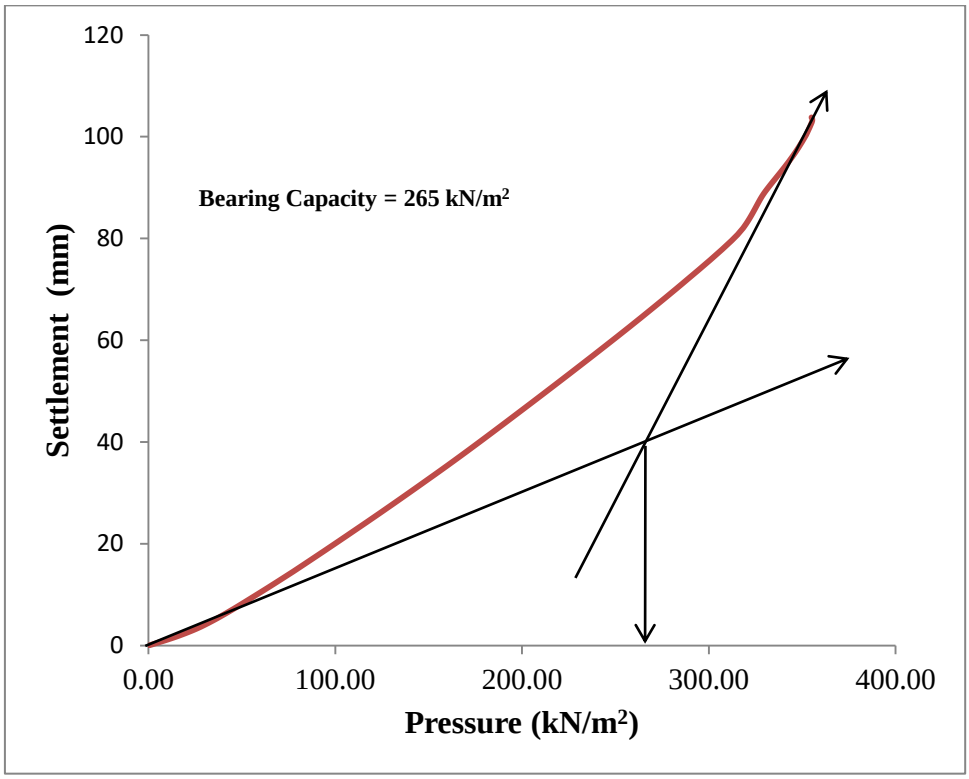

Fig 5.4 :- Pressure vs Displacement Curve for Model-1 (Strip Footing B = 2m, $D_f/B = 0.5$, $L_1/L_2 = 1/3$)

5.2 MODEL 2 (Strip Footing, B = 2m, $D_f/B = 0.5$, $L_1/L_2 = 1/1$)

Final Output deformed mesh & load-displacement curve of the corresponding model is presented.

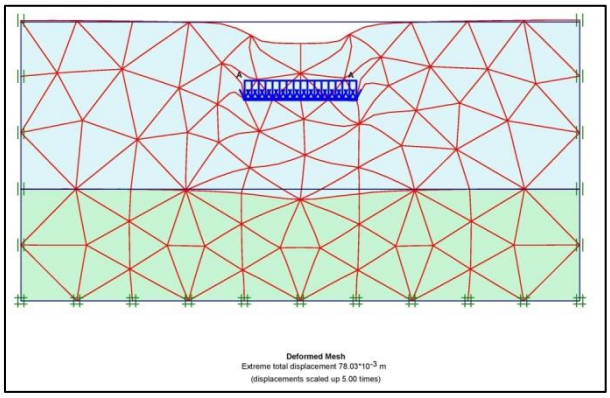

Fig 5.5 :- Final Output deformed mesh of Model-2

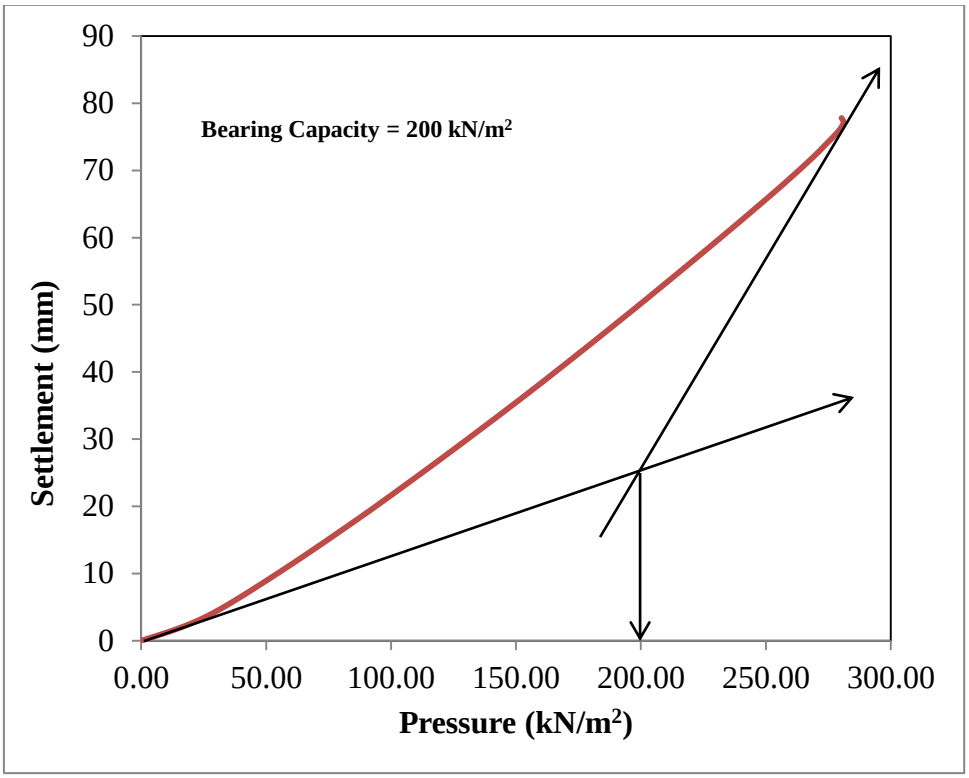

Fig 5.6 :- Pressure vs Displacement Curve for Model -2 (Strip Footing B = 2m, $D_f/B = 0.5$, $L_1/L_2 = 1/1$)

5.3 MODEL 3 (Strip Footing, B = 2m, $D_f/B = 0.5$, $L_1/L_2 = 3/1$)

Final Output deformed mesh & load-displacement curve of the corresponding model is presented.

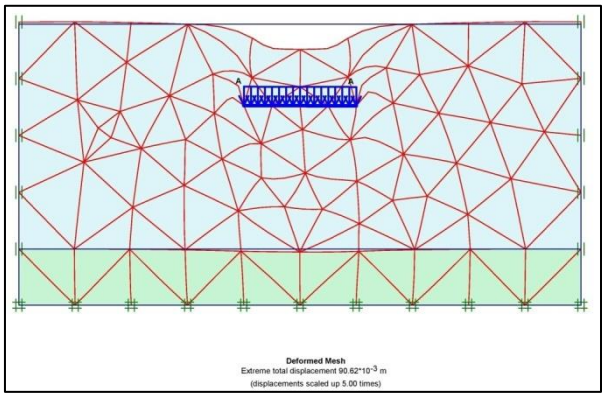

Fig 5.7 :- Final output deformed mesh of Model-3

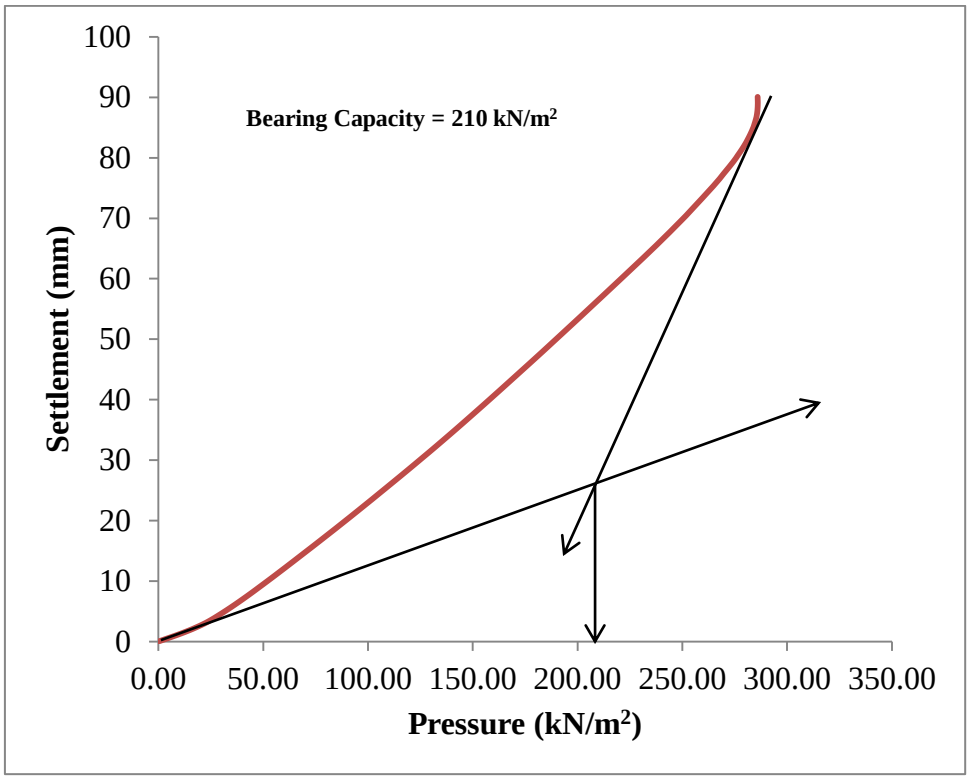

Fig 5.8 :- Pressure vs Displacement Curve for Model-3 (Strip Footing B = 2m, $D_f/B = 0.5$, $L_1/L_2 = 3/1$)

5.4 MODEL 4 (Strip Footing, B = 2m, $D_f/B = 1$, $L_1/L_2 = 1/3$)

Final Output deformed mesh & load-displacement curve of the corresponding model is presented.

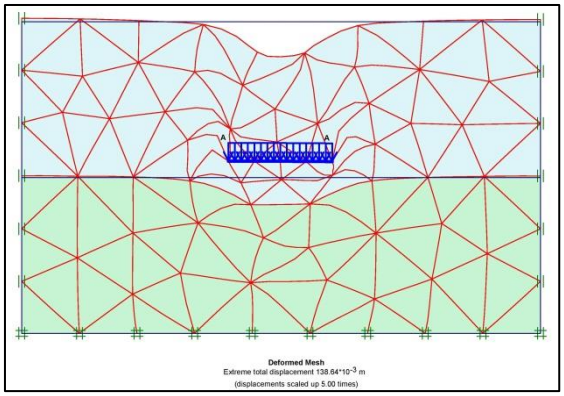

Fig 5.9 :- Final output deformed mesh of Model-4

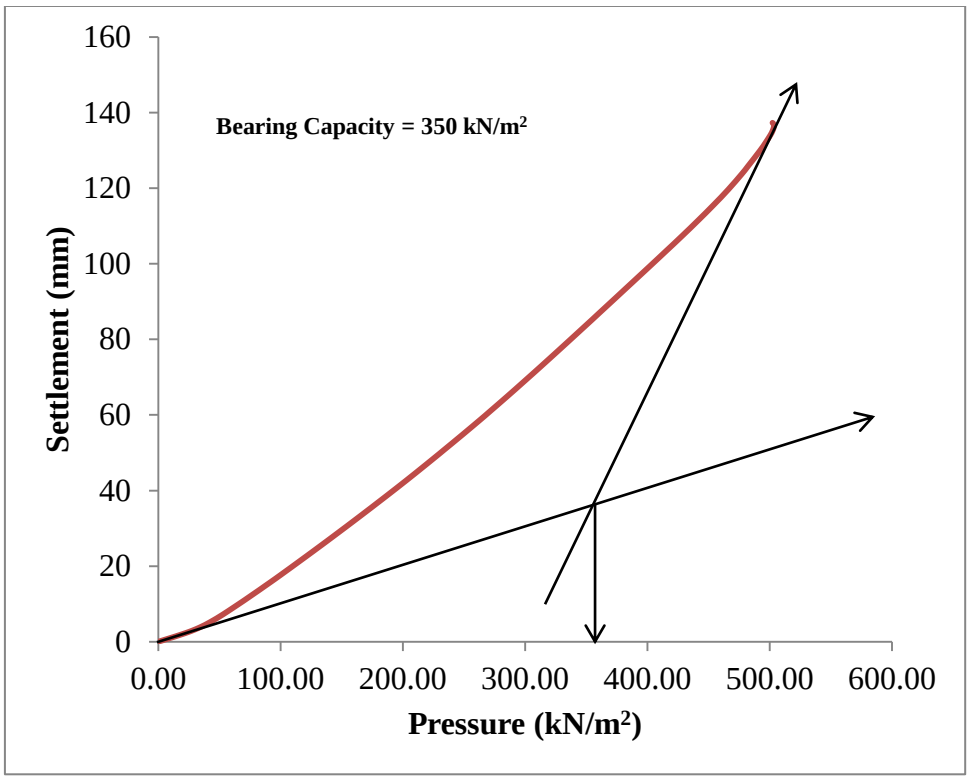

Fig 5.10 :- Pressure vs Displacement Curve for Model-4 (Strip Footing B = 2m, $D_f/B = 1$, $L_1/L_2 = 1/3$)

5.5 MODEL 5 (Strip Footing, B = 2m, $D_f/B = 1$, $L_1/L_2 = 1/1$)

Final Output deformed mesh & load-displacement curve of the corresponding model is presented.

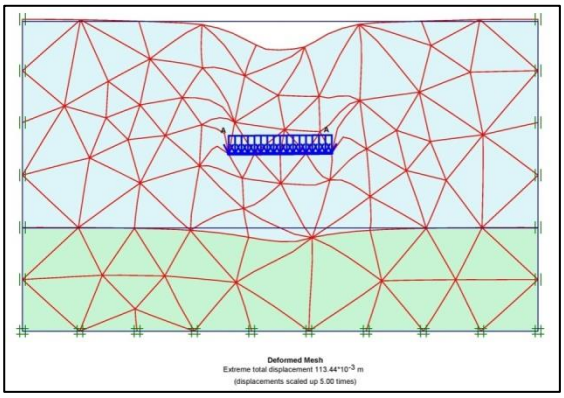

Fig 5.11 :- Final output deformed mesh of Model-5

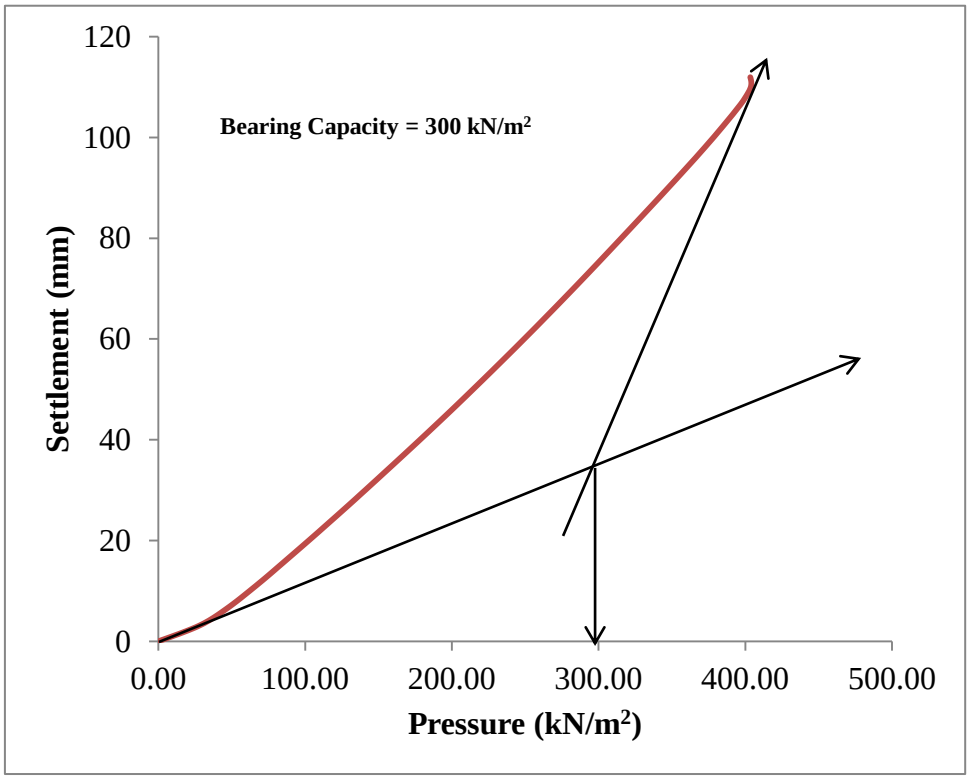

Fig 5.12 :- Pressure vs Displacement Curve for Model-5 (Strip Footing B = 2m, $D_f/B = 1$, $L_1/L_2 = 1/1$)

5.6 MODEL 6 (Strip Footing, B = 2m, $D_f/B = 1$, $L_1/L_2 = 3/1$)

Final Output deformed mesh & load-displacement curve of the corresponding model is presented.

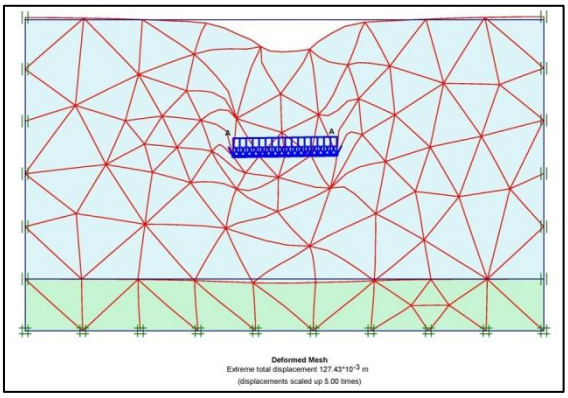

Fig 5.13 :- Final output deformed mesh of Model-6

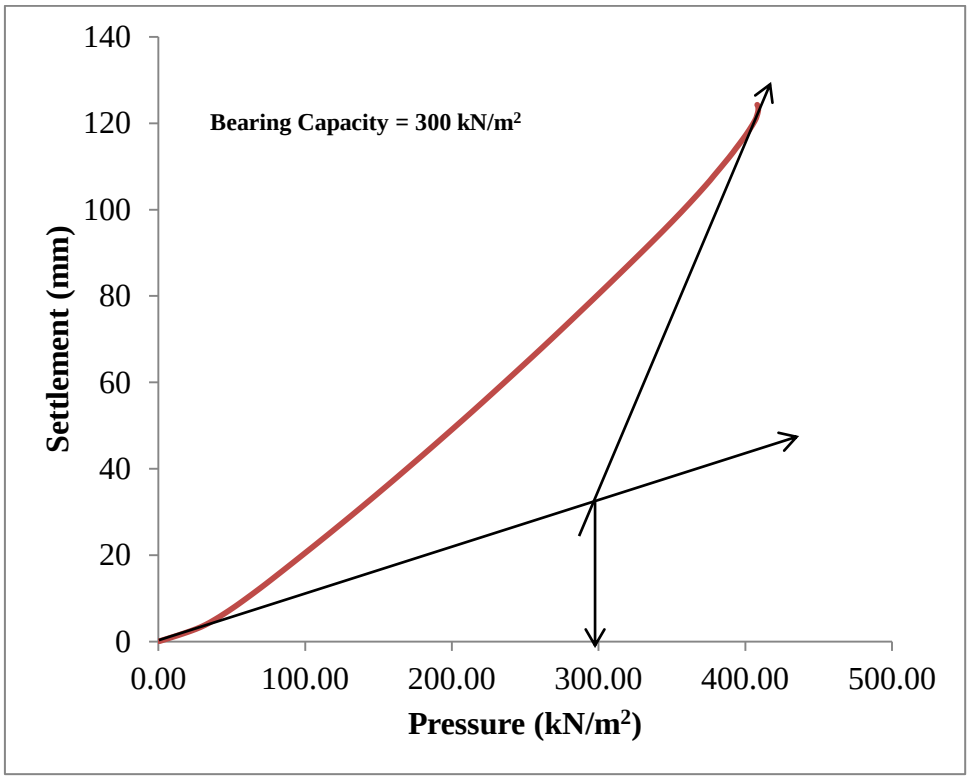

Fig 5.14 :- Pressure vs Displacement Curve for Model-6 (Strip Footing B = 2m, $D_f/B = 1$, $L_1/L_2 = 3/1$)

5.7 MODEL 7 (Strip Footing, B = 2m, D_f/B = 1.5, L_1/L_2 = 1/3)

Final Output deformed mesh & load-displacement curve of the corresponding model is presented.

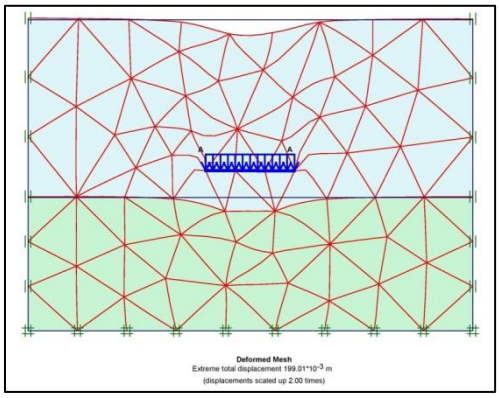

Fig 5.15:- Final output deformed mesh of Model-7

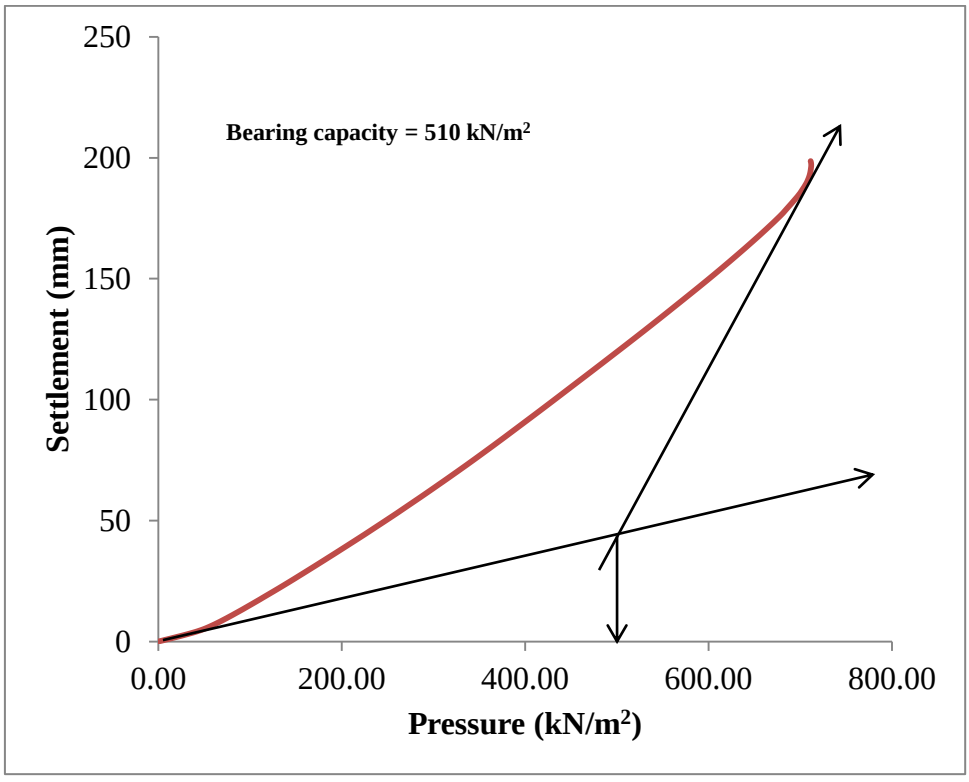

Fig 5.16:- Pressure vs Displacement Curve for Model-7(Strip Footing B = 2m, D_f/B = 1.5, L_1/L_2 = 1/3)

5.8 MODEL 8 (Strip Footing, B = 2m, D_f/B = 1.5, L_1/L_2 = 1/1)

Final Output deformed mesh & load-displacement curve of the corresponding model is presented.

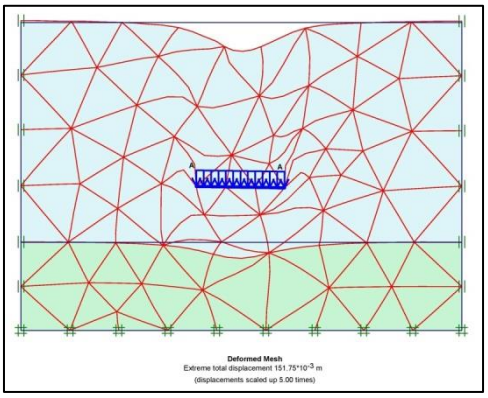

Fig 5.17:- Final output deformed mesh of Model-8

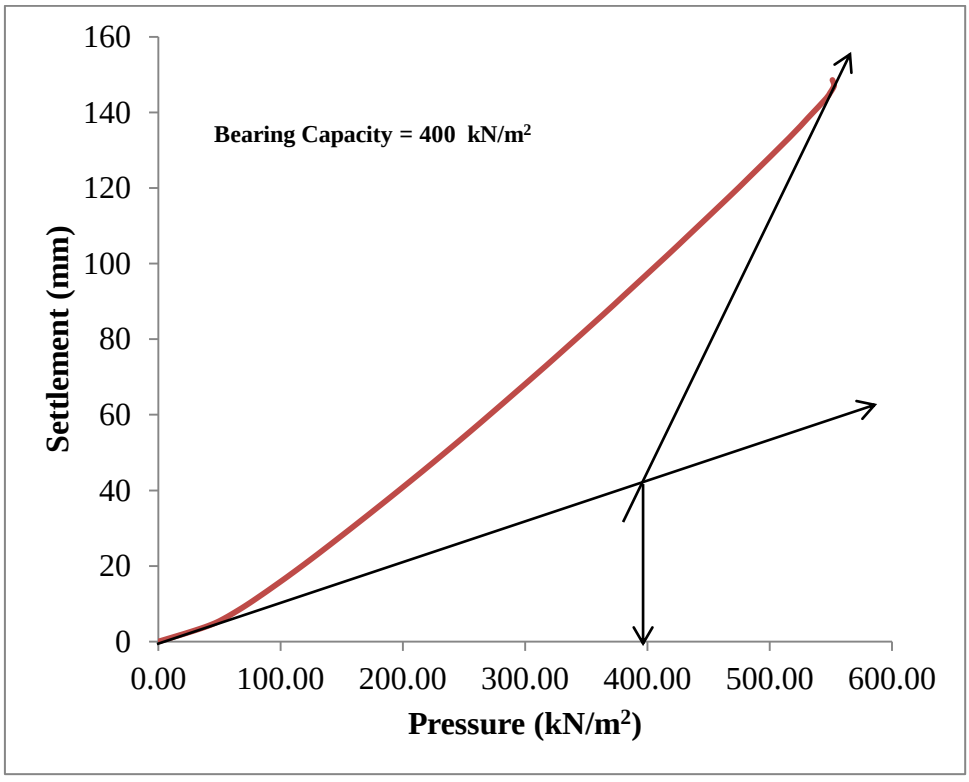

Fig 5.18:- Pressure vs Displacement Curve for Model-8 (Strip Footing B = 2m, D_f/B = 1.5, L_1/L_2 = 1/1)

5.9 MODEL 9 (Strip Footing, B = 2m, D_f/B = 1.5, L_1/L_2 = 3/1)

Final Output deformed mesh & load-displacement curve of the corresponding model is presented.

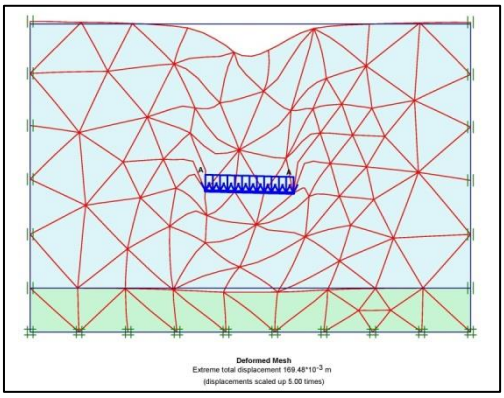

Fig 5.19:- Final output deformed mesh of Model-9

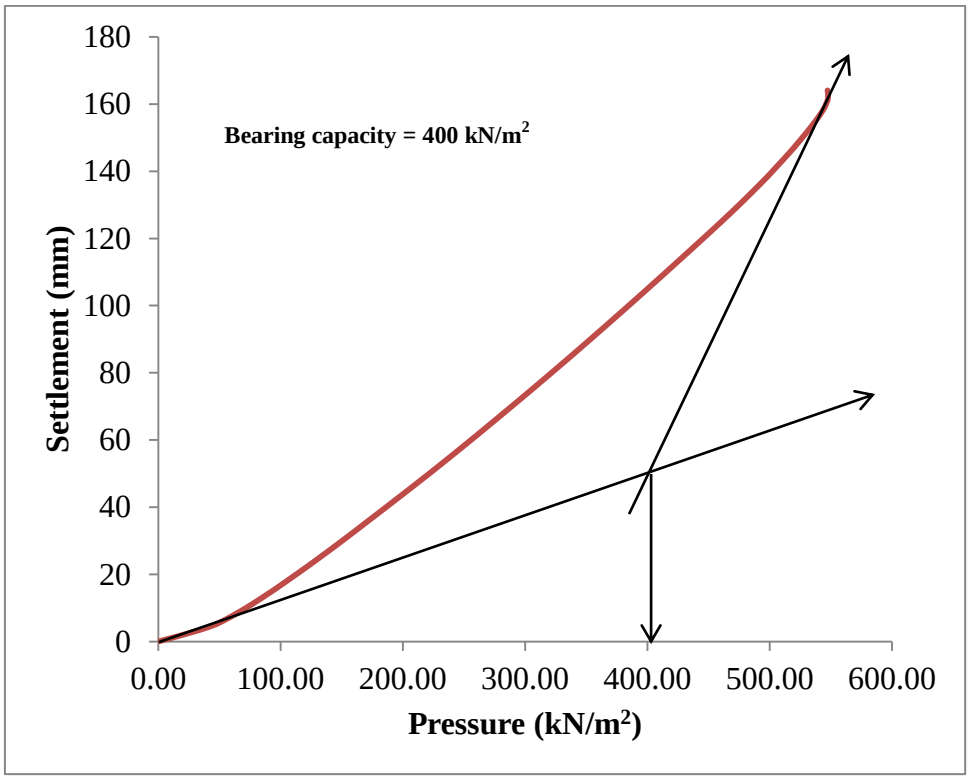

Fig 5.20:- Pressure vs Displacement Curve for Model-9 (Strip Footing B = 2m, D_f/B = 1.5, L_1/L_2 = 3/1)

5.10 MODEL 10 (Strip Footing, B = 3m, $D_f/B = 0.5$, $L_1/L_2 = 1/3$)

Final Output deformed mesh & load-displacement curve of the corresponding model is presented.

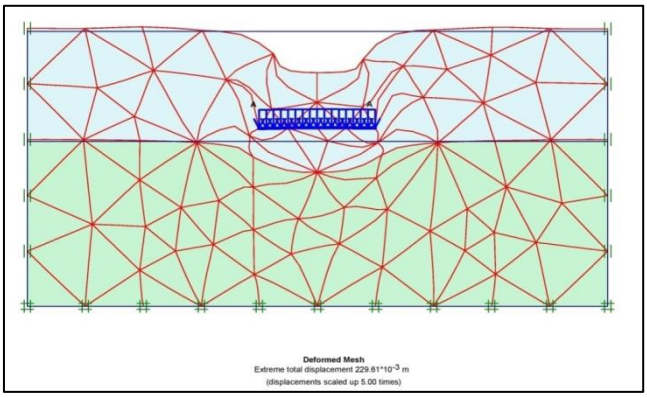

Fig 5.21:- Final output deformed mesh of Model-10

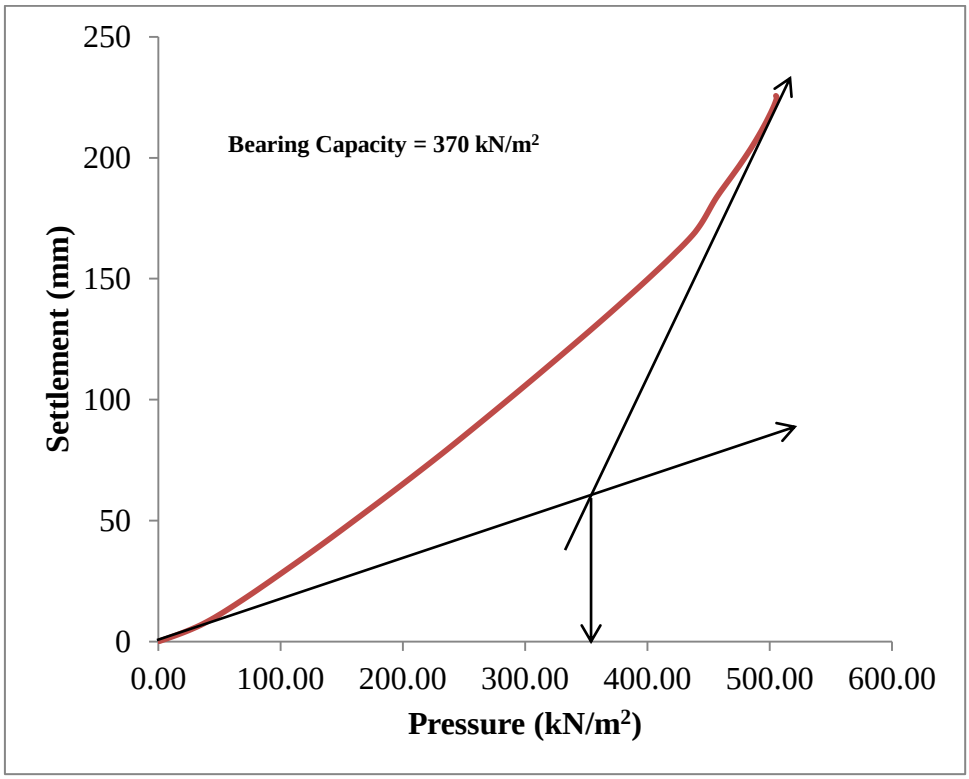

Fig 5.22:- Pressure vs Displacement Curve for Model-10 (Strip Footing B = 3m, $D_f/B = 0.5$, $L_1/L_2 = 1/3$)

5.11 MODEL 11 (Strip Footing, B = 3m, $D_f/B = 0.5$, $L_1/L_2 = 1/1$)

Final Output deformed mesh & load-displacement curve of the corresponding model is presented.

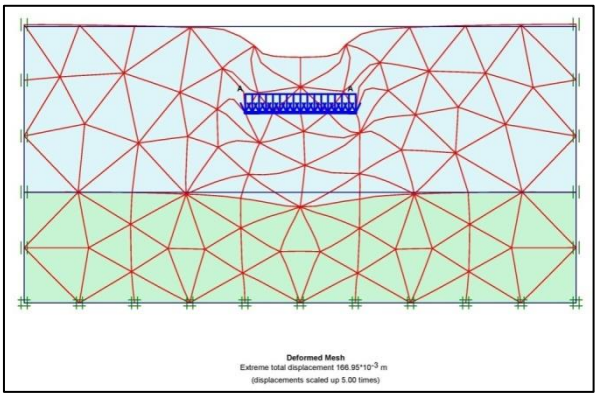

Fig 5.23:- Final output deformed mesh of Model-11

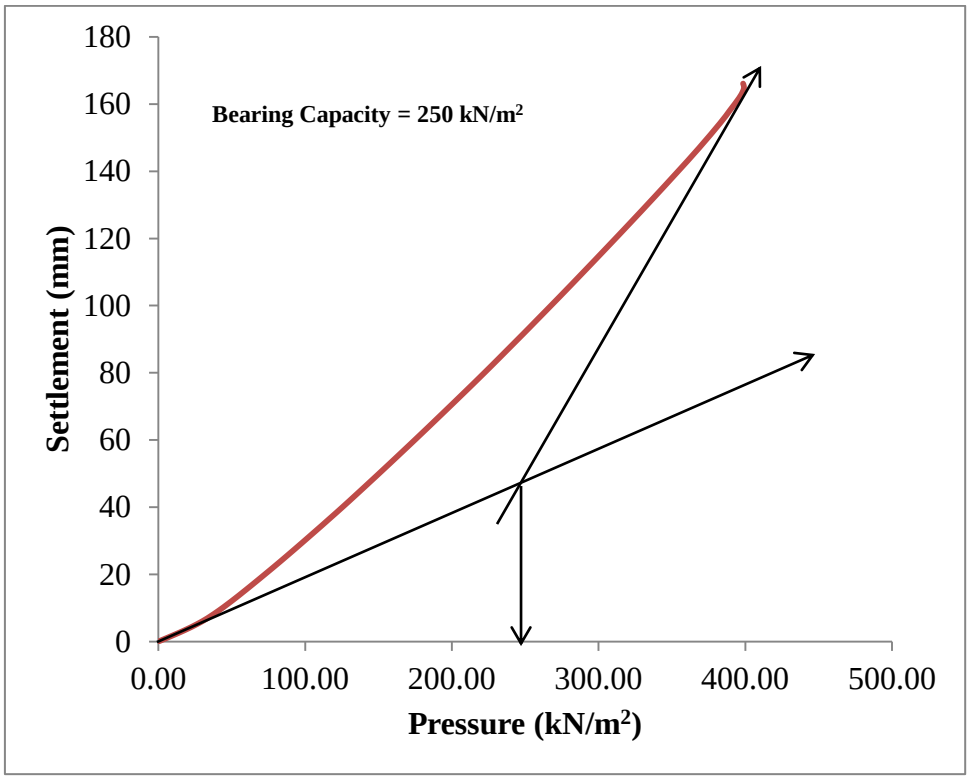

Fig 5.24:- Pressure vs Displacement Curve for Model-11 (Strip Footing B = 3m, $D_f/B = 0.5$, $L_1/L_2 = 1/1$)

5.12 MODEL 12 (Strip Footing, B = 3m, $D_f/B = 0.5$, $L_1/L_2 = 3/1$)

Final Output deformed mesh & load-displacement curve of the corresponding model is presented.

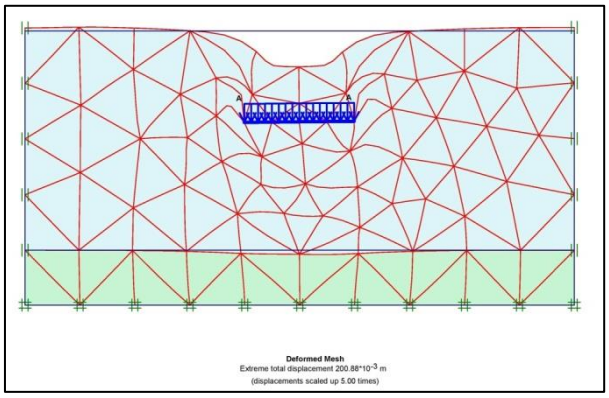

Fig 5.25:- Final output deformed mesh of Model-12

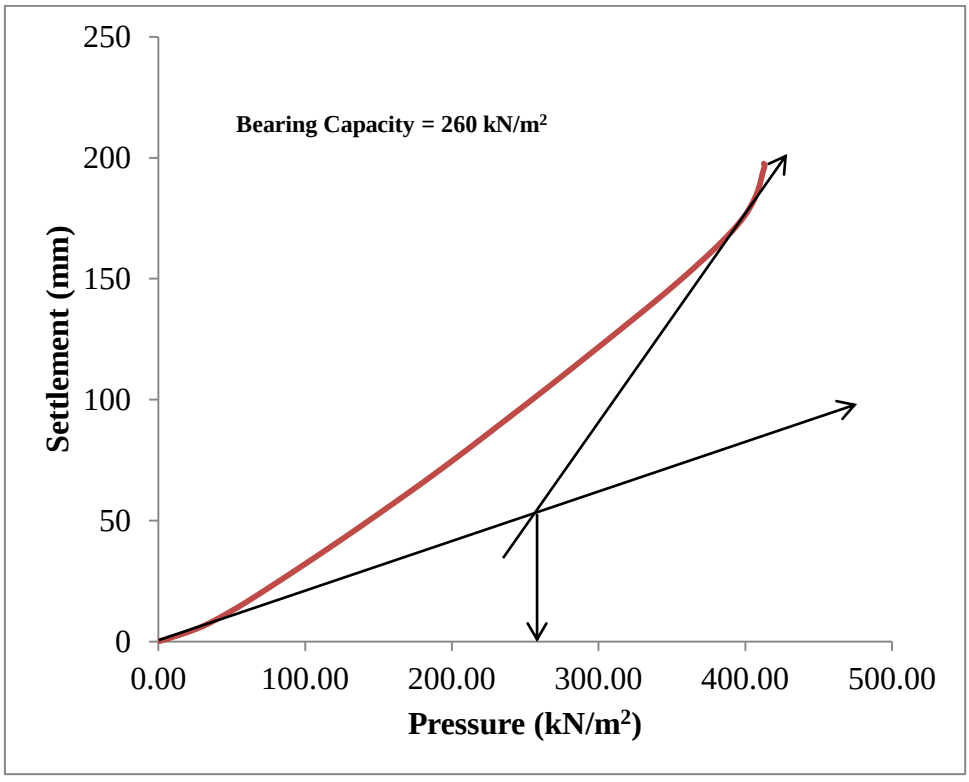

Fig 5.26:- Pressure vs Displacement Curve for Model-12 (Strip Footing B = 3m, $D_f/B = 0.5$, $L_1/L_2 = 3/1$)

5.13 MODEL 13 (Strip Footing, B = 3m, D_f/B = 1.0, L_1/L_2 = 1/3)

Final Output deformed mesh & load-displacement curve of the corresponding model is presented.

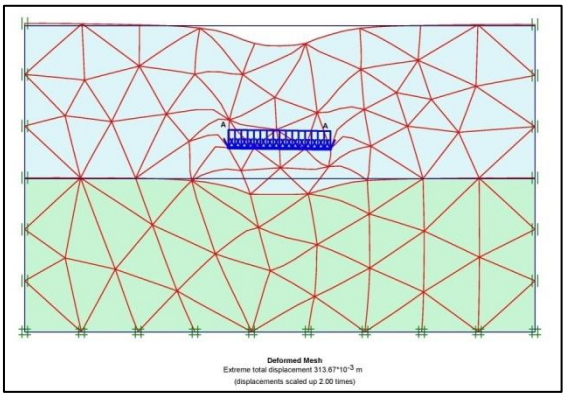

Fig 5.27:- Final output deformed mesh of Model - 13

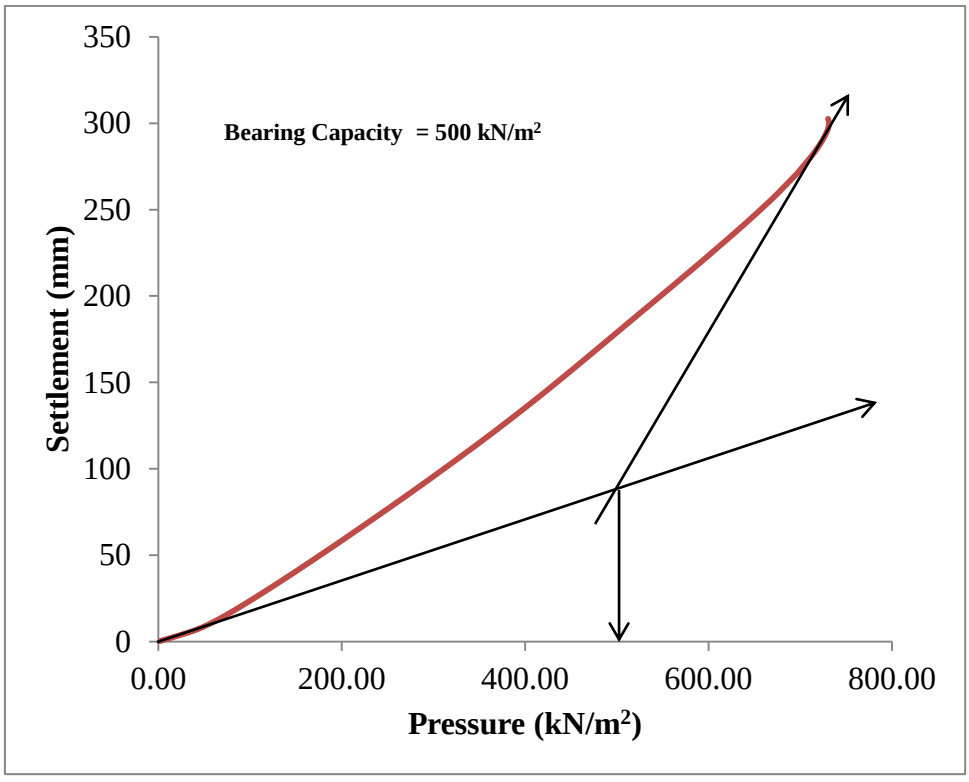

Fig 5.28:- Pressure vs Displacement Curve for Model-13 (Strip Footing B = 3m, D_f/B = 1.0, L_1/L_2 = 1/3)

‘

5.14 MODEL 14 (Strip Footing, B = 3m, D_f/B = 1.0, L_1/L_2 = 1/1)

Final Output deformed mesh & load-displacement curve of the corresponding model is presented.

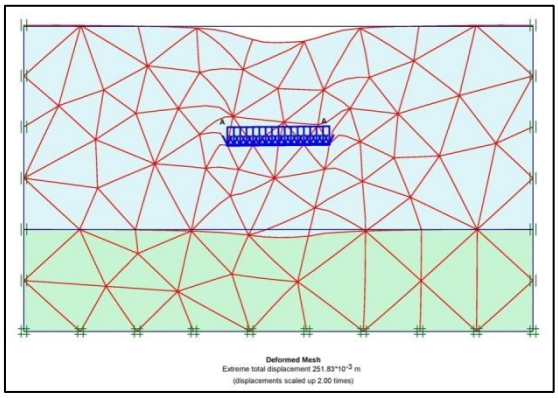

Fig 5.29:- Final output deformed mesh of Model - 14

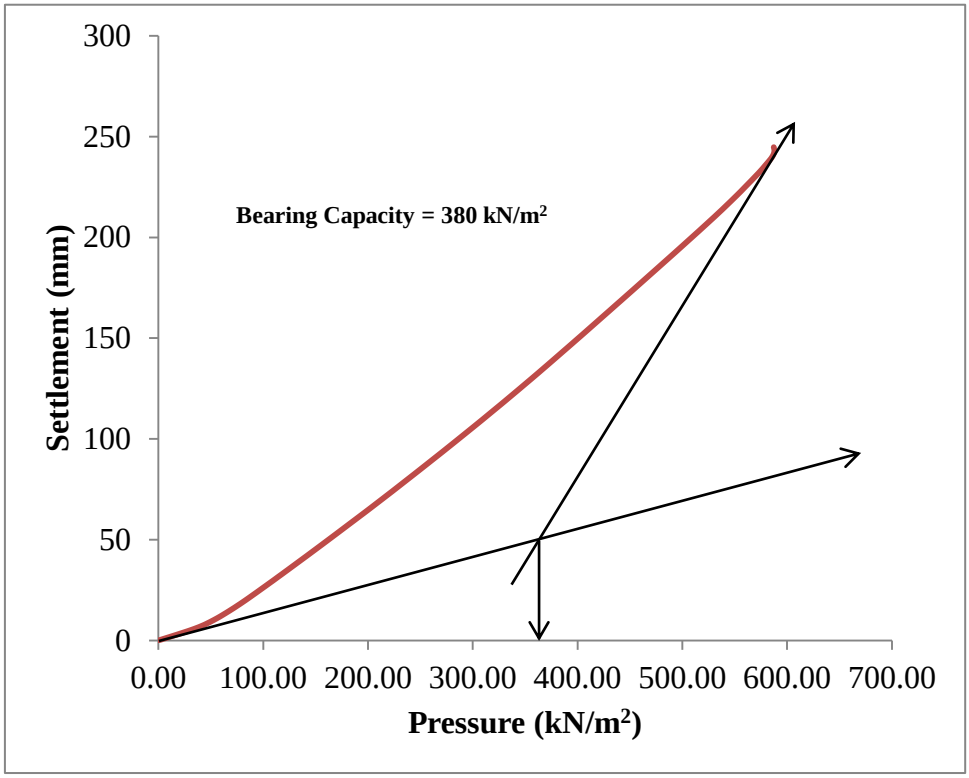

Fig 5.30:- Pressure vs Displacement Curve for Model-14 (Strip Footing B = 3m, D_f/B = 1.0, L_1/L_2 = 1/1)

5.15 MODEL 15 (Strip Footing, B = 3m, D_f/B = 1.0, L_1/L_2 = 3/1)

Final Output deformed mesh & load-displacement curve of the corresponding model is presented.

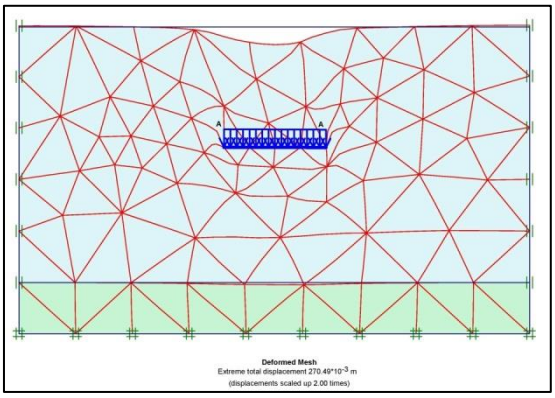

Fig 5.31:- Final output deformed mesh of Model - 15

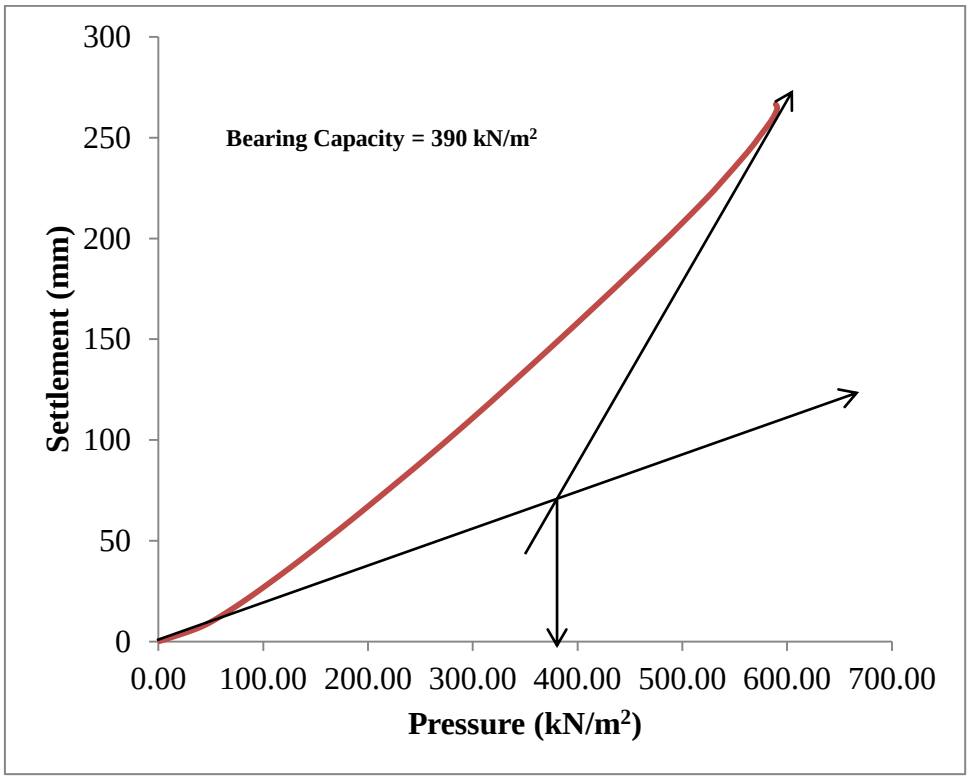

Fig 5.32:- Pressure vs Displacement Curve for Model-15 (Strip Footing B = 3m, D_f/B = 1.0, L_1/L_2 = 3/1)

5.16 MODEL 16 (Strip Footing, B = 3m, D_f/B = 1.5, L_1/L_2 = 1/3)

Final Output deformed mesh & load-displacement curve of the corresponding model is presented.

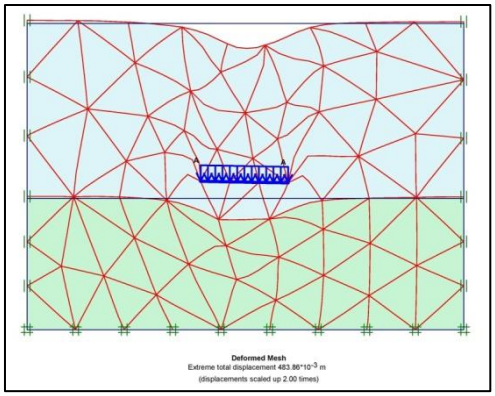

Fig 5.33:- Final output deformed mesh of Model - 16

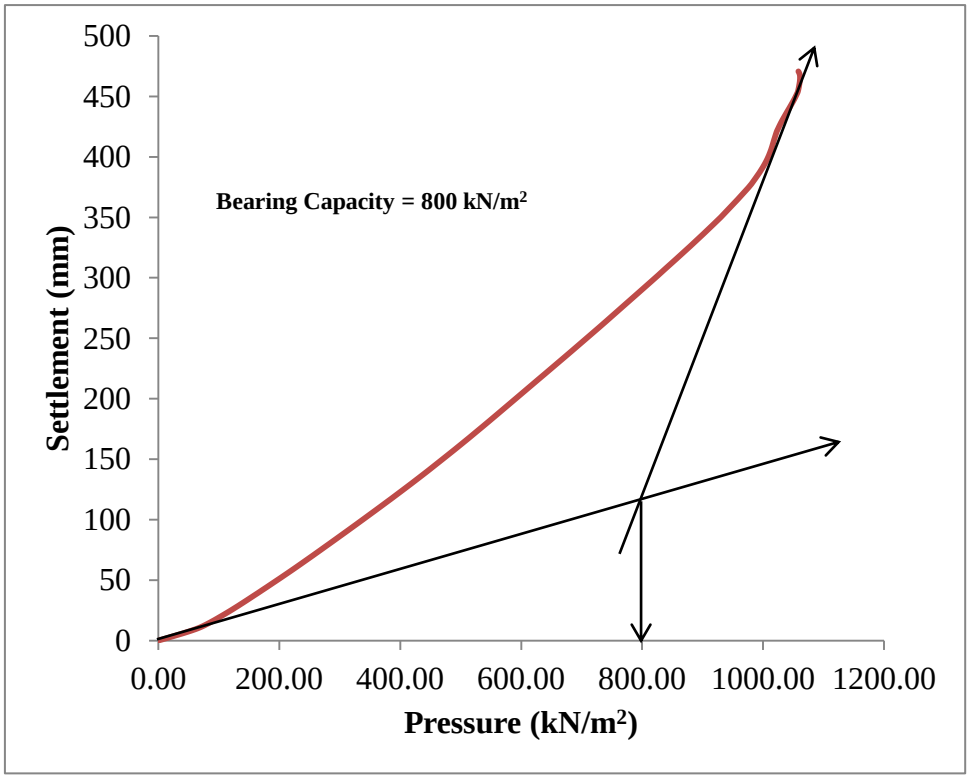

Fig 5.34:- Pressure vs Displacement Curve for Model-16 (Strip Footing B = 3m, D_f/B = 1.5, L_1/L_2 = 1/3)

5.17 MODEL 17 (Strip Footing, B = 3m, D_f/B = 1.5, L_1/L_2 = 1/1)

Final Output deformed mesh & load-displacement curve of the corresponding model is presented.

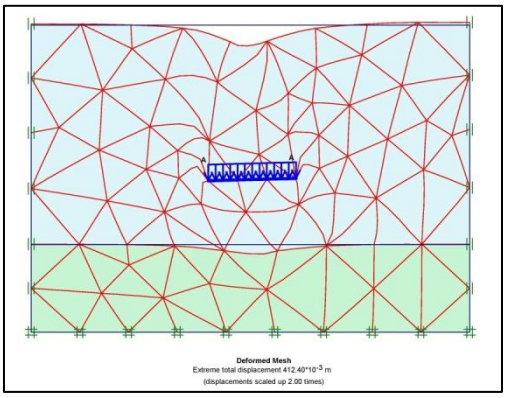

Fig 5.35:- Final output deformed mesh of Model - 17

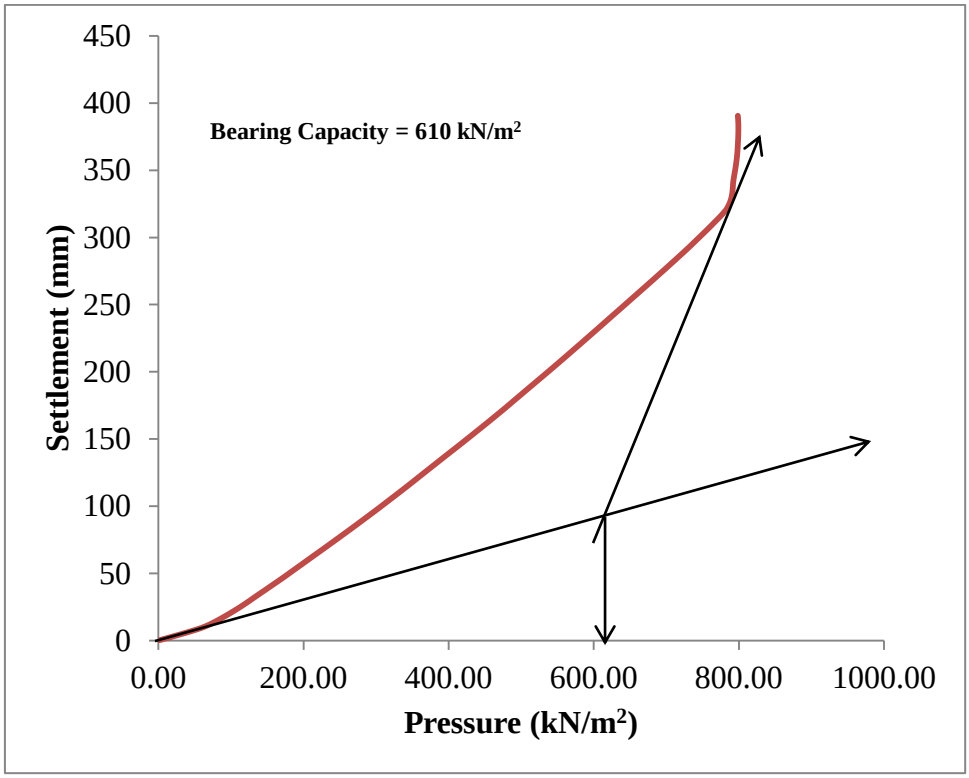

Fig 5.36:- Pressure vs Displacement Curve for Model-17 (Strip Footing B = 3m, D_f/B = 1.5, L_1/L_2 = 1/1)

5.18 MODEL 18 (Strip Footing, B = 3m, D_f/B = 1.5, L_1/L_2 = 3/1)

Final Output deformed mesh & load-displacement curve of the corresponding model is presented.

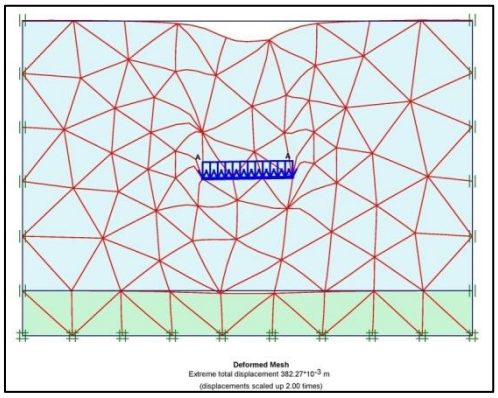

Fig 5.37:- Final output deformed mesh of Model – 18

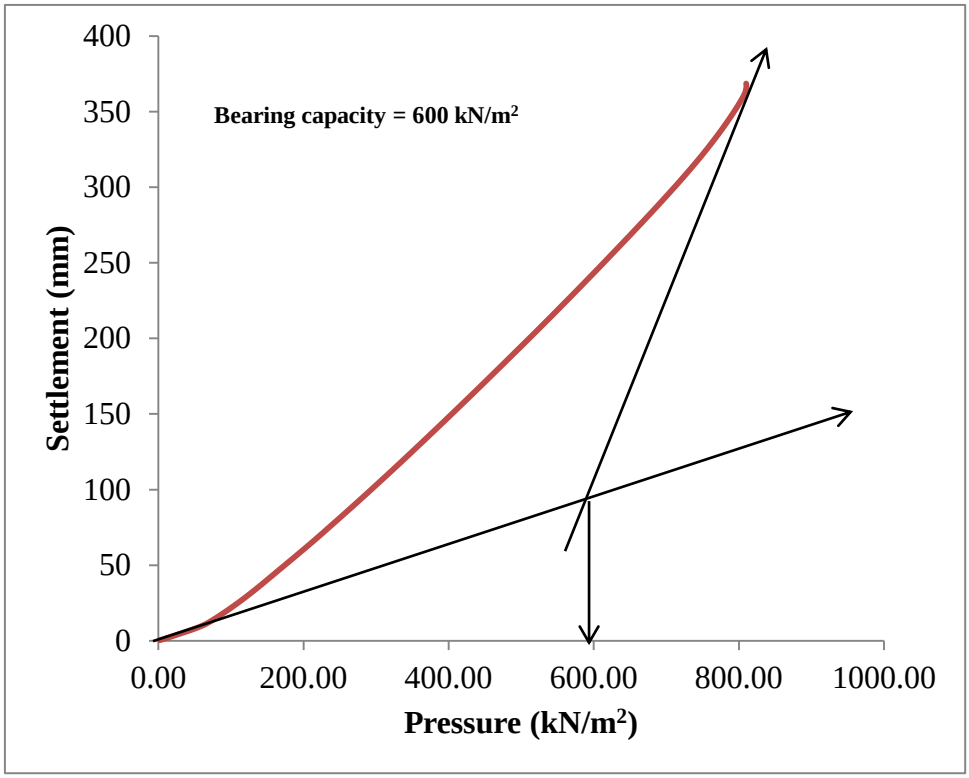

Fig 5.38:- Pressure vs Displacement Curve for Model-18 (Strip Footing B = 3m, D_f/B = 1.5, L_1/L_2 = 3/1)

5.19 MODEL 19 (Circular Footing, B = 2m, $D_f/B = 0.5$, $L_1/L_2 = 1/3$)

Final Output deformed mesh & load-displacement curve of the corresponding model is presented.

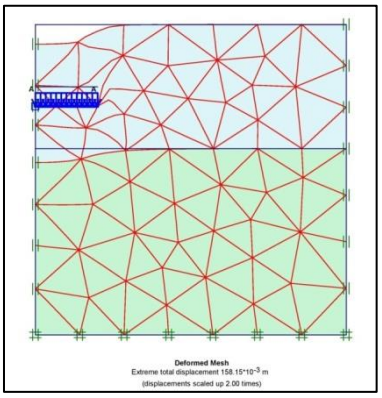

Fig 5.39:- Final output deformed mesh of Model - 19

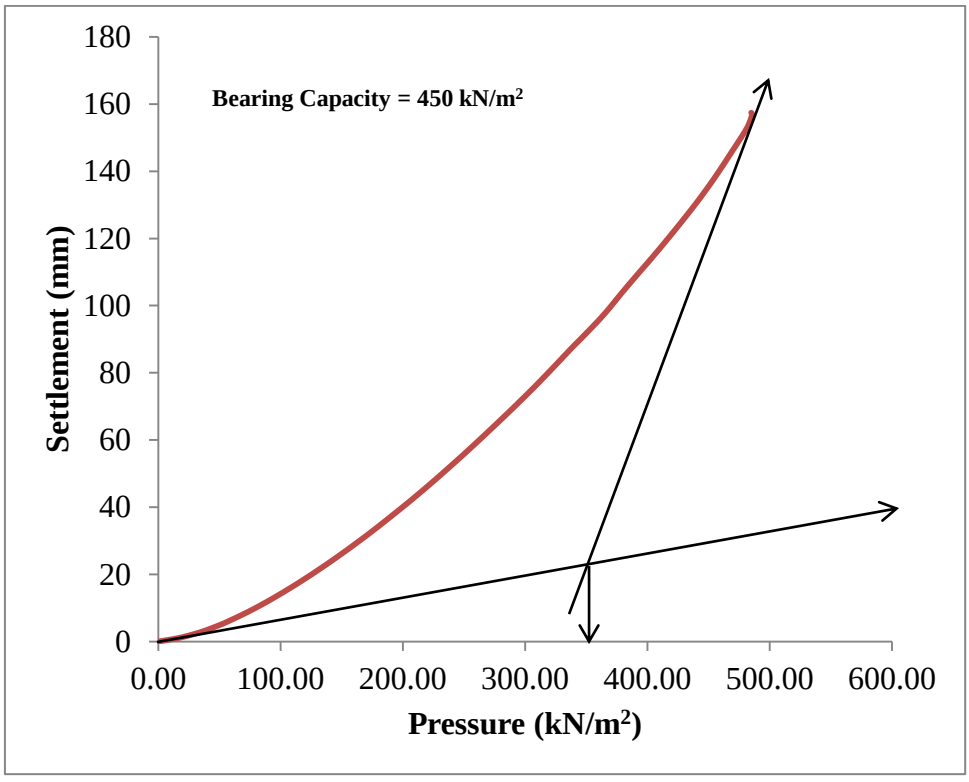

Fig 5.40:- Pressure vs Displacement Curve for Model-19 (Circular Footing B = 2m, $D_f/B = 0.5$, $L_1/L_2 = 1/3$)

5.20 MODEL 20 (Circular Footing, B = 2m, $D_f/B = 0.5$, $L_1/L_2 = 1/1$)

Final Output deformed mesh & load-displacement curve of the corresponding model is presented.

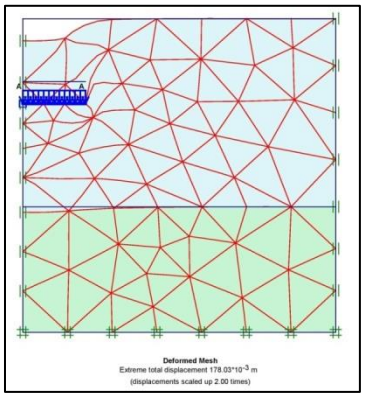

Fig 5.41:- Final output deformed mesh of Model - 20

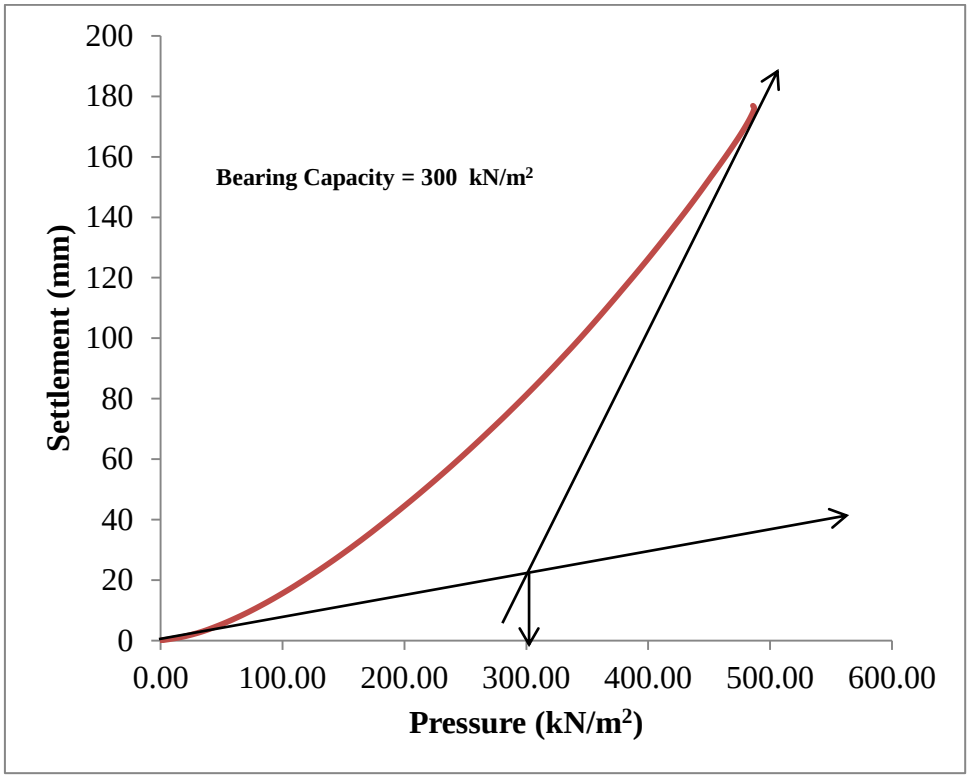

Fig 5.42:- Pressure vs Displacement Curve for Model-20 (Circular Footing B = 2m, $D_f/B = 0.5$, $L_1/L_2 = 1/1$)

5.21 MODEL 21 (Circular Footing, B = 2m, $D_f/B = 0.5$, $L_1/L_2 = 3/1$)

Final Output deformed mesh & load-displacement curve of the corresponding model is presented.

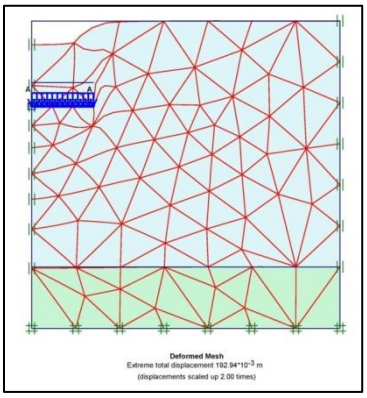

Fig 5.43:- Final output deformed mesh of Model - 21

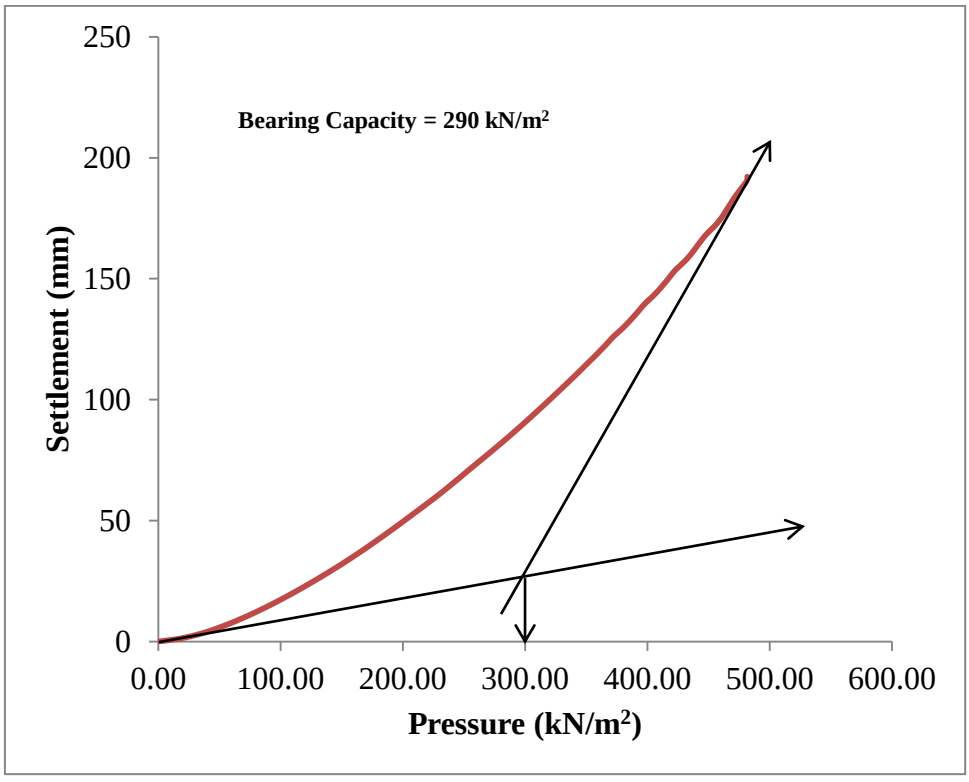

Fig 5.44:- Pressure vs Displacement Curve for Model-21 (Circular Footing B = 2m, $D_f/B = 0.5$, $L_1/L_2 = 3/1$)

5.22 MODEL 22 (Circular Footing, B = 2m, D_f/B = 1.0, L_1/L_2 = 1/3)

Final Output deformed mesh & load-displacement curve of the corresponding model is presented.

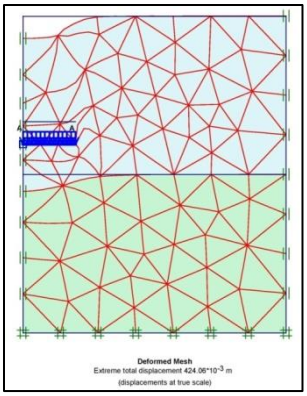

Fig 5.45:- Final output deformed mesh of Model – 22

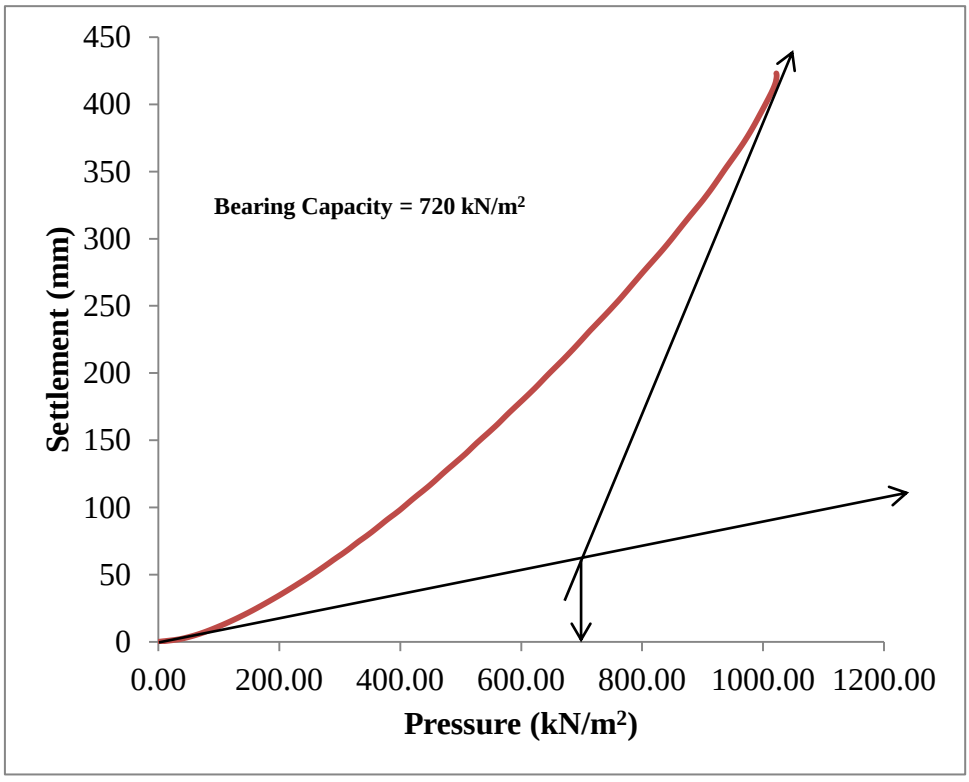

Fig 5.46:- Pressure vs Displacement Curve for Model-22 (Circular Footing B = 2m, D_f/B = 1.0, L_1/L_2 = 1/3)

5.23 MODEL 23 (Circular Footing, B = 2m, D_f/B = 1.0, L_1/L_2 = 1/1)

Final Output deformed mesh & load-displacement curve of the corresponding model is presented.

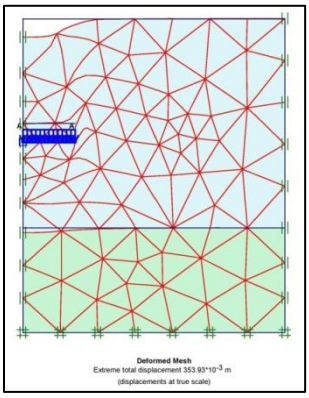

Fig 5.47:- Final output deformed mesh of Model - 23

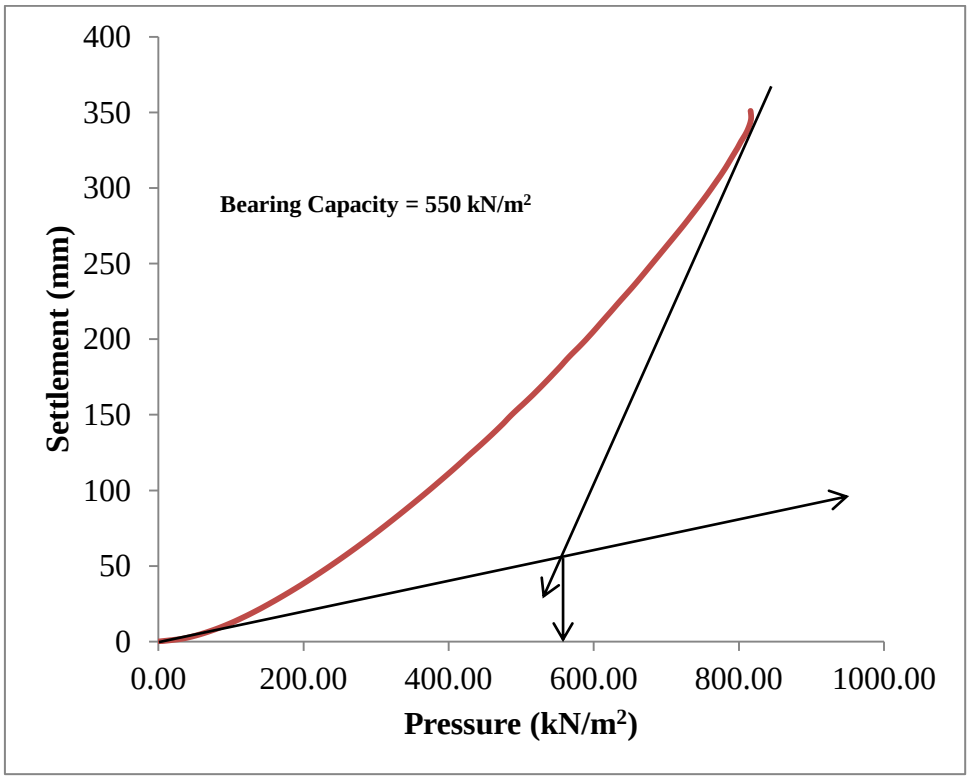

Fig 5.48:- Pressure vs Displacement Curve for Model-23 (Circular Footing B = 2m, D_f/B = 1.0, L_1/L_2 = 1/1)

5.24 MODEL 24 (Circular Footing, B = 2m, D_f/B = 1.0, L_1/L_2 = 3/1)

Final Output deformed mesh & load-displacement curve of the corresponding model is presented.

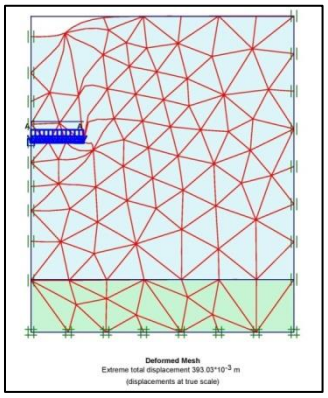

Fig 5.49:- Final output deformed mesh of Model - 24

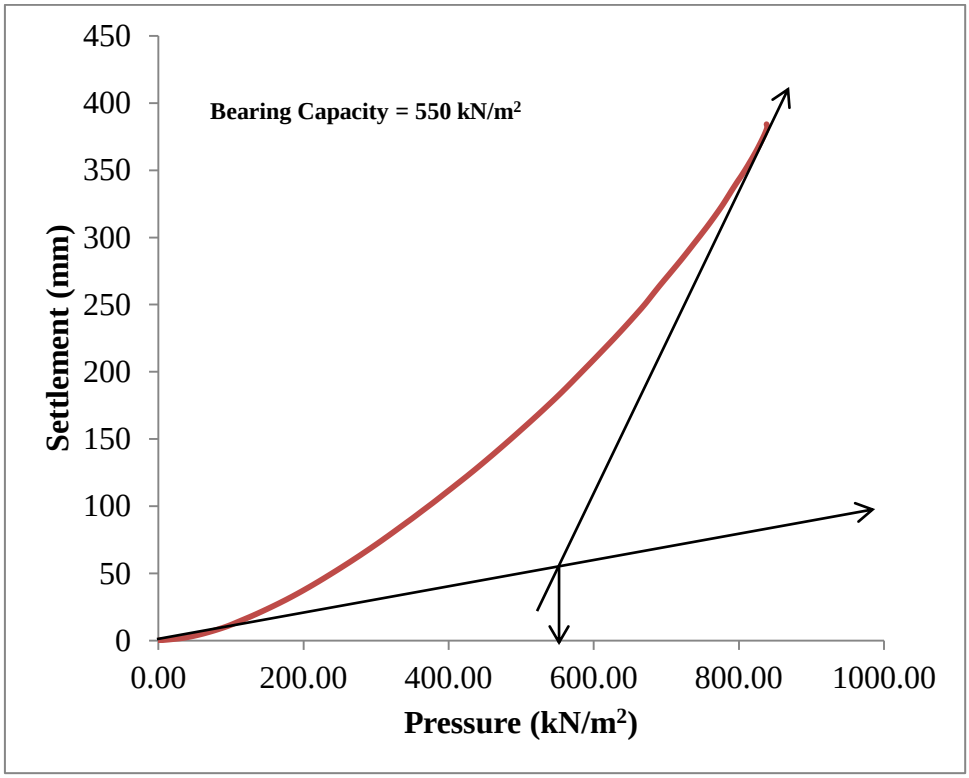

Fig 5.50:- Pressure vs Displacement Curve for Model-24 (Circular Footing B = 2m, D_f/B = 1.0, L_1/L_2 = 3/1)

5.25 MODEL 25 (Circular Footing, B = 2m, D_f/B = 1.5, L_1/L_2 = 1/3)

Final Output deformed mesh & load-displacement curve of the corresponding model is presented.

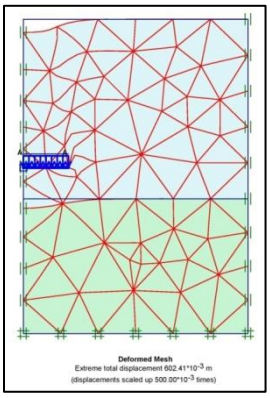

Fig 5.51:- Final output deformed mesh of Model - 25

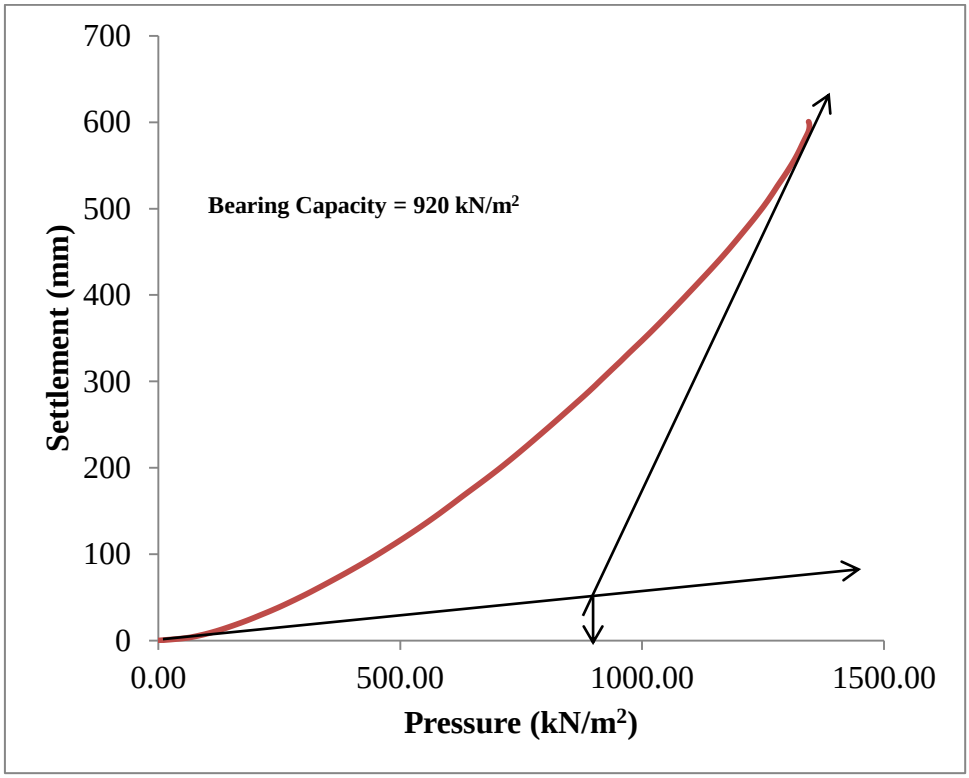

Fig 5.52:- Pressure vs Displacement Curve for Model-25 (Circular Footing B = 2m, D_f/B = 1.5, L_1/L_2 = 1/3)

5.26 MODEL 26 (Circular Footing, B = 2m, D_f/B = 1.0, L_1/L_2 = 3/1)

Final Output deformed mesh & load-displacement curve of the corresponding model is presented.

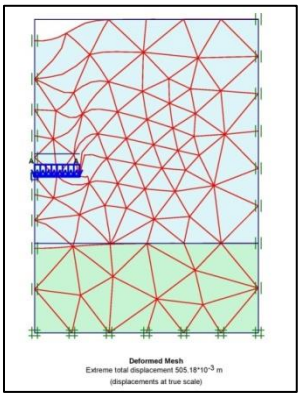

Fig 5.53:- Final output deformed mesh of Model - 26

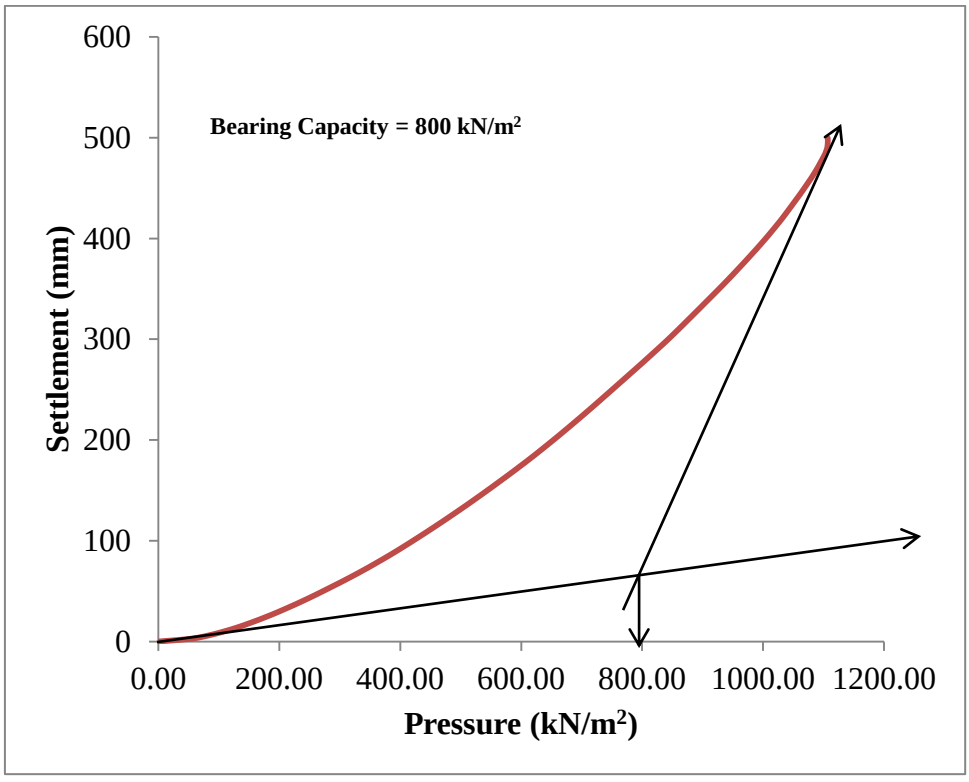

Fig 5.54:- Pressure vs Displacement Curve for Model 26 (Circular Footing B = 2m, D_f/B = 1.0, L_1/L_2 = 3/1)

5.27 MODEL 27 (Circular Footing, B = 2m, D_f/B = 1.5, L_1/L_2 = 3/1)

Final Output deformed mesh & load-displacement curve of the corresponding model is presented.

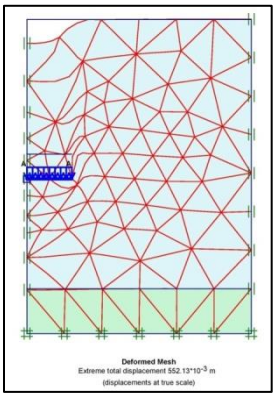

Fig 5.55:- Final output deformed mesh of Model - 27

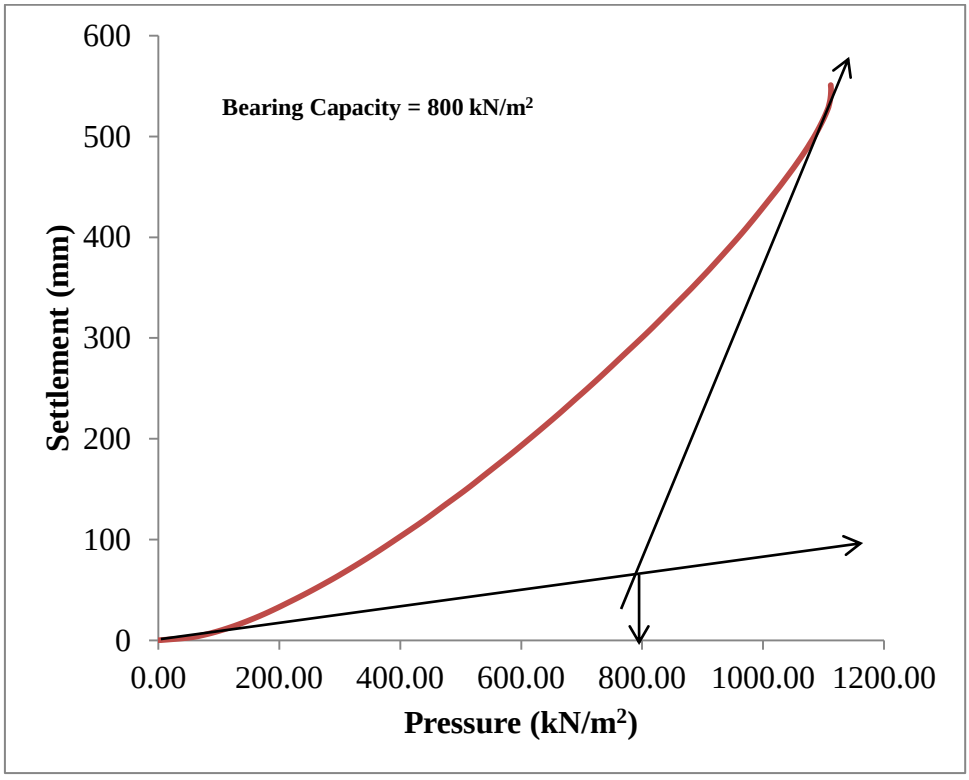

Fig 5.56:- Pressure vs Displacement Curve for Model-27 (Circular Footing B = 2m, D_f/B = 1.5, L_1/L_2 = 3/1)

5.28 MODEL 28 (Circular Footing, B = 3m, $D_f/B = 0.5$, $L_1/L_2 = 1/3$)

Final Output deformed mesh & load-displacement curve of the corresponding model is presented.

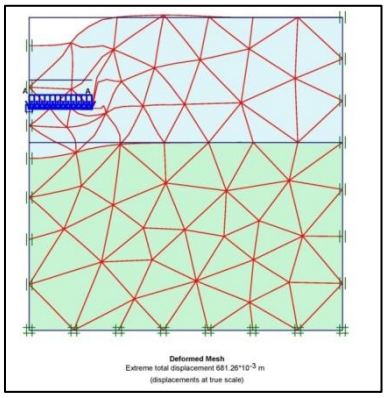

Fig 5.57:- Final output deformed mesh of Model - 28

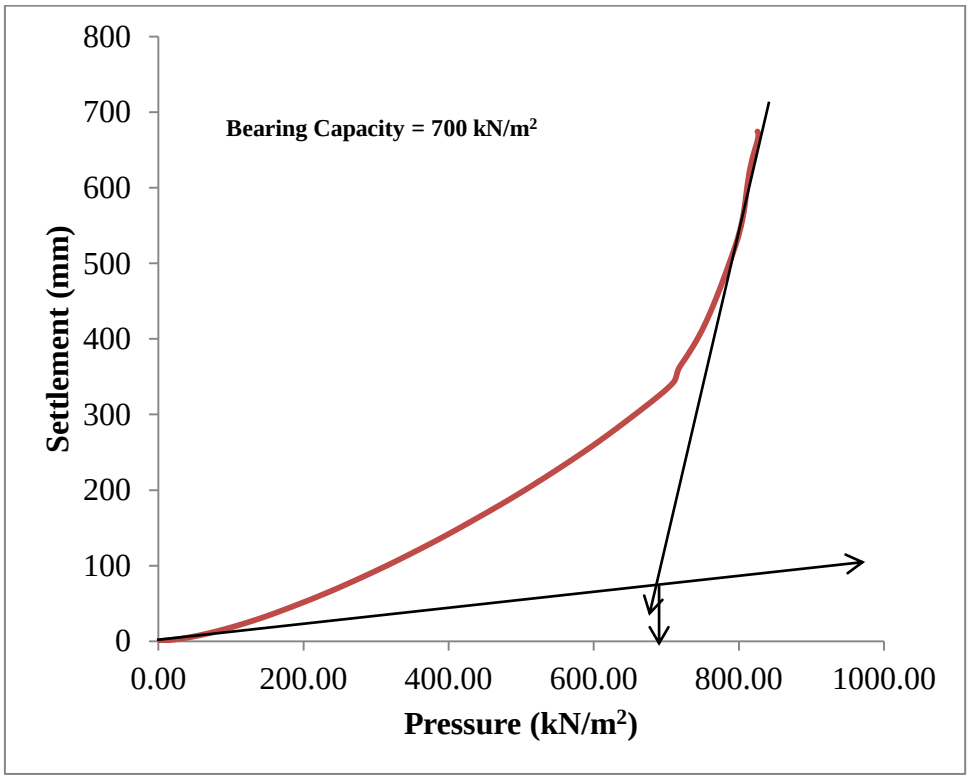

Fig 5.58:- Pressure vs Displacement Curve for Model-28 (Circular Footing B = 3m, $D_f/B = 0.5$, $L_1/L_2 = 1/3$)

5.29 MODEL 29 (Circular Footing, B = 3m, D_f/B = 0.5, L_1/L_2 = 1/1)

Final Output deformed mesh & load-displacement curve of the corresponding model is presented.

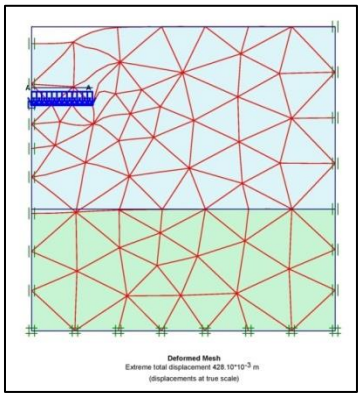

Fig 5.59:- Final output deformed mesh of Model - 29

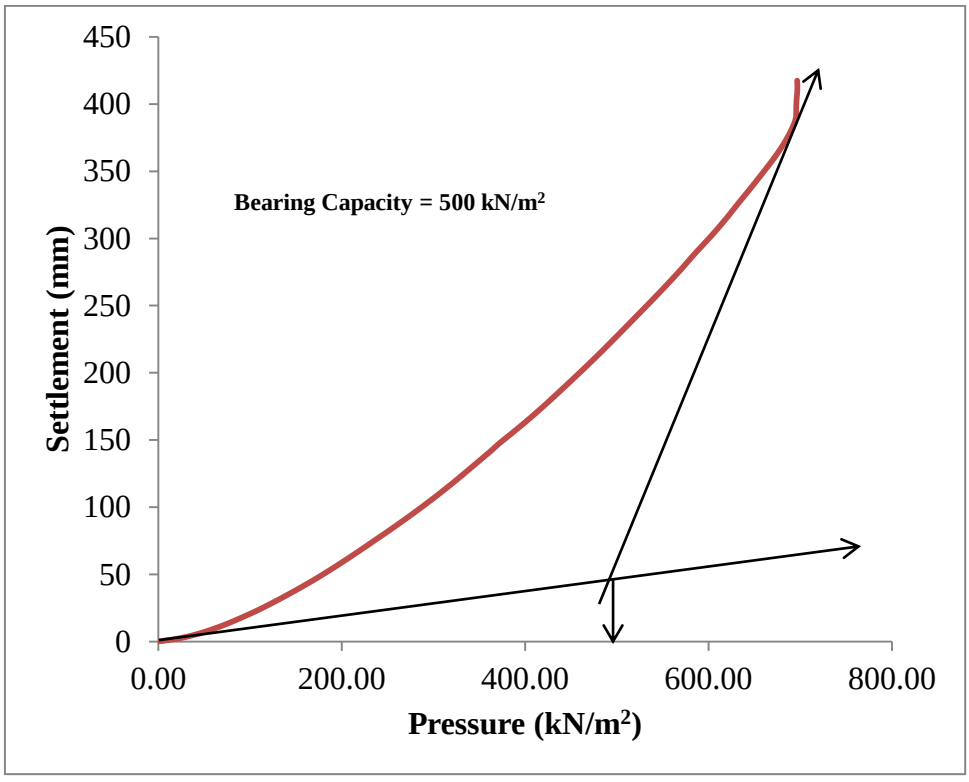

Fig 5.60:- Pressure vs Displacement Curve for Model-29 (Circular Footing B = 3m, D_f/B = 0.5, L_1/L_2 = 1/1)

5.30 MODEL 30 (Circular Footing, B = 3m, D_f/B = 0.5, L_1/L_2 = 3/1)

Final Output deformed mesh & load-displacement curve of the corresponding model is presented.

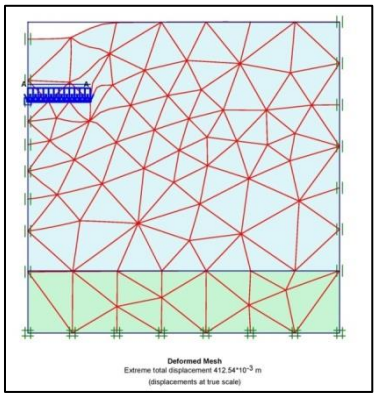

Fig 5.61:- Final output deformed mesh of Model - 30

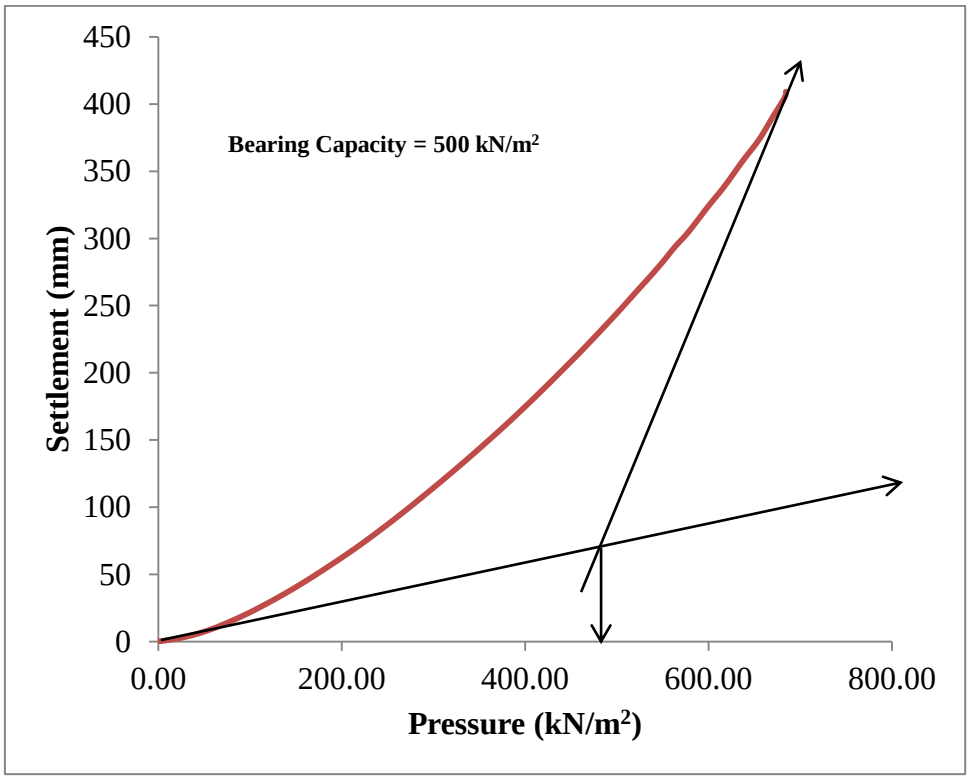

Fig 5.62:- Pressure vs Displacement Curve for Model-30 (Circular Footing B = 3m, D_f/B = 0.5, L_1/L_2 = 3/1)

5.31 MODEL 31 (Circular Footing, B = 3m, D_f/B = 1.0, L_1/L_2 = 1/3)

Final Output deformed mesh & load-displacement curve of the corresponding model is presented.

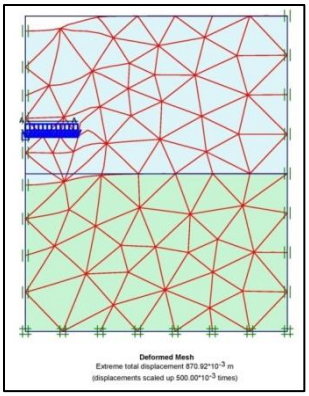

Fig 5.63:- Final output deformed mesh of Model - 31

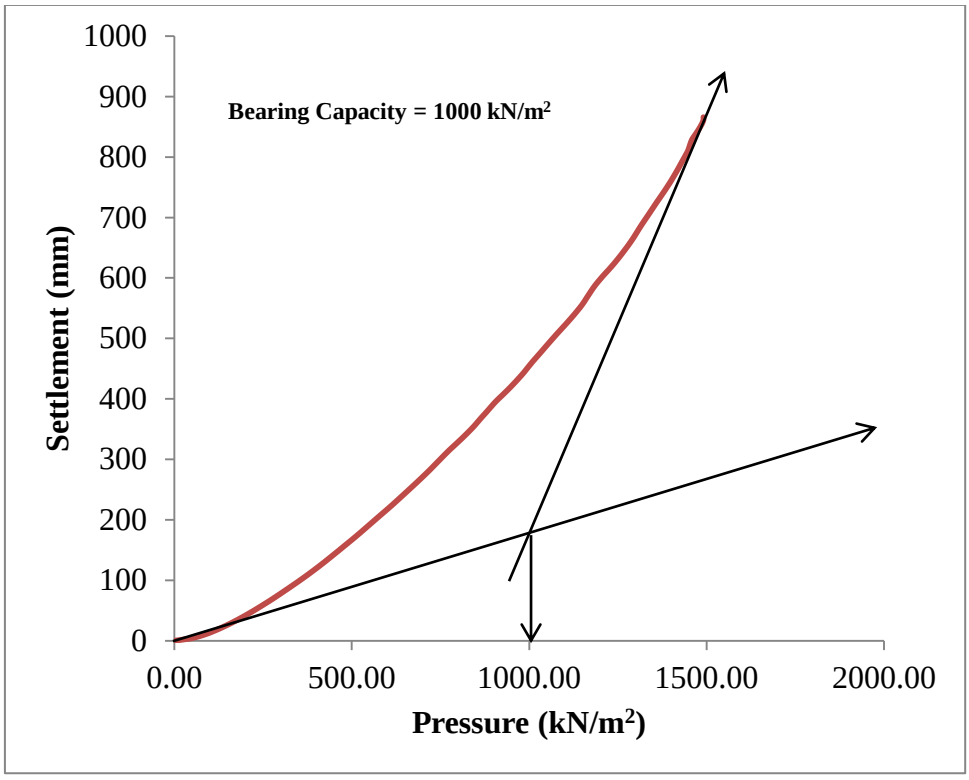

Fig 5.64:- Pressure vs Displacement Curve for Model-31 (Circular Footing B = 3m, D_f/B = 1.0, L_1/L_2 = 1/3)

5.32 MODEL 32 (Circular Footing, B = 3m, D_f/B = 1.0, L_1/L_2 = 1/1)

Final Output deformed mesh & load-displacement curve of the corresponding model is presented.

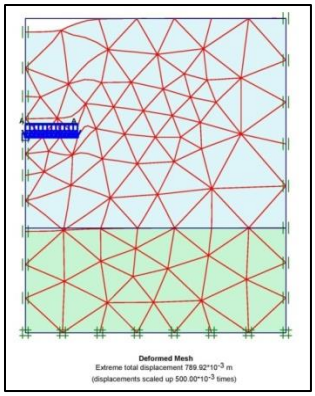

Fig 5.65:- Final output deformed mesh of Model - 32

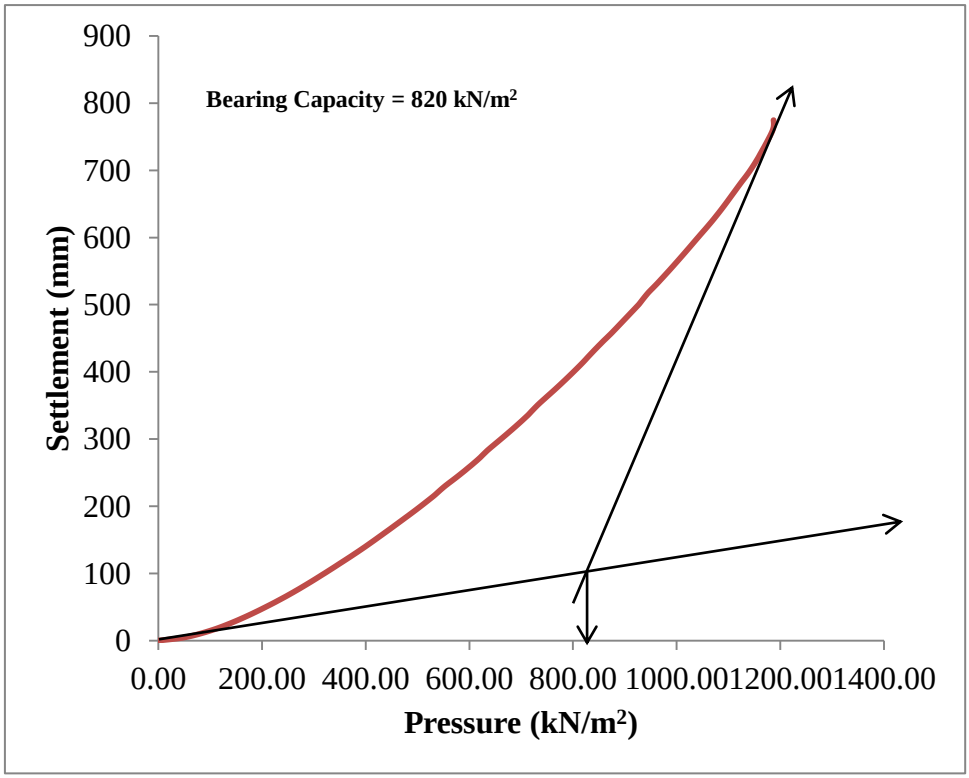

Fig 5.66:- Pressure vs Displacement Curve for Model-32 (Circular Footing B = 3m, D_f/B = 1.0, L_1/L_2 = 1/1)

5.33 MODEL 33 (Circular Footing, B = 3m, D_f/B = 1.0, L_1/L_2 = 3/1)

Final Output deformed mesh & load-displacement curve of the corresponding model is presented.

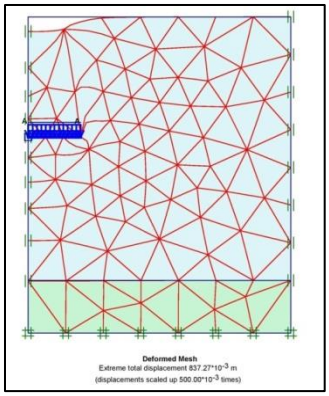

Fig 5.67:- Final output deformed mesh of Model - 33

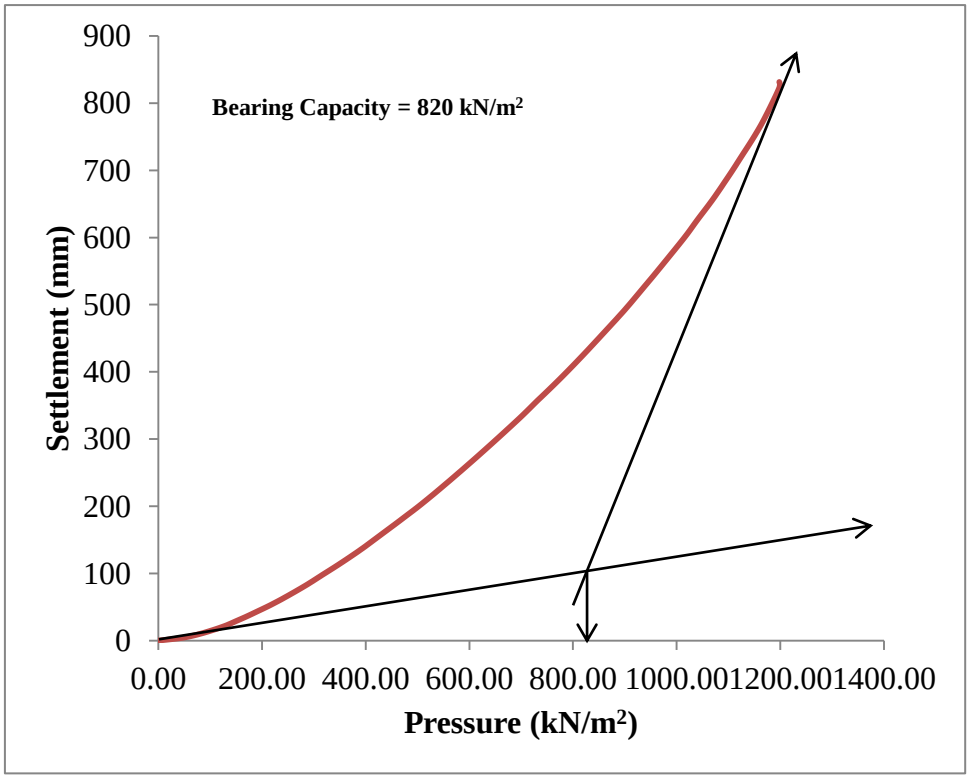

Fig 5.68:- Pressure vs Displacement Curve for Model-33 (Circular Footing B = 3m, D_f/B = 1.0, L_1/L_2 = 3/1)

5.34 MODEL 34 (Circular Footing, B = 3m, D_f/B = 1.5, L_1/L_2 = 1/3)

Final Output deformed mesh & load-displacement curve of the corresponding model is presented.

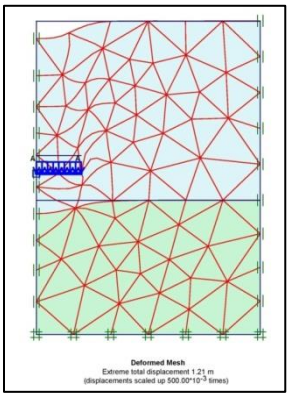

Fig 5.69:- Final output deformed mesh of Model – 34

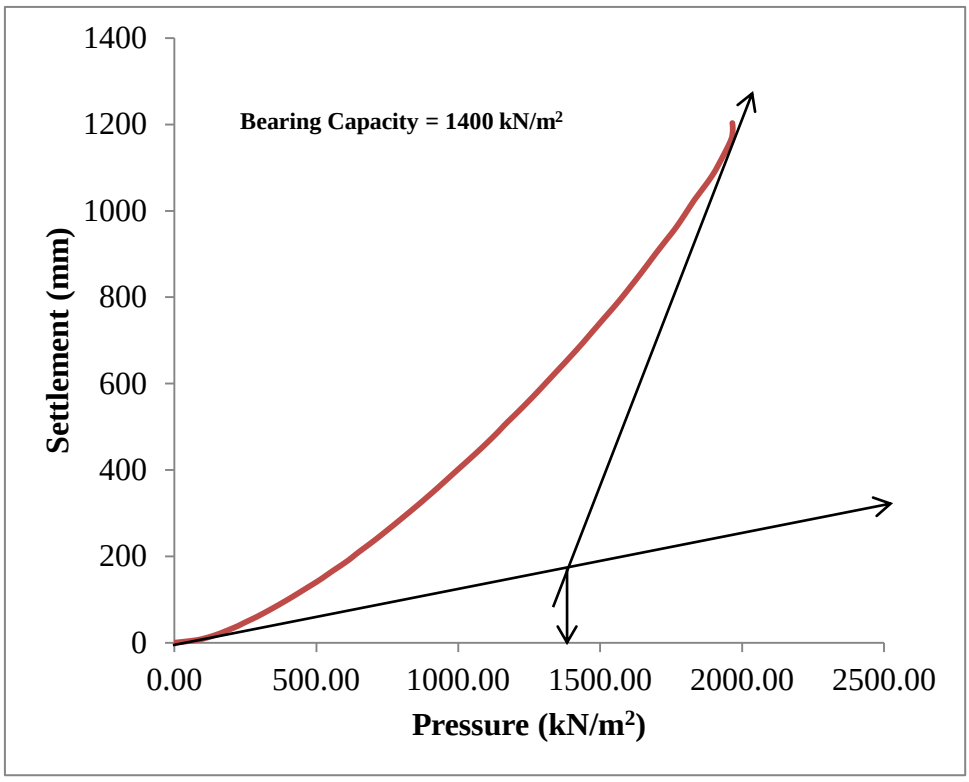

Fig 5.70:- Pressure vs Displacement Curve for Model-34 (Circular Footing B = 3m, D_f/B = 1.5, L_1/L_2 = 1/3)

5.35 MODEL 35 (Circular Footing, B = 3m, D_f/B = 1.5, L_1/L_2 = 1/1)

Final Output deformed mesh & load-displacement curve of the corresponding model is presented.

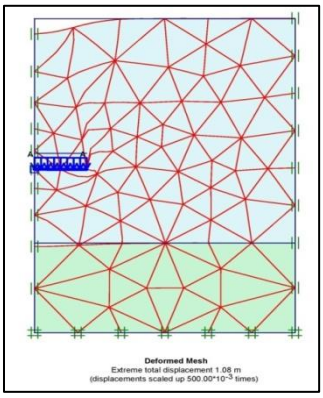

Fig 5.71:- Final output deformed mesh of Model – 35

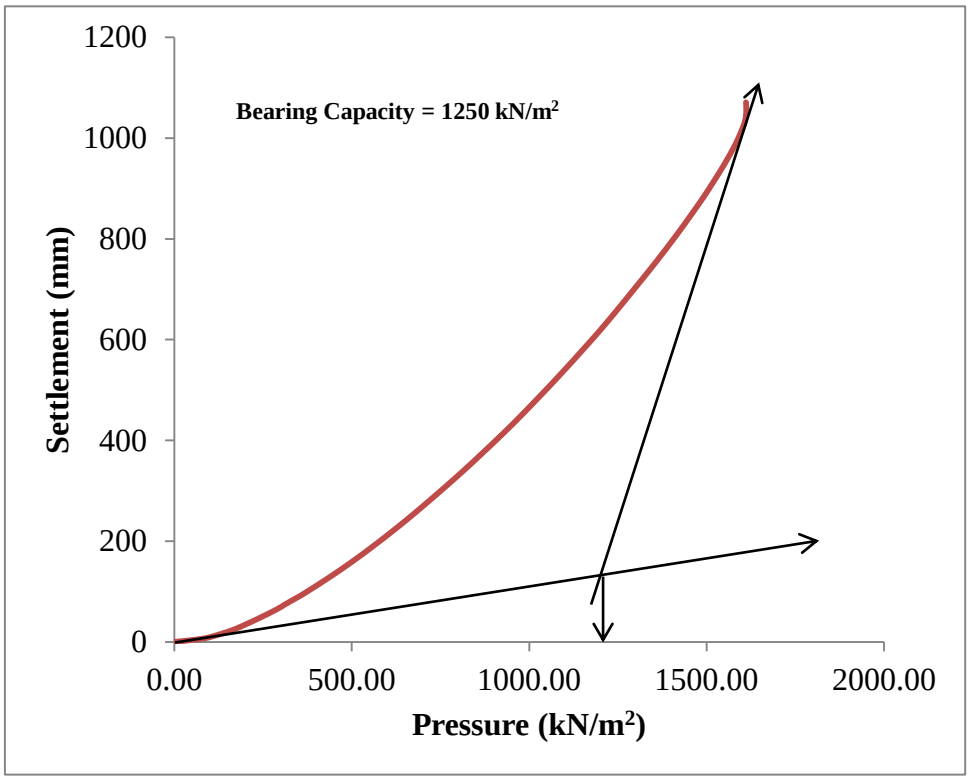

Fig 5.72:- Pressure vs Displacement Curve for Model-35 (Circular Footing B = 3m, D_f/B = 1.5, L_1/L_2 = 1/1)

5.36 MODEL 36 (Circular Footing B = 3m, D_f/B = 1.5, L_1/L_2 = 3)

Final Output deformed mesh & load-displacement curve of the corresponding model is presented.

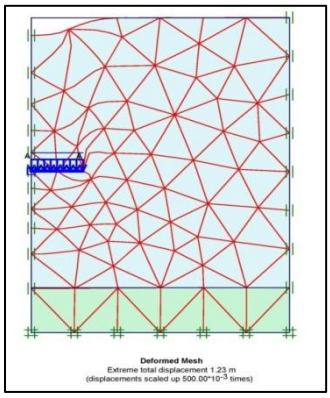

Fig 5.73:- Final output deformed mesh of Model - 36

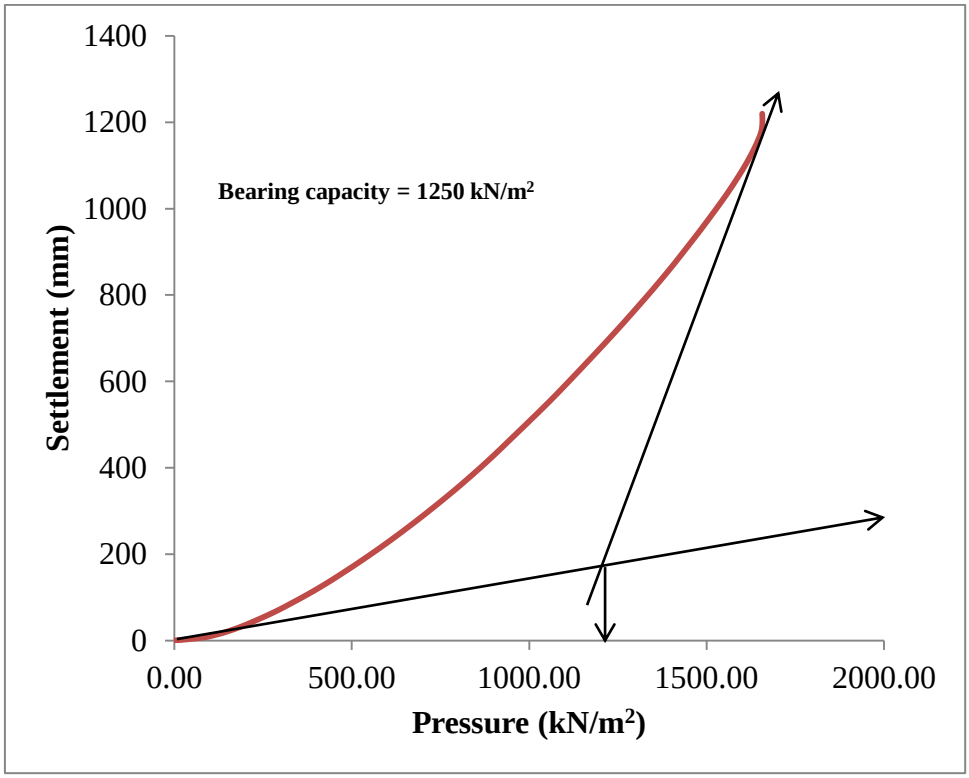

Fig 5.74:- Pressure vs Displacement Curve for Model-36 (Circular Footing B = 3m, D_f/B = 1.5, L_1/L_2 = 3)

CHAPTER 6: RESULTS AND DISCUSSION

6.0 GENERAL

Based on the results obtained from numerical analysis an attempt has been made in this chapter to study the effect of D_f/B ratio, ratio of thickness of upper & lower layer subsoil (L_1/L_2), type of footings (strip and circular) on ultimate bearing capacity of footings.

6.1 LOAD - SETTLEMENT CURVES

Load - settlement curves for strip footings (of width 2 m and 3 m) and circular footing (of diameter 2 m and 3 m) as obtained from output of PLAXIS 2D software have been presented earlier in Chapter 5 (Figs. 5.1 to 5.74). It is observed that the numerically obtained curves follow continuously curvilinear trend and hence the ultimate loads have been obtained from these curves by double tangent method. Thus, for total 36 numerical cases considered for the numerical study, as mentioned in Chapter 5, the ultimate bearing capacities obtained from load settlement curves presented in Chapter 5 are furnished in Table 6.1.

Table 6.1 Ultimate Bearing Capacities Obtained from Numerical Analysis

Model No.	Type of Footing	Width of Footing (m)	D_f/B	L_1/L_2	Bearing Capacity (KN/m^2)
1	Strip (F1)	2	0.5	1/3	265
2	Strip (F1)	2	0.5	1	200
3	Strip (F1)	2	0.5	3	210
4	Strip (F1)	2	1	1/3	350
5	Strip (F1)	2	1	1	300
6	Strip (F1)	2	1	3	300
7	Strip (F1)	2	1.5	1/3	510
8	Strip (F1)	2	1.5	1	400
9	Strip (F1)	2	1.5	3	400
10	Strip (F2)	3	0.5	1/3	370

11	Strip (F2)	3	0.5	1	250
12	Strip (F2)	3	0.5	3	260
13	Strip (F2)	3	1	1/3	500
14	Strip (F2)	3	1	1	380
15	Strip (F2)	3	1	3	390
16	Strip (F2)	3	1.5	1/3	800
17	Strip (F2)	3	1.5	1	610
18	Strip (F2)	3	1.5	3	600
19	Circular (F3)	2	0.5	1/3	450
20	Circular (F3)	2	0.5	1	300
21	Circular (F3)	2	0.5	3	290
22	Circular (F3)	2	1	1/3	720
23	Circular (F3)	2	1	1	550
24	Circular (F3)	2	1	3	550
25	Circular (F3)	2	1.5	1/3	920
26	Circular (F3)	2	1.5	1	800
27	Circular (F3)	2	1.5	3	800
28	Circular (F4)	3	0.5	1/3	700
29	Circular (F4)	3	0.5	1	500
30	Circular (F4)	3	0.5	3	500
31	Circular (F4)	3	1	1/3	1000
32	Circular (F4)	3	1	1	820
33	Circular (F4)	3	1	3	810
34	Circular (F4)	3	1.5	1/3	1400
35	Circular (F4)	3	1.5	1	1250
36	Circular (F4)	3	1.5	3	1240

6.2 EFFECT OF D_f/B RATIO ON ULTIMATE BEARING CAPACITY

In order to study the effect of D_f/B ratio on ultimate bearing capacity, ultimate bearing capacity vs. D_f/B ratio graphs have been plotted for different ratio of thickness of upper & lower layer subsoil (L_1/L_2) as shown in Figs. 6.1, 6.2, 6.3 and 6.4 for four different footing types F1, F2, F3 and F4 respectively.

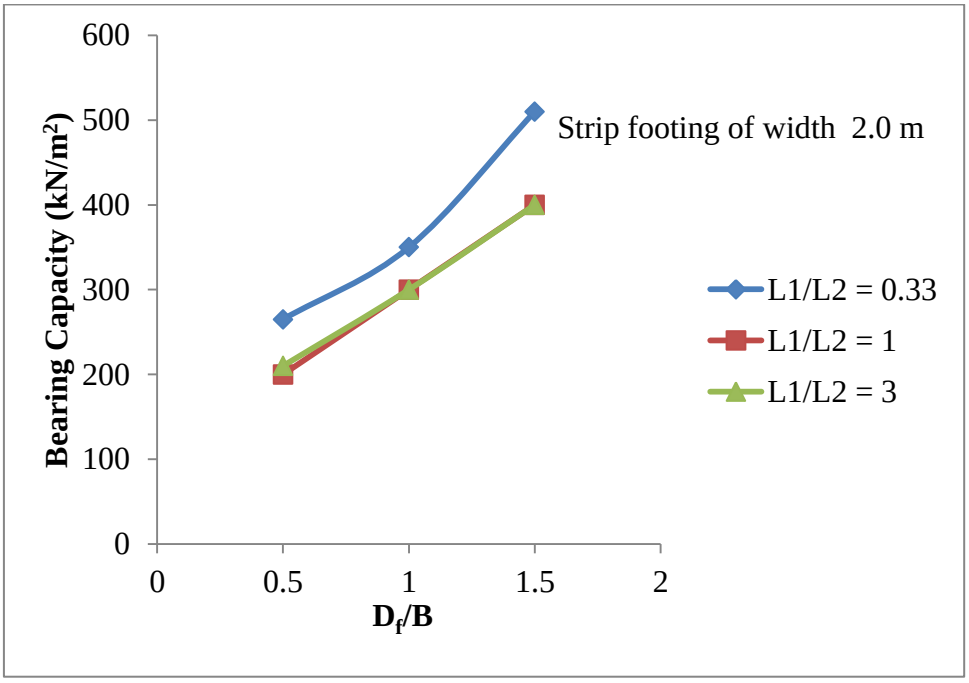

Fig. 6.1: Variation of Bearing Capacity with D_f/B Ratio for Various L_1/L_2 Ratio for Footing Type F1

From the above figure it is observed that for strip footing of width 2.0 m and L_1/L_2 of 0.33, bearing capacity increases by almost 30% when D_f/B ratio is increased from 0.5 to 1 and by 45% when D_f/B ratio is increased from 1 to 1.5.

For the values of L_1/L_2 of 1 and 3, increment of bearing capacity with D_f/B ratio is almost same. Bearing capacity increases by 45% when D_f/B ratio is increased from 0.5 to 1 and by 33% when D_f/B ratio is increased from 1 to 1.5.

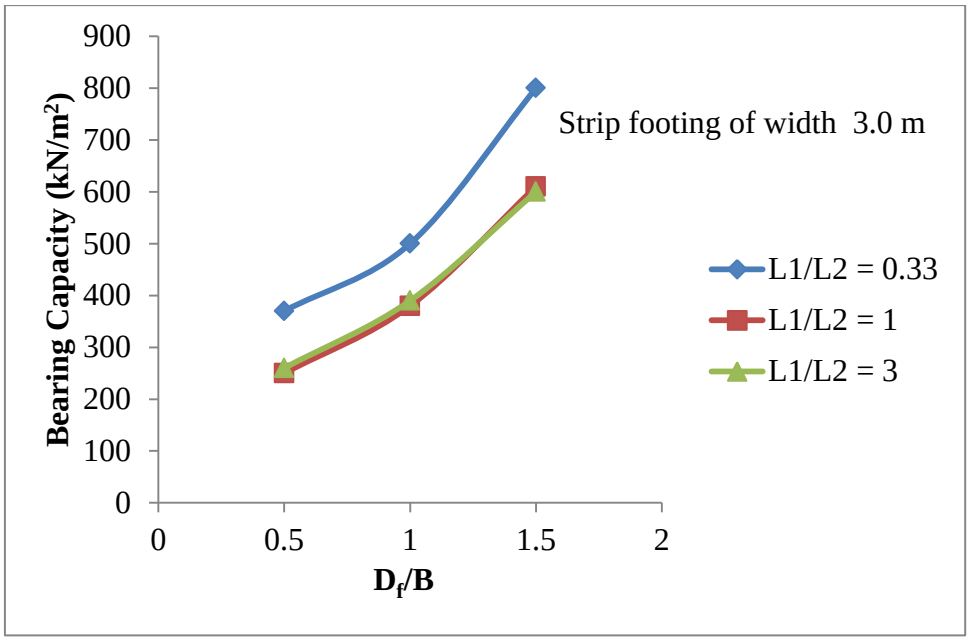

Fig. 6.2: Variation of Bearing Capacity with D_f/B Ratio for Various L_1/L_2 Ratio for Footing Type F2

From the above figure it is observed that for strip footing of width 3.0 m and L_1/L_2 of 0.33, bearing capacity increases by almost 35% when D_f/B ratio is increased from 0.5 to 1 and by 60% when D_f/B ratio is increased from 1 to 1.5.

For the values of L_1/L_2 of 1 and 3, increment of bearing capacity with D_f/B ratio is almost same. Bearing capacity increases by 50% when D_f/B ratio is increased from 0.5 to 1 and by 55-60% when D_f/B ratio is increased from 1 to 1.5.

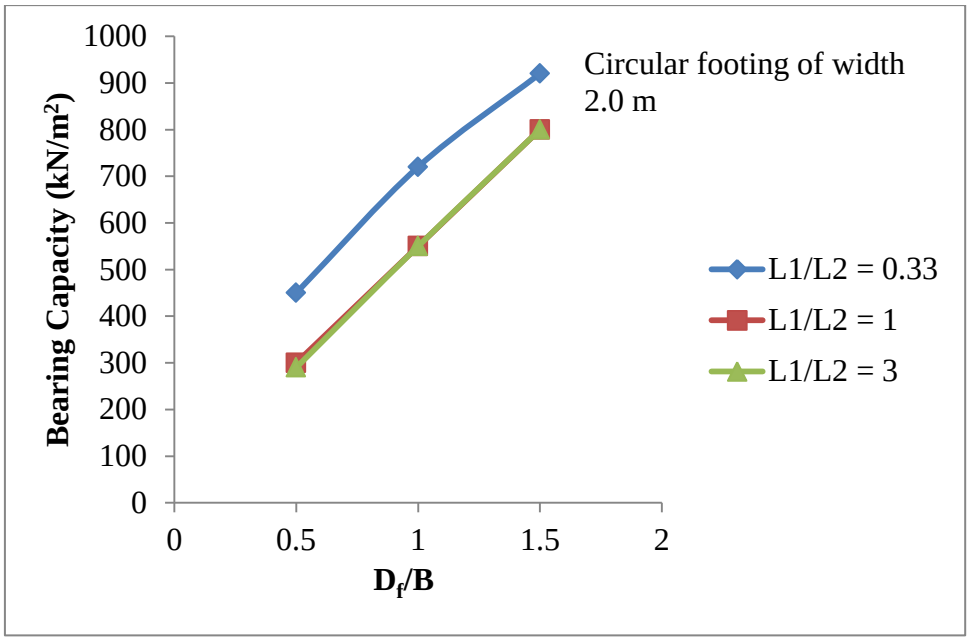

Fig. 6.3: Variation of Bearing Capacity with D_f/B Ratio for Various L_1/L_2 Ratio for Footing Type F3

From the above figure it is observed that for circular footing of width 2.0 m and L_1/L_2 of 0.33, bearing capacity increases by almost 60% when D_f/B ratio is increased from 0.5 to 1 and by 30% when D_f/B ratio is increased from 1 to 1.5.

For the values of L_1/L_2 of 1 and 3, increment of bearing capacity with D_f/B ratio is almost same. Bearing capacity increases by 85% when D_f/B ratio is increased from 0.5 to 1 and by 45% when D_f/B ratio is increased from 1 to 1.5.

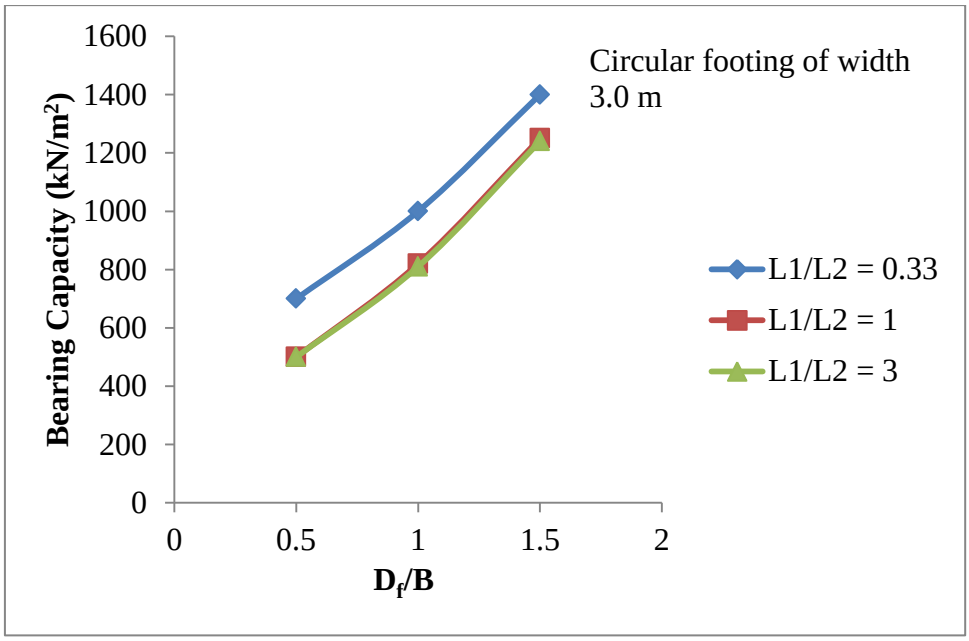

Fig. 6.4: Variation of Bearing Capacity with D_f/B Ratio for Various L_1/L_2 Ratio for Footing Type F4

From the above figure it is observed that for circular footing of width 3.0 m and L_1/L_2 of 0.33, bearing capacity increases by almost 42% when D_f/B ratio is increased from 0.5 to 1 and by 40% when D_f/B ratio is increased from 1 to 1.5.

For the values of L_1/L_2 of 1 and 3, increment of bearing capacity with D_f/B ratio is almost same. Bearing capacity increases by 63% when D_f/B ratio is increased from 0.5 to 1 and by 53% when D_f/B ratio is increased from 1 to 1.5.

6.3 EFFECT OF L_1/L_2 RATIO ON ULTIMATE BEARING CAPACITY

In order to study the effect of L_1/L_2 ratio on ultimate bearing capacity, ultimate bearing capacity vs. L_1/L_2 ratio graphs have been plotted for different D_f/B ratio as shown in Figs. 6.5, 6.6, 6.7 and 6.8 for four different footing types F1, F2, F3 and F4 respectively.

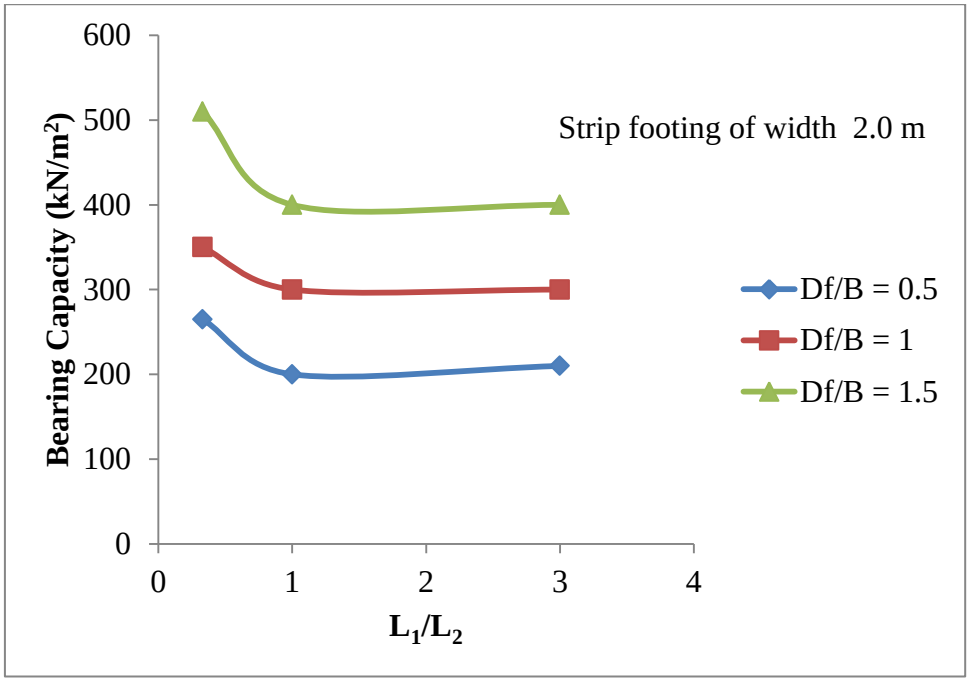

Fig. 6.5: Variation of Bearing Capacity with L_1/L_2 Ratio for Various D_f/B Ratio for Footing Type F1

From the above figure it is observed that for strip footing of width 2.0 m and Df/B of 0.5, when L_1/L_2 is increased from 0.33 to 1, bearing capacity is decreased by 25%. Similarly for D_f/B = 1, when L_1/L_2 is increased from 0.33 to 1, bearing capacity is decreased by 15% and for D_f/B = 1.5, bearing capacity is decreased by 21% when L_1/L_2 is increased 0.33 to 1.

It is also observed that for all values of D_f/B, when L_1/L_2 s increases from 1 to 3, the change in bearing capacity is almost nil.

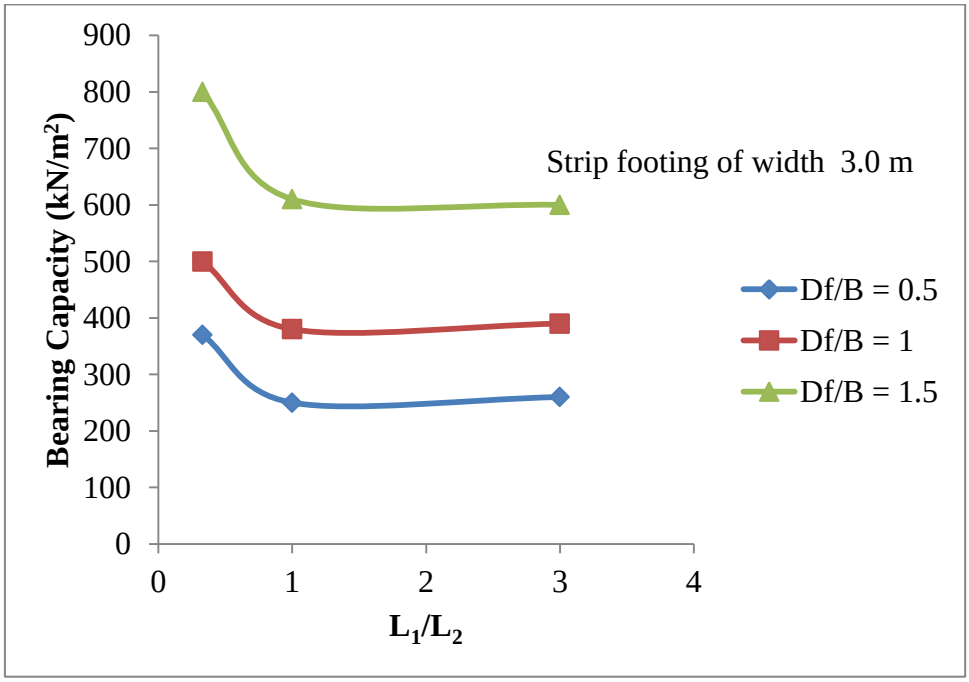

Fig. 6.6: Variation of Bearing Capacity with L_1/L_2 Ratio for Various D_f/B Ratio for Footing Type F2

From the above figure it is observed that for strip footing of width 3.0 m and Df/B of 0.5, when L_1/L_2 is increased from 0.33 to 1, bearing capacity is decreased by 33%. Similarly for D_f/B = 1, when L_1/L_2 is increased from 0.33 to 1, bearing capacity is decreased by 25% and for D_f/B = 1.5, bearing capacity is decreased by 24% when L_1/L_2 is increased 0.33 to 1.

It is also observed that for all values of D_f/B, when L_1/L_2 s increases from 1 to 3, the change in bearing capacity is almost nil.

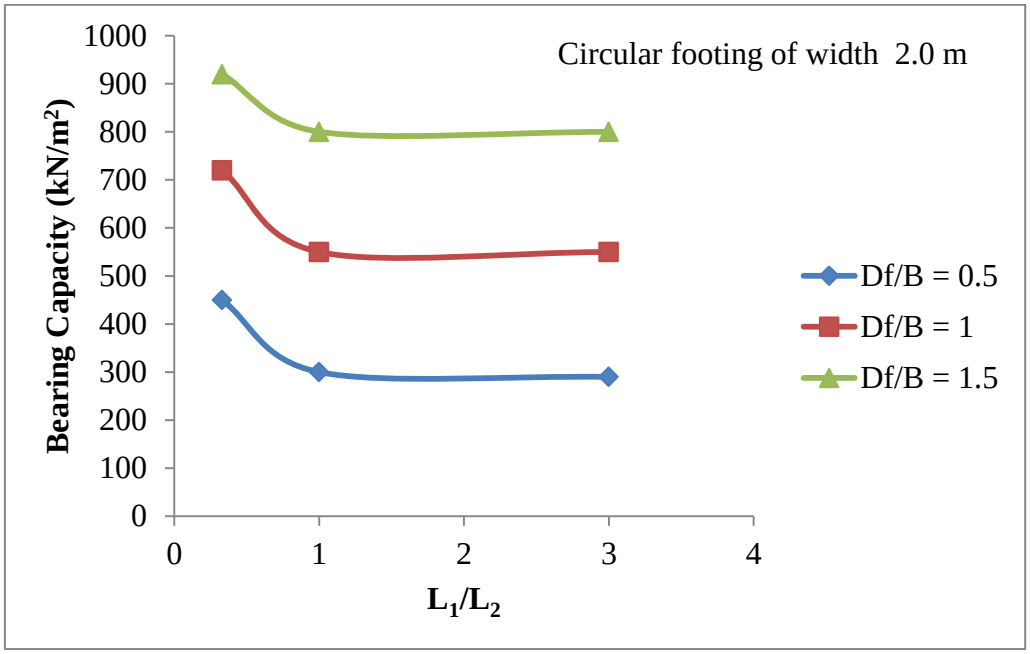

Fig. 6.7: Variation of Bearing Capacity with L_1/L_2 Ratio for Various D_f/B Ratio for Footing Type F3

From the above figure it is observed that for circular footing of width 2.0 m and Df/B of 0.5, when L_1/L_2 is increased from 0.33 to 1, bearing capacity is decreased by 33%. Similarly for D_f/B = 1, when L_1/L_2 is increased from 0.33 to 1, bearing capacity is decreased by 23% and for D_f/B = 1.5, bearing capacity is decreased by 13% when L_1/L_2 is increased 0.33 to 1.

It is also observed that for all values of D_f/B, when L_1/L_2 s increases from 1 to 3, the change in bearing capacity is almost nil.

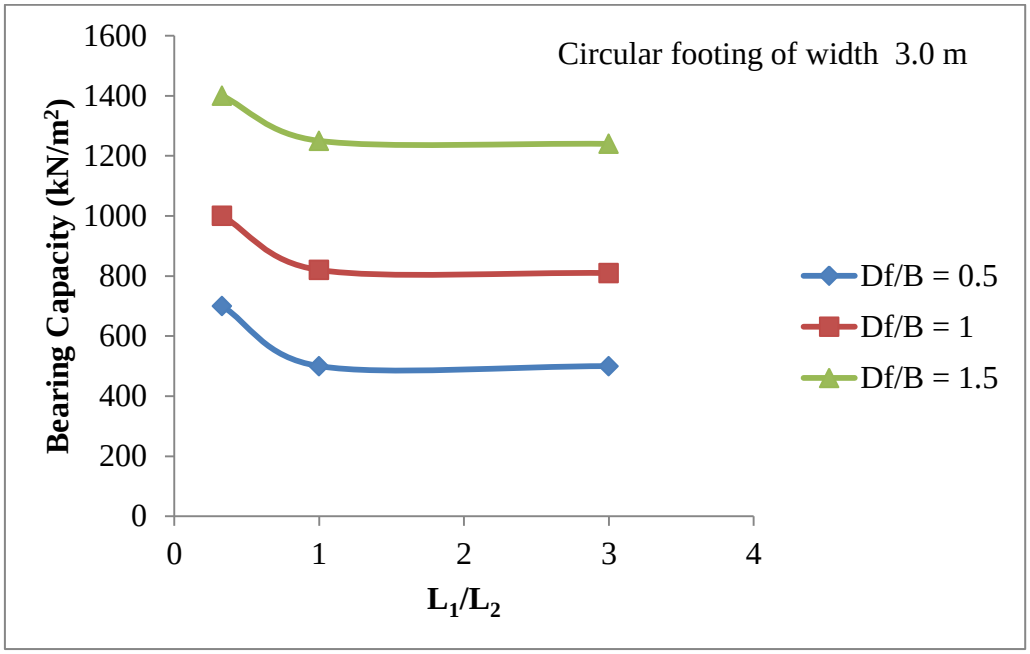

Fig. 6.8: Variation of Bearing Capacity with L_1/L_2 Ratio for Various D_f/B Ratio for Footing Type F4

From the above figure it is observed that for strip footing of width 2.0 m and D_f/B of 0.5, when L_1/L_2 is increased from 0.33 to 1, bearing capacity is decreased by 28%. Similarly for D_f/B = 1, when L_1/L_2 is increased from 0.33 to 1, bearing capacity is decreased by 18% and for D_f/B = 1.5, bearing capacity is decreased by 10% when L_1/L_2 is increased 0.33 to 1.

It is also observed that for all values of D_f/B, when L_1/L_2 s increases from 1 to 3, the change in bearing capacity is almost nil.

6.4 SHAPE FACTOR DETERMINATION :

For all the D_f/B, L_1/L_2 and width of footing combinations considered in the present study, bearing capacity has been evaluted separately for both strip and circular footing using PLAXIS 2D. From the obtained results, shape factor for circular footing is calculated for different cases. Shape factors for different combinations of parameters have been presented in Table 6.2.

Table 6.2 : Shape Factors for Different Combinations of Non-Dimensional Parameters

Width of footing (m)	D_f/B	L_1/L_2	Bearing capacity of strip footing (kN/m^2)	Bearing capacity of circular footing (kN/m^2)	Shape factor
2	0.5	0.33	265	450	**1.70**
2	0.5	1	200	300	**1.50**
2	0.5	3	210	290	**1.38**
2	1	0.33	350	720	**2.06**
2	1	1	300	550	**1.83**
2	1	3	300	550	**1.83**
2	1.5	0.33	510	920	**1.80**
2	1.5	1	400	800	**2.00**
2	1.5	3	400	800	**2.00**
3	0.5	0.33	370	700	**1.89**
3	0.5	1	250	500	**2.00**
3	0.5	3	260	500	**1.92**
3	1	0.33	500	1000	**2.00**
3	1	1	380	820	**2.16**
3	1	3	390	810	**2.08**
3	1.5	0.33	800	1400	**1.75**
3	1.5	1	610	1250	**2.05**
3	1.5	3	600	1240	**2.07**

It is found that bearing capacity of circular footing of 2.0 m dia increases by 70% to 100%, compared to that of strip footing of same width. The values of shape factor for 2.0 m width is found to vary between 1.7 to 2.

It is also observed that bearing capacity of circular footing of 3.0 m dia increases by 89% to 100%, compared to that of strip footing of same width. The values of shape factor for 3.0 m width is found to vary between 1.89 to 2.

6.5 STATISTICAL MODELLING

From the results found from numerical analysis, an attempt has been made to obtain a statistical model by performing regression analysis so that bearing capacity (q) can be predicted in terms of depth of footing D_f, and L_1/L_2 ratio. The values of different parameters for the statistical modelling are given in the Table 6.3.

Table 6.3 Values of various parameters for Regression Analysis

Model No.	Type of Footing	Width of Footing, B (m)	Depth of footing, D_f	L_1/L_2	Bearing Capacity, q (KN/m^2)
1	Strip (F1)	2	1	1/3	265
2	Strip (F1)	2	1	1	200
3	Strip (F1)	2	1	3	210
4	Strip (F1)	2	2	1/3	350
5	Strip (F1)	2	2	1	300
6	Strip (F1)	2	2	3	300
7	Strip (F1)	2	3	1/3	510
8	Strip (F1)	2	3	1	400
9	Strip (F1)	2	3	3	400
10	Strip (F2)	3	1.5	1/3	370
11	Strip (F2)	3	1.5	1	250
12	Strip (F2)	3	1.5	3	260
13	Strip (F2)	3	3	1/3	500
14	Strip (F2)	3	3	1	380
15	Strip (F2)	3	3	3	390
16	Strip (F2)	3	4.5	1/3	800
17	Strip (F2)	3	4.5	1	610

18	Strip (F2)	3	4.5	3	600
19	Circular (F3)	2	1	1/3	450
20	Circular (F3)	2	1	1	300
21	Circular (F3)	2	1	3	290
22	Circular (F3)	2	2	1/3	720
23	Circular (F3)	2	2	1	550
24	Circular (F3)	2	2	3	550
25	Circular (F3)	2	3	1/3	920
26	Circular (F3)	2	3	1	800
27	Circular (F3)	2	3	3	800
28	Circular (F4)	3	1.5	1/3	700
29	Circular (F4)	3	1.5	1	500
30	Circular (F4)	3	1.5	3	500
31	Circular (F4)	3	3	1/3	1000
32	Circular (F4)	3	3	1	820
33	Circular (F4)	3	3	3	810
34	Circular (F4)	3	4.5	1/3	1400
35	Circular (F4)	3	4.5	1	1250
36	Circular (F4)	3	4.5	3	1240

The 36 sets of data have been used for regression analysis as illustrated in the following section.

6.5.1 Regression Analysis

Multiple linear regression has been done using Microsoft Excel, with ultimate bearing capacity (q) as response and depth of footing (D_f), and L_1/L_2 ratio as predictors. From the values of parameters furnished in Table 6.3, the values from serial nos. 1 to 9 and 19 to 27 have been used to obtain the required equation 6.1 with R^2 value of 0.902 and equation 6.2 with R^2 value of 0.943, respectively for strip and circular footing type.

$$q = 143.732 + 105.833*(D_f) – 20.292*(L_1/L_2) \quad \text{……..... (6.1)}$$

$$q = 167.454 + 246.667*(D_f) – 43.655*(L_1/L_2) \quad \text{……..... (6.2)}$$

The testing of the above equations has been done respectively with the help of the values of serial nos. 10 to 18 and 28 to 36 given in Table 6.3 and variations of result as obtained are given in Table 6.4 below. It can be seen that the variation of results obtained from the above equation and numerical analysis are well within 25.28 %.

Table 6.4a: Validation of the Regression Equation for Strip Footing

Model No.	Type of Footing	Width of Footing, B (m)	Depth of footing, D_f	L_1/L_2	q (from PLAXIS analysis) (kN/m^2)	q (from Regression analysis) (kN/m^2)	Percentage variation in results (%)
10	Strip (F2)	3	1.5	1/3	370	295.7851	20.05807
11	Strip (F2)	3	1.5	1	250	282.1895	-12.8758
12	Strip (F2)	3	1.5	3	260	241.6055	7.074808
13	Strip (F2)	3	3	1/3	500	454.5346	9.093072
14	Strip (F2)	3	3	1	380	440.939	-16.0366
15	Strip (F2)	3	3	3	390	400.355	-2.65513
16	Strip (F2)	3	4.5	1/3	800	613.2841	23.33948
17	Strip (F2)	3	4.5	1	610	599.6885	1.69041
18	Strip (F2)	3	4.5	3	600	559.1045	6.815917

Table 6.4b: Validation of the Regression Equation for Circular Footing

Model No.	Type of Footing	Width of Footing, B (m)	Depth of footing, D_f	L_1/L_2	q (from PLAXIS analysis) (kN/m^2)	q (from Regression analysis) (kN/m^2)	Percentage variation in results (%)
28	Circular (F4)	3	1.5	1/3	700	523.0484	25.27881
29	Circular (F4)	3	1.5	1	500	493.7995	1.2401
30	Circular (F4)	3	1.5	3	500	406.4895	18.7021
31	Circular (F4)	3	3	1/3	1000	893.0489	10.69512
32	Circular (F4)	3	3	1	820	863.8	-5.34146
33	Circular (F4)	3	3	3	810	776.49	4.137037
34	Circular (F4)	3	4.5	1/3	1400	1263.049	9.782189
35	Circular (F4)	3	4.5	1	1250	1233.801	1.29596
28	Circular (F4)	3	1.5	1/3	700	1146.491	7.541089

CHAPTER 7: SUMMARY AND CONCLUSIONS

7.0 GENERAL

Summary, conclusion and scope of future work are presented in this chapter.

7.1 SUMMARY

Conventional bearing capacity theories for determining the ultimate load carrying capacity of shallow foundations assume that the thickness of the bearing stratum is homogenous and semi-infinite. However, this is not true in all cases. Multilayered soils are commonly encountered in practice. From the review of literature, it may be noted that the bearing capacity equations proposed for the homogenous soils by Terzaghi (1943), Hansen (1960) and Meyerhof (1963) are not applicable to layered soils.

In the present study, in order to evaluate bearing capacity of shallow footing in layered cohesionless soil, an attempt is made on 2m and 3m wide strip and circular footing in PLAXIS 2D. It has been considered here the ratio of thickness of upper subsoil layer to the thickness of lower subsoil layer is 0.33,1 and 3, accordingly the numerical study has been done for different cases. One type of subsoil combination is taken in the present study, medium dense sand layer is overlain by weak loose sand layer. A parametric study has also been carried out to understand the influence of different parameters like footing width, thickness of different layers etc. on ultimate bearing capacity of shallow footings.

7.2 CONCLUSIONS

The following conclusions have been drawn from the present study:-

- Load - settlement curves for strip footings (of width 2 m and 3 m) and circular footing (of diameter 2 m and 3 m) as obtained from output of PLAXIS 2D software have been presented earlier in Chapter 5 and it is observed that the numerically obtained curves follow continuously curvilinear trend.

- In case of strip footing of width 2.0 m and 3.0 m having L_1/L_2 = 0.33, bearing capacity increases by almost 30% to 35% when D_f/B ratio is increased from 0.5 to 1 and by 45% to 60% when D_f/B ratio is increased from 1 to 1.5, respectively. For the values of L_1/L_2 = 1 and 3, the increment in bearing capacity with D_f/B ratio is almost same. Also, bearing capacity has been found to increase by 45% to 50% when D_f/B

ratio is increased from 0.5 to 1 and by 33% to 55% when D_f/B ratio is increased from 1 to 1.5, respectively.

- In case of circular footing of width 2.0 m and 3.0 m and L_1/L_2 = 0.33, bearing capacity increases by almost 42% to 60% when D_f/B ratio is increased from 0.5 to 1 and by 30% to 40% when D_f/B ratio is increased from 1 to 1.5, respectively. For the values of L_1/L_2 = 1 and 3, the increment in bearing capacity with D_f/B ratio is almost same. It has also been found that the bearing capacity increases by 63% to 85% when D_f/B ratio is increased from 0.5 to 1 and by 45% to 53% when D_f/B ratio is increased from 1 to 1.5, respectively.

- In case of strip footing of width 2.0 m and 3.0 m having D_f/B = 0.5, when L_1/L_2 is increased from 0.33 to 1, bearing capacity has been found to decrease by 25%-33%. Similarly for D_f/B = 1, when L_1/L_2 is increased from 0.33 to 1, the decrease in bearing capacity is 15%-25% and for D_f/B = 1.5, bearing capacity decreases by 21%-24% when L_1/L_2 is increased from 0.33 to 1. It is also observed that for all values of D_f/B, when L_1/L_2 increases from 1 to 3, change of bearing capacity value is almost nil.

- In case of circular footing of width 2.0 m and 3.0 m having D_f/B = 0.5, when L_1/L_2 is increased from 0.33 to 1, bearing capacity has been found to decrease by 28% to 33%. Similarly for D_f/B = 1, when L_1/L_2 is increased from 0.33 to 1, the decrease in bearing capacity is 18% to 23% and for D_f/B = 1.5, bearing capacity decreases by 10% to 13% when L_1/L_2 is increased 0.33 to 1. It is also observed that for all values of D_f/B, when L_1/L_2 increases from 1 to 3, change of bearing capacity value is almost nil.

- It is also observed that bearing capacity of circular footing of 2.0 m dia increases by 70% to 100%, compared to that of strip footing of same width. The values of shape factor for 2.0 m width is found to vary between 1.7 to 2.

- It is also found that bearing capacity of circular footing of 3.0 m dia increases by 89% to 100%, compared to that of strip footing of same width. The values of shape factor for 3.0 m width is found to vary between 1.89 to 2.

- From the output of deformed mesh, it has been observed that there is very little or negligible heaving or bulging of ground surface adjacent to shallow footing. So local shear failure is predominant.

- From the multiple linear regression done using Microsoft Excel, with ultimate bearing capacity (q) as response and depth of footing (D_f), and L_1/L_2 ratio as predictors, equation 7.1 with R^2 value of 0.902 and equation 7.2 with R^2 value of 0.943, respectively for strip and circular footing type, have been found.
    - $q = 143.732 + 105.833*(D_f) – 20.292*(L_1/L_2)$ ……..... (7.1)
    - $q = 167.454 + 246.667*(D_f) – 43.655*(L_1/L_2)$ ……..... (7.2)

7.4 SCOPE OF FUTURE WORK

The further studies may be extended towards the following directions.

- This study will be extended for cohesive layered soil and square footing for different cases.
- Seismic bearing capacity of footing in layered cohesive and cohesionless soil can be worked out.
- Bearing Capacity of shallow footing in layered soil near slope may also be studied under seismic condition.

REFERENCES

- Al-Karni A. A. and Budhu M.(2001). "An Experimental Study Of Seismic Bearing Capacity Of Shallow Footings". Missouri S&T, International Conferences on Recent Advances in Geotechnical Earthquake Engineering and Soil Dynamics, Mar 26th - Mar 31st.
- Azam G. and Wang M.C. (2015). "Bearing Capacity of Strip Footing Supported by Two-Layer c-φ Soils". Transportation Research Record 1331.
- Benmebarek S., Benmoussa S., Belounar L. & Benmebarek N. (2012). "Bearing Capacity of Shallow Foundation on Two Clay Layers by Numerical Approach". Geotechnical and Geological Engineering, ISSN 0960-3182, Volume 30, Number 4.
- Bera A.K., Sasmal S.(2017). "Ultimate Bearing Capacity Analysis of Square Footing on Two Layered Soil". Journal of Geotechnical Studies. Vol 2, No 1 (2017).
- Brown, J.D. and Meyerhof, G.G. (1969). "Experimental Study of Bearing Capacity in Layered Clays". Proceedings of the 7th International Conference on Soil Mechanics and Foundation Engineering, Mexico, vol. 2, pp. 45-51.
- Burd, H.J. and Frydman, S. (1996). "Discussion on Bearing Capacity of Footings over Two-Layer Foundation Soils". Journal of Geotechnical Engineering, ASCE, vol. 122(8), pp. 699-700.
- Burd, H.J. and Frydman, S. (1997). "Bearing Capacity of Plane-Strain Footings on Layered Soils". Canadian Geotechnical Journal, vol. 34, pp. 241-253.
- Button, S.J. (1953). "The Bearing Capacity of Footing on Two-Layer Cohesive Subsoil". Proceedings of the 3rd International Conference on Soil Mechanics and Foundation Engineering, vol. 1, pp. 332-335.
- Caputo V., Cascone E. , Cillo C.(2011). "Seismic Bearing Capacity Factors for Shallow Foundations through Different Methods of Analysis". 5th International conference on Earthquake Geotechnical Engineering, January 2011, 10-13.
- Carlos, A. F. (2004). "Ultimate Bearing Capacity of Shallow Foundations on Layered Soils". Thesis submitted at Concordia University, Montreal, Quebec, Canada.
- Choudhury D. and Rao K.S.S (2006)."Seismic Bearing Capacity Of Shallow Strip Footings Embedded In Slope". International Journal of Geomechanics, Vol. 6, No.3, May 1, 2006.

- Choudhury D., Kanakapura and Rao S. S.(2015). “Seismic Bearing Capacity Of Shallow Strip Footings”. August 2005, Volume 23, Issue 4, pp 403–418.
- Das, B. (1988). “Principles of Foundation Engineering”. Fourth Edition 1999.
- Dey S., Chattopadhyay B.C., Maity J.(2017). “Seismic Bearing Capacity Of Strip Footing”. International Journal of Engineering and Advanced Research Technology (IJEART) ISSN: 2454-9290, Volume-3, Issue-5, May 2017.
- Fazeli P. and Ghareh P.(2012). “A Numerical Study of Bearing Capacity Coefficients of Soil Beneath Foundation under Earthquake Load”. EJGE, Vol. 17, 2012.
- Francesco Castelli and Ernesto Motta(2012). “SEISMIC BEARING CAPACITY OF SHALLOW FOUNDATIONS”. ResearchGate, Chapter · February 2012.
- Georgiadis, M. and Michalopoulos, A. (1985). “Bearing Capacity of Gravity Bases on Layered Soil”. Journal of Geotechnical Engineering, vol. 111, n. 6, pp. 712-729.
- Hanna, A.M. (1981). “Experimental Study of Footings in Layered Soil”. Journal of Geotechnical Engineering, ASCE, 107(GT8), pp. 1113-1127.
- Hanna, A.M. (1981). “Foundations on Strong Sand Overlying Weak Sand”. Journal of Geotechnical Engineering, ASCE, 107(GT7), pp. 915-927.
- Hanna, A.M. (1982). “Bearing Capacity of Foundations on a Weak Sand Layer Overlying a Strong Deposit”. Canadian Geotechnical Journal, vol. 19, no. 3, pp. 392-396.
- Hanna, A.M. and Meyerhof, G.G. (1981). “Experimental Evaluation of Bearing Capacity of Footings Subjected to Inclined Loads”. Canadian Geotechnical Journal, vol. 18, no. 4, pp. 599- 603.
- Huang C.C., and Kang W.W.,(2008). “Seismic Bearing Capacity Of Rigid Footing Adjacent To A Cohesionless Slope”. Soils And Foundations, Japanese Geotechnical Society, vol. 48, No. 5, 641-651.
- IS code (IS: 6403-1981) - Code of practice for determination of bearing capacity of shallow foundations..
- Khan A., Jawaid S.M.Ali.(2017). “Review On Determining Seismic Bearing Capacity Of Shallow Strip Footing”. International Journal of Innovative Research in Science, Engineering and Technology. Vol. 6, Issue 4, April 2017.
- Maeda Y., Irie T. and Yokota Y. (2004). “Bearing Capacity Formura For Shallow

Foundations During Earthquake".13th World Conference on Earthquake Engineering. August 1-6, 2004 Paper No. 3293.

- Meherhof, G. G. (1963). "Some recent research on the bearing capacity of foundations".Canadian Geotechnical Journal 1: 16-26.
- Meyerhof, G.G. (1974). "Ultimate Bearing Capacity of Footings on Sand Layer Overlying Clay". Canadian Geotechnical Journal, vol. 11, pp. 223-229.
- Meyerhof, G.G. and Hanna, A.M. (1978). "Ultimate Bearing Capacity of Foundations on Layered Soils under Inclined Load". Canadian Geotechnical Journal, vol. 15, no. 4, pp. 565-572.
- Meyerhof, G.G. and Hanna, A.M. (1979). "Ultimate Bearing Capacity of Foundations on a Three- Layer Soil, With Special Reference to Layered Sand". Canadian Geotechnical Journal, vol. 16, no. 2, pp. 412-414.
- Misir G., Laman M. (2017)."A Modern Approach to Estimate the Bearing Capacity of Layered Soil". Periodica Polytechnica Civil Engineering. 61(3), pp. 434‑446, 2017
- Mosadegh, A. and Nikraz, H. (2015). "Bearing Capacity Evaluation of Footing on a Layered - Soil using ABAQUS". Journal of Earth Science & Climatic Change. Volume 6 • Issue 3 • 1000264.
- Oda, M. and Win, S. (1990). "Ultimate Bearing Capacity Tests on Sand with Clay Layer". Journal of Geotechnical Engineering, vol. 116, n. 12, pp. 1902-1906.
- Pane V., Vecchietti A. and Cecconi M.(2016)."A Numerical Study On The Seismic Bearing Capacity Of Shallow Foundations". Springer Science+Business Media Dordrecht 2016.
- Pfeifle, T.W. and Das, B.M. (1979). "Model Tests for Bearing Capacity in Sand". Journal of Geotechnical Engineering, ASCE, 105(GT9), pp. 1112-1116.
- PLAXIS Tutorial Manual, Material Models Manual, Reference Manual and Scientific Manual. Version 8.
- Saha A., Saha A.K., and Ghosh S.(2018). "Pseudodynamic Bearing Capacity Analysis Of Shallow Strip Footing Using The Advanced Optimization Technique "Hybrid Symbiosis Organisms Search Algorithm" With Numerical Validation". Hindawi, Advances in Civil

Engineering, Volume 2018, Article ID 3729360.

- Shafiee A. H., Jahanandish M. (2010).” Seismic Bearing Capacity Factors For Strip Footings”. 5th National Congress on Civil Engineering, May 4-6, 2010, Ferdowsi University of Mashhad, Mashhad, Iran.
- Soubra A. H.(1997).” Seismic bearing capacity of shallow strip footings in seismic conditions”. Proc. Instn Civ. Engrs Geotech. Engng, 1997, 125, Oct., 230-241,Paper 11179.
- Szypcio, Z. and Dolzyk, K. (2006). “The Bearing Capacity of Layered Subsoil”. Studia Geotechnica et Mechanica, Vol. XXVIII, No. 1, 2006.
- Terzaghi, K. (1943). Bearing Capacity Theory. Theoretical soil mechanics, John wiley & sons, New York.
- Verma, S. K., Jain, P.K. and Kumar, R. (2013). “Prediction of Bearing Capacity of Granular Layered Soils by Plate Load Test”. International Journal of Advanced Engineering Research and Studies, Vol. II/ Issue III/April-June, 2013/142-149.
- Yadav A.P., Jawaid S.M.Ali(2016).”Seismic Bearing Capacity And Settlements Of Foundations” International Journal of Innovative Research in Science, Engineering and Technology. Vol. 5, Issue 4, April 2016.
- Zhu, M. (2004). “Bearing Capacity of Strip Footings on Two-Layer Clay Soil by Finite Element Method”. ABAQUS User’s Conference.
- Zhu, M. and Michalowski, R. L. (2010). “Bearing Capacity of Rectangular Footings on Two-Layer Clay”. American Society of Civil Engineers, 191(15), pp. 933-947.